INSTITUTE OF PAPER SCIENCE AND TECHNOLOGY

Atlanta, Georgia

THE EFFECTS OF RETENTION AID DOSAGE AND MECHANICAL ENERGY DISSIPATION ON FIBER FLOCCULATION IN A FLOW CHANNEL

9490 Doctoral Thesis

December 23, 2004

Submitted to:

Dr. Fred Ahrens--Advisor
Dr. Yulin Deng
Dr. Timothy Patterson
Dr. Roman Popil
Dr. David White
Office of Academic Affairs

Submitted by:

Brian D. Weseman

I dedicate this thesis to my wife Sarah and my son Benjamin.

ABSTRACT

Formation plays an important role in the end-use properties of paper products, but before formation can be optimized to achieve superior properties, an understanding about the causes of formation must be developed. Formation is caused by variations in the basis weight of paper that are results of fiber floc formation before and during the forming of the sheet. This project is a first step in a larger research program aimed at studying formation. By observing the effects that mechanical energy dissipation (in the form of turbulence) and retention chemical dosage have on floc formation, we may develop a better understanding of how to control formation.

In this study, a rectangular cross-section flow channel was constructed to aid in the acquisition of digital images of a flowing fiber suspension. The furnish consisted of a 55:45 spruce:pine bleached market pulp mix from a Western Canadian mill. Turbulence was varied by changing the flow rate; Reynolds numbers achieved range from 20,000 to 40,000. The retention aid used was a cationic polyacrylamide with a medium charge density. Dosage of the retention aid was varied from 0 to 2 pounds per ton OD fiber. Digital images of the flowing fiber suspension were acquired with a professional digital SLR camera with a forensics-quality lens. Three separate image analysis techniques were used to measure the flocculation state of the fiber suspension: morphological image operations, formation number analysis, and fast Fourier transform analysis.

Morphological image analysis was capable of measuring floc size increases seen in the acquired floc images. It was shown how floc diameter could increase simultaneously with decreasing total floc area and total floc number. A regression model relating retention aid dosage and energy dissipation was constructed in an effort to predict flocculation. The regression model was used to predict F^2 (formation number squared) results from the study. The interaction effect RE was shown to have a differing effect

across the retention aid dosage levels. As a result, this model and technique may prove to be a beneficial tool in optimizing retention aid applications.

TABLE OF CONTENTS

LIST OF TABLES

LIST OF FIGURES

INTRODUCTION

The formation quality of paper is related to the degree of variation in the local basis weight of the sheet. These variations in local basis weight are primarily the result of fiber flocs created before or within the forming section of the paper machine. Because formation quality has a significant influence on the end use properties of paper (as will be shown), improving formation quality is a key goal for the papermaker. Knowing that formation is determined by the presence, structure and quantity of fiber flocs, an effort to improve formation is also an effort to understand and control fiber flocs.

Measuring Paper Formation

Much work has been done in the area of measuring the formation of paper. There are many ways to describe the formation quality of a sheet of paper. Subjectively, the papermaker may call the sheet formation blotchy, or non-uniform, after completing a visual test such as with transmitted light. This is often termed *look-through appearance*. Many instruments have been developed that try to measure formation on a transmitted light basis. The drawback to these types of instruments is that results for different grades cannot be compared because light scattering is different for each grade (Norman and Wahren, 1974). Since each grade of paper has its own specialized furnish (fines, fillers, and fiber types), each grade will have different optical properties. For example, a sheet with high mineral filler content will have a much higher light scattering capability than a sheet without high filler content. The differences in optical properties make each grade exhibit different results under the transmitted light formation test methods.

For more objective purposes, it is necessary to use a different procedure that can distinguish between *mass variations* in the paper without the drawbacks associated with scattering. One such way is through the use of beta radiography (Norman and Wahren, 1974). Beta particles are not scattered when they travel through a sheet—they are absorbed only by the mass in the path through the sheet. The final result of a beta radiography test is the coefficient of variation of basis weight. A higher coefficient means a poorer formation. Today, the beta radiographic method is one of the best methods for measuring the formation of paper (Popil, 1996).

Measuring formation accurately is important when evaluating the quality of paper. As will be shown in the next section, formation does not just play a role in the visual appeal of paper, but it can also significantly affect the physical properties of the paper.

The Effect of Formation on the Strength Properties of Paper

The basis weight variations arising out of sheet formation play a large role in how the sheet will perform under the intended conditions. Many studies have shown that the physical properties of paper are affected by formation. Göttsching (1979) studied the effect of formation on different strength properties. In this work, formation was varied in two ways: changing the sedimentation time of the sheet formation, and changing the consistency. In both cases, increasing the variable decreased the quality of formation. Formation was indirectly evaluated using a caliper measurement that was shown to correlate with visual observations of formation; a direct measure of basis weight variation was not done. From the study, Göttsching concluded that, with decreasing formation quality, breaking length, breaking stretch, burst strength, and tear strength all decreased. In order to realize the full strength potential of a sheet, this study showed that it is important to have good formation.

Norman and Wahren (1973) discussed unpublished data by Calvin and Rudström from an investigation about the influence of mass distribution on the strength properties of paper. The study looked at three types of sheets: a laboratory sheet, paper made on an experimental paper machine, and paper made on an industrial paper machine. Formation on the machine-made papers was adjusted by changing the consistency inside the headbox. The strength property compared was the geometric mean breaking stress divided by the sheet density (to obtain a specific strength that was proportional to the breaking length). The machine-made papers experienced a maximum 40% decrease in their strength properties as formation quality was decreased.

In another strength properties study, Libertucci, et al. (1992) looked at the effect of formation on the fracture toughness of handsheets. They came to the conclusion that the mean fracture toughness is relatively unaffected by formation, but that the coefficient of variance of fracture toughness is increased by decreased formation quality.

The Effect of Formation on the Printability and Optical Properties of Paper

In an early study by Madsen and Aneliunas (1968), the printability difference between the light and dark areas in a newsprint sheet was found to be caused by a lack of smoothness in the light areas. They also came to the conclusion "…that the effectiveness of the usual calender stack is limited by the structure of the paper."

Kajanto (1991) found that formation played a larger role in the printability of experimental or laboratory sheets and a lesser role in commercial sheets. Correlations did exist for both sheets. Kajanto stressed the point that it was not the actual basis weight variations that were causing the changes in printability. It is the effect on other paper properties, namely surface topography and porosity, that changes the printability. Figure 1 displays this statement graphically. This echoes the conclusions of Madsen and Aneliunas. Another confirmation of previous work is the conclusion Kajanto came to about the effectiveness of hard nip calendering. Kajanto stated that hard nip calendering cannot be used to overcome deficiencies caused by poor formation—the effectiveness of usual calendering is limited by the structure of the paper.

The previous work was confirmed again by Shallhorn and Heintze (1996). In their study of the effect of formation on offset printing, they found that the areas of light basis weight received less ink and the areas of higher basis weight received more. Microscopic evidence of the structure of the lighter weight areas revealed that there were fewer fibers at the surface. This is an indication of a rougher surface. Further data suggested that calendering seemed to accentuate the negative effects of poor formation.

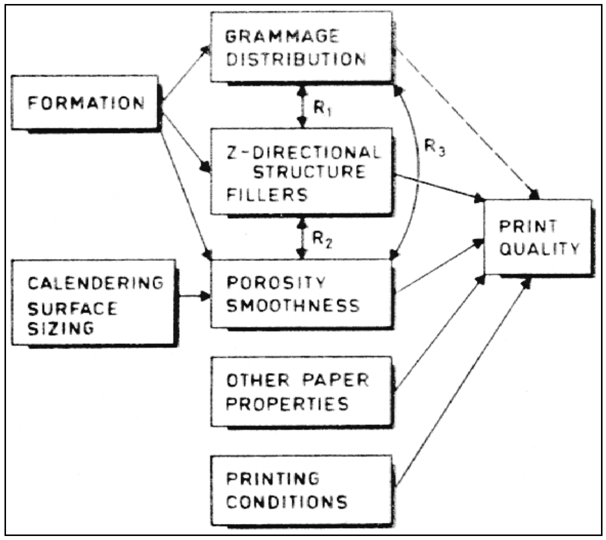

Figure 1. How formation indirectly affects printability. (Source: Kajanto, I. "Effect of Formation on Print Unevenness." In *The Proceedings of the TAPPI International Paper Physics Conference Held in Kona, HI, 22-26 September 1991*, 281-290.)

The optical properties of paper are also affected by the quality of formation. Kulikova, et al. (1995) varied the formation of paper while keeping the fluorescent dye addition constant. What they found was an increase in variability of brightness with decreased formation quality, and that the increased variability could be attributed to differences in surface roughness. This confirms previous work.

The formation of paper and board products has been shown to have a substantial influence on the printed appearance of both coated and uncoated printing paper and board. Formation may also have a substantial effect on the strength of these products. Therefore, formation is an important product quality attribute that is of continuing interest.

The Importance of Floc Formation

The composition, size, and density of fiber flocs during the manufacture of paper is thought to be affected by both mechanical and chemical influences within the paper machine, as well as fiber morphology and concentration (as expressed by consistency). Paper machine suppliers strive to provide equipment that maximizes the energy input to the stock and de-waters the stock as rapidly as possible in an effort to both diminish the rate of floc formation as well as to disrupt flocs that may already be in the process of forming. Chemical suppliers have developed a number of new products over the last two decades in a parallel effort to improve paper and board formation.

Unfortunately, most published studies in the area of formation have focused exclusively on either mechanical or chemical influences on formation. By understanding the combined effects of mechanical energy input and the chemical influences of formation, it may be possible to more accurately determine the extent of energy input required to improve formation by disrupting fiber flocs, or to more intelligently synthesize retention systems and more appropriately choose points of chemical addition.

BACKGROUND

DEFINITION OF A FIBER FLOC

For further discussion about flocculation, it is necessary to clarify the definition that will be used for the term *floc*. In the previous section, the term floc was used to describe the basis weight variations in a dry sheet of paper. What is of interest in this project is floc *formation*. The definition of the term floc in a dry sheet of paper is not appropriate for this discussion. What is needed is a definition of floc as it pertains to fibers in a water suspension. For this discussion, a floc is defined as a region of increased fiber mass concentration in a fiber slurry. As will be explained later, with respect to the data analysis in the study, flocs will be defined as any region of fiber mass concentration that has an area greater than 0.785 mm^2 (i.e. has an equivalent diameter of 1 mm or more); These fiber mass concentrations have a typical size of one to three times the fiber length of the pulp in question (Wrist 1961). In addition, it will be helpful to visualize flocculation as a sum of processes—processes that encourage floc formation and processes that encourage floc disruption.

FIBER EFFECTS ON FLOC DYNAMICS

Since flocs are made of fibers, it is logical to expect that certain properties of fibers are going to play an important role in how flocs form. What are the important fiber properties that affect flocculation? An easy way to approach this question is to consider flocculation as a type of statistical process. Flocs form only when fibers can interact with each other. As a result, any parameter that can increase the probability of fiber interaction will increase the chances of flocculation. If the parameters of the system are set such that the chance of interactions between fibers is low, flocculation may not occur. To answer the question, properties of fibers and fiber slurries that affect the ability of fibers to interact need to be considered. The kinetics of floc formation is a give and take situation.

On one side, the kinetics are affected by changing the ability of the fibers to flocculate, and on the other side, the kinetics are affected by changing the ability of flocs to disperse. As a result, not only are fiber properties that affect fiber interaction important, but fiber properties that affect floc toughness or the ability of a floc to persist in the suspension will be just as important to the kinetics of floc formation.

To explain one fiber parameter, think of flocculation as analogous to a typical chemical reaction. One way to push a reaction to completion is to increase the concentration of the reactants. In this case, the reactant is fibers and the concentration is the consistency of the fibers in the suspension. By increasing the consistency of the fibers, the fibers are more likely to come in contact with one another because there is less free space available. In work by Mason (1954), a critical concentration for fiber interaction was developed much along the lines of the previous thought experiment. He thought of the fiber as a rigid cylinder that could sweep out a characteristic sphere with a diameter equal to the length of the cylinder. By using the geometric properties of the fiber, Mason showed that the critical concentration for flocculation (as a volume percent) is given by equation 1.

$$c_0 = \frac{3}{2r^2} \qquad \textbf{(1)}$$

In equation 1, c_0 is the critical concentration expressed as a volume percent, and r is the axis ratio (length/diameter) of the cylinder. The critical concentration is the point at which there is one fiber within the sphere swept out by a fiber and collision through rotation is possible. When more than one fiber exists within the sphere, fiber interaction begins to take place. Notice that the only fiber properties in equation 1 are fiber diameter and fiber length. To decrease the critical concentration, the fiber length can be increased or the fiber diameter can be decreased. This concept was recently further developed by

Kerekes and Schell (1991). They developed a crowding factor that described the number of fibers within the sphere (equation 2).

$$N = 5C_m \frac{L^2}{\omega} \qquad \textbf{(2)}$$

In equation 2, N is the crowding factor (the number of fibers within the characteristic sphere), C_m is the mass concentration of fibers expressed as a percent, L is the fiber length in m and ω is the fiber coarseness in kg/m. For the sake of comparison, Mason's critical concentration occurs at a crowding factor of 1. The crowding factor can be used as an indicator of the amount of fiber interaction within a suspension by relating it to the number of fiber-to-fiber contacts. The amount of fiber-to-fiber contacts plays a large role in the dispersing ability of flocs. The lower the number of fiber contacts, the more mobile the fibers are. This results in a more dispersible floc. As stated by Kerekes and Schell, the relationship between the crowding factor and the number of fiber-to-fiber contacts is given by equation 3.

$$N \cong \frac{4\pi n_c^3}{3(n_c - 1)} \qquad \textbf{(3)}$$

In equation 3, n_c is the number of fiber-to-fiber contacts per fiber. The number of fiber contacts affect the dispersibility of flocs. As the crowding number increases, the number of fiber contacts also increases. This results in fiber entanglement and flocs that are difficult to disperse. Figure 2 displays the two most common forms of fiber cohesion. Elastic fiber bending (Figure 2a) occurs via frictional forces that arise as fibers are restrained in the network (Kerekes et al., 1985). Mechanical surface linkage (Figure 2b) is a hooking entanglement between fibers that depends heavily on the amount of surface fibrillation the fiber has.

Although consistency plays a part in determining the crowding factor and the amount of fiber interaction, Kerekes and Schell (1991) were quick to point out that consistency is not the sole determinant of flocculation. By examining equations 1 and 2, more fiber properties that affect flocculation are revealed. Both equations display the importance of fiber length to flocculation. Length is contained within the variable r in equation 1. All sources in the literature reviewed state that **fiber length is the most important fiber property that affects flocculation**. One convincing piece of evidence that fiber length is the important variable is that floc sizes are usually in the range of 1-2 fiber lengths. Why is fiber length so important? Fibers can move in translation, but as pointed out by Mason (1954) the important motion is rotation. Fibers sweep out a much larger volume than themselves. Therefore, rotational motion results in more collisions than translational motion. The fiber property that leads to a larger swept out volume is obviously the length. This importance of length is witnessed by the square relationship in equation 2. Fiber length affects the kinetics of floc formation in two ways: the interaction of the fibers and the number of fiber contacts.

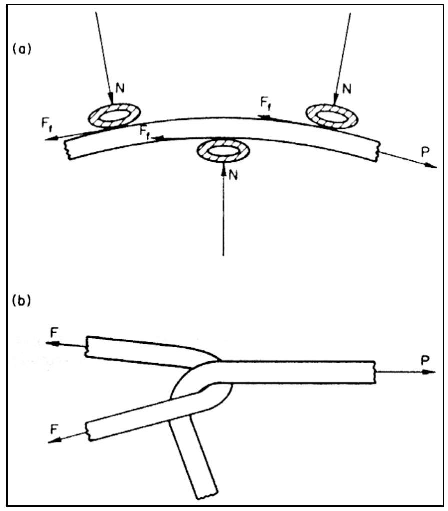

Figure 2. Types of fiber cohesion: (a) elastic fiber bending, (b) mechanical surface linkage. (Source: Kerekes, R., R. Soszynski, and P. Tam Doo. "The Flocculation of Pulp Fibers." In *The Proceedings of the Papermaking Raw Materials Conference* edited by Punton, 1985.)

Coarseness is also an important fiber property that affects flocculation. It is important to note that, as Kerekes and Schell wrote (1995), it is difficult to separate the effects of fiber length and fiber coarseness because longer fibers tend to be coarser fibers. Coarseness affects the kinetics of flocculation through fiber interaction, but plays a larger role in the dispersibility of fibers. Coarse fibers tend to be stiffer fibers. As a result, they are more resistant to bending. As the number of fiber contacts increase, fibers become less mobile and become entangled. Coarser fibers lend strength to the fiber network because of their stiffness, therefore making a stronger floc. The complicated relationship of consistency, fiber length and fiber coarseness as it applies to flocculation is displayed by experimental data from Kerekes and Soszynski in Figure 3.

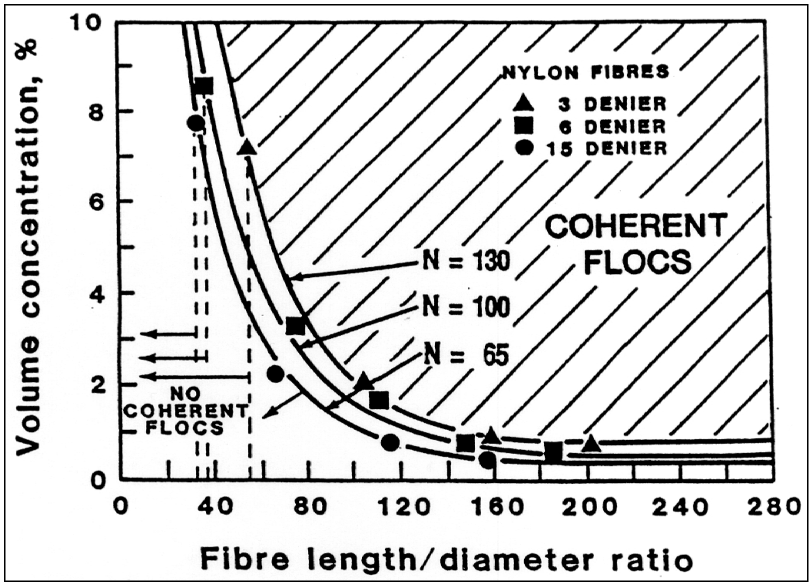

Figure 3. Experimental data showing the affect of fiber length, fiber diameter and volume consistency on the flocculation tendency of a fiber suspension. (Source: Kerekes, R. "Perspectives on Fibre Flocculation in Papermaking." In *The Proceedings of the International Paper Physics Conference Held in Niagra-on-the-Lake, Ontario, 11 September 1995*, 23-31.)

A denier is another measure of fiber coarseness that is used more commonly in the textiles industry (1 denier = 1 g/9000 m). The three coarseness levels used in Figure 3 expressed in units of mg/100 m are: 33, 67, and 167. Notice in Figure 3, that as fiber coarseness increases, the maximum fiber length/diameter ratio before flocculation occurs, decreases. At a constant fiber concentration, increasing the fiber length/diameter ratio will result in increased flocculation. At a constant fiber length/diameter ratio, increasing the volume concentration of the fibers will result in increased flocculation. In both cases, there comes a point where coherent flocs (flocs that aren't continuously forming and dispersing) just will not occur. This point is at low concentrations and low fiber length/diameter ratios.

To summarize, it has been shown that the important fiber properties and fiber suspension properties that affect the tendency of fibers to flocculate are fiber length, consistency and fiber coarseness. Another set of parameters that might affect the kinetics of floc formation is chemical effects. For years, scientists thought that flocculation was the result of colloidal forces only. Although the literature is full of evidence to show this is an incomplete view, colloidal forces still play an important role in flocculation.

CHEMICAL EFFECTS ON FLOC DYNAMICS

We have seen that several *physical* fiber and fiber slurry properties affect floc formation, but these properties are not exclusive in the paper machine system. Because paper formation occurs in an aqueous environment, flocculation is also affected by both the chemical properties of the fiber and the chemical properties of the wet end as a whole. Of particular importance is the electrostatic properties of the fibers and the aqueous environment. The papermaker uses electrostatic properties to enhance the properties of the final product. This is accomplished through the use of a class of chemicals collectively referred to as *retention aids*. Retention aids work via electrostatic forces at the colloidal level to aggregate fines and fillers and attach them to fibers so they are present in the final product. Retention is most commonly accomplished through the use of polymers of differing functionality and structure. These polymers enhance retention by taking part in a variety of retention mechanisms. Examples of retention mechanisms include charge neutralization, heterocoagulation, bridging, and patching (Eklund and Lindström, 1991). The following section will discuss colloidal theory, and the effects of chemical dosage and type on the flocculation of fibers.

Colloidal Theory

Colloidal theory serves as a way to begin to explain phenomena occurring in the wet end of a paper machine. It is important to remember, however, that colloidal theory has been developed with the aid of laboratory conditions that are extremely difficult (if not impossible) to achieve in the wet end of a paper machine. The paper machine wet end represents an environment of vastly different components, from a chemical perspective, that are moving at speeds much higher than the relatively static conditions on which colloidal theory is based. Colloidal theory allows explanation of the general trends and phenomena in the wet end, but because of the non-ideal nature of the wet end, specific application of theory to practice is not always successful.

Many of the particle interactions occurring in the wet end of a paper machine involve surface charges that particles develop upon being introduced into water. Surface charges develop on particles because of ionizable groups and ion adsorption at the surface. Since the sum total of charges in the system must be zero, an equilibrium structure of charges surrounds the surface of particles. This equilibrium structure has come to be known as the electrostatic double layer (Figure 4). Aside from the negative surface charge that most particles possess, two other layers exist: the Stern layer and the Gouy layer. The layers are named after the researchers that proposed the respective layers. The Stern layer is a layer of positive counterions that are held near the surface by electrostatic attraction, the van der Waals force, and thermal movement (Eklund and Lindström, 1991). In the Stern layer, potential generally drops off linearly with distance from the particle surface. The Gouy layer is a diffuse layer of ions that are affected only by electrostatic attraction and thermal movement (Eklund and Lindström, 1991). Potential drops off exponentially in the Gouy layer.

One important parameter that affects how particles interact is the thickness of the double layer. The thinner the double layer, the easier it is for particles to come in close contact with each other. The thickness of the double layer is usually taken as the distance over which potential decreases exponentially (Shaw, 1992). This distance is equal to the inverse of the Debye parameter κ which is also known as the Debye length. Equations 4 and 5 show how the Debye parameter is calculated.

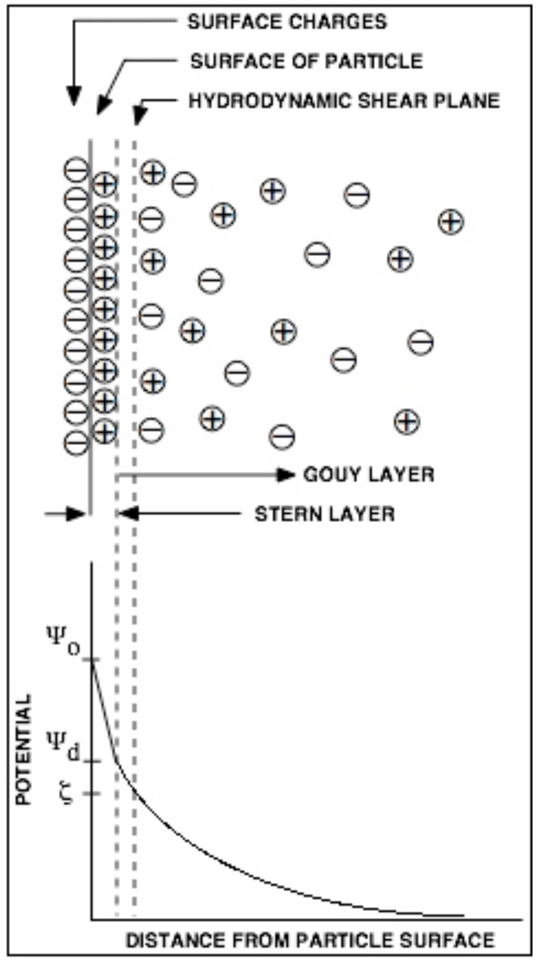

Figure 4. The electrostatic double layer.

$$\frac{1}{\kappa} = \sqrt{\frac{\varepsilon_r \varepsilon_o \mathrm{R}T}{2\mathrm{F}^2}} \frac{1}{\sqrt{I}} \qquad \textbf{(4)}$$

$$I = \sum C_{ia} z_i^2 \qquad \textbf{(5)}$$

In equations 4 and 5, ε_r is the dielectric constant of the material, ε_o is the permittivity of a vacuum, R is the gas constant, T is the temperature in kelvin, F is Faraday's constant, I is the ionic strength, C_{ia} is the average ion concentration, and z_i is the valency of the ion.

Equation 4 shows that the double layer thickness is governed mostly by constants and the inherent properties of the particles. The only two variables are temperature and the ionic strength. At constant temperature, it is apparent that to decrease the double layer, an increase in ionic strength must occur. Equation 5 shows that to increase ionic strength either the electrolyte concentration or the valence of the electrolyte must be changed. These are the parameters that are key to optimizing retention at the colloidal level on a paper machine.

The double layer plays a large role in the ease at which particles can get close to one another. It is the balance of attractive and repulsive forces arising out of electrostatics that determine the aggregation of particles in the wet end of a paper machine. This balance is explained by what is known as DLVO (Deryagin-Landau-Verwey-Overbeek) theory. Equations 6 and 7 show how the attractive force of two like particles is calculated.

$$V_{att} = \frac{\mathrm{A_H}}{12\pi s^2} \qquad \textbf{(6)}$$

$$\mathrm{A_H} = \text{the Hamaker constant} = \frac{3}{4}\pi^2 \mathrm{N_V^2} \mathrm{h} \nu^2 \alpha^2 \qquad \textbf{(7)}$$

For equations 6 and 7, s is the interfacial separation of atomic centers at contact, x is a geometric factor, $\mathrm{N_V}$ is the number of molecules per unit volume, h is Planck's constant, ν is the characteristic vibration frequency for the weakest bound electrons in the molecules, and α is the polarizability. Repulsion forces counteract the attractive forces. Equations 8 and 9 show how the repulsion force is calculated.

$$V_{rep} = 32\pi\varepsilon_r \varepsilon_o r \left(\frac{\mathrm{k_B}T}{z\mathrm{e}}\right)^2 \phi^2 \ln(1+\exp(-\kappa d)) \qquad \textbf{(8)}$$

$$\phi = \tanh\left(\frac{z\mathrm{e}\Psi_d}{4\mathrm{k_B}T}\right) \qquad \textbf{(9)}$$

For equations 8 and 9, r is the particle radius, e is the elementary charge, d is the interparticle distance, and Ψ_d is the potential of the Gouy layer. Here again we see the role of colloidal theory serving as a baseline to explain phenomena in the wet end. Equations 8 and 9 are only valid for systems at low electrolyte concentrations. It is difficult to argue that low electrolyte concentrations are found in the wet end of the paper machine.

Equations 6 and 8 can be combined to produce a total interparticle force that is displayed by equation 10 and graphically by Figure 5.

$$V_{tot} = V_{att} + V_{rep} \qquad \textbf{(10)}$$

DLVO theory demonstrates that two energies of interaction exist between particles: attraction and repulsion. For particles to come in contact easier it is necessary to lower the energy barrier showed in Figure 5. This is done by lowering the repulsion energy. A decrease in repulsion energy requires a decrease in the double layer thickness and this is achieved by increasing the ionic strength of the electrolyte. Retention aids employ this technique using several different mechanisms to affect the flocculation on the paper machine.

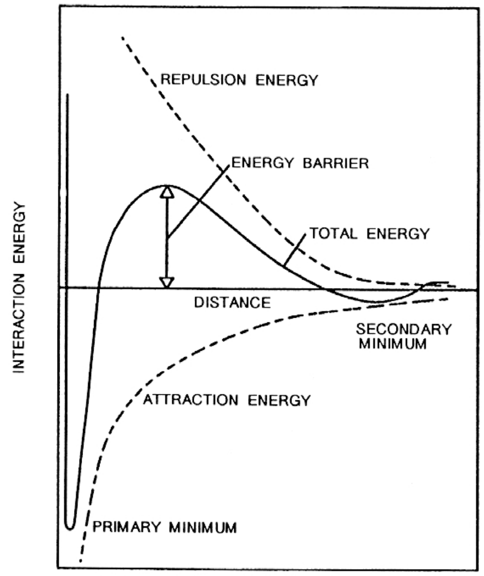

Figure 5. Particle interaction according to DLVO theory. (Source: Eklund, D, and T. Lindström. *Paper Chemistry: An Introduction*. Grankulla, Finland: DT Paper Science, 1991.)

Retention Mechanisms

There are a number of different retention mechanisms that employ exactly what DLVO theory predicts about the depression of the double layer resulting in aggregation of particles. One such mechanism, *charge neutralization*, is accomplished by adding cationic electrolytes (salts) to the system. The electrolytes neutralize or decrease the negative surface charge of the fibers and fines. This causes compression of the electrostatic double layer and allows the fibers and fines to come into contact with one another more readily (Eklund and Lindström, 1991). The ultimate result of charge neutralization is coagulation.

Heterocoagulation is similar to charge neutralization, but is achieved through the use of polyelectrolytes of high charge density, and high molecular weight. Examples of polyelectrolytes are polyamines, polyethyleneimines, and polyamideamine epichlorohydrins (Scott, 1996). The "hetero" in heterocoagulation arises out of the fact that these polyelectrolytes are selective in what they neutralize. For instance, polyethyleneimines (PEI) are thought to be preferentially deposited on fibers instead of fines and fillers. In a paper machine, one would typically see a different polyelectrolyte added for each component in the system.

The *patching* flocculation mechanism is another means to induce aggregation. Although the same chemicals that are used for patching are also used for charge neutralization, for patching it is necessary to use low molecular weight polymers. The patching flocculation mechanism is different from charge neutralization in that the polymer is creating point sources of positive charge on the fiber which allow other negatively charged particles (fines and fillers) to attach to it. Another difference between charge neutralization and patching flocculation lies in the rate of coagulation. "Coagulation rate increases with increasing electrolyte content during charge neutralization, whereas it decreases during patching after the optimum electrolyte content has been attained" (Eklund and Lindström, 1991).

Another way to induce flocculation is by the *bridging* mechanism. During the bridging mechanism, a moderate charge density, high molecular weight cationic polymer is used to attach to a fiber in numerous places and create "loops" that reach far out into the slurry away from the fiber. These loops then serve to attach to other fines and fibers. The application of these retention aids is done with some precaution in the selection of an addition point. Since the main functionality of these polymers lies in its high molecular weight, shear is an important consideration in the use of the polymer. Too high a shear rate will decrease the chain length and lower the effectiveness of the bridging mechanism. Some bridging polymers are polyacrylamides (PAM) and polyethyleneoxides (PEO).

Some applications employ both a bridging polymer and a patching polymer. These are commonly referred to as *dual-polymer systems*. A patching polymer (called in this case a *cationic promoter*) is added to the stock to create the small patches of cationic charge on the fibers. Further down the process, an anionic long chain polymer is added to attach at the sites created by the patching polymer.

A retention system that is relatively new in application is *microparticle retention systems*. This mechanism uses a long chain polymer such as a cationic polyacrylamide or starch and a small anionic particle like colloidal silica or montmorillonite clay. What sets this system apart from the other system, is its suggested ability to re-flocculate after being disturbed by shear forces. The re-flocculation, however, is on a microscale and does not contribute to the coarse scale formation of the sheet (Eklund and Lindström, 1991). In a bridging or patching system, if the flocs that are formed are dispersed, the system has no ability to reform the flocs.

Not many sources in the literature comment on the direct effect retention aid type has on the kinetics of floc formation. Of the studies reviewed, the general consensus is that dual-polymer retention systems provide, by far, the most intense flocculation of all the retention mechanisms, however there is no mention about the time frame of this intense flocculation (Penniman, 1978; Britt, 1979). Dual-polymer systems generally give the papermaker an increase in drainage and retention at the expense of formation quality.

Wågberg and Lindström (1987) completed a study of three different retention system types: polyethyleneoxide (PEO) with phenol formaldehyde resin (PFR), anionic polyacrylamide (A-PAM) with polyamine epichlorohydrin (PAE), and a cationic polyacrylamide (C-PAM). The PEO system reached flocculation equilibrium after two seconds. Both the A-PAM and C-PAM systems reached an equilibrium in under one second. The A-PAM had a higher flocculation intensity than the C-PAM system. It appears in Wågberg and Lindström's work that there is not much difference in flocculation with respect to retention system type.

Unpublished work by Robbins et al. (1991) produced similar results to that of Wågberg and Lindström. Their study was concerned more with the actual formation of the sheet rather than the flocculation of the fibers. Using a beta radiographic technique to characterize the formation of the paper, Robbins was able to show that at constant single pass pigment retention, several different types of retention mechanisms produced the same quality of formation. Figure 6 displays these results.

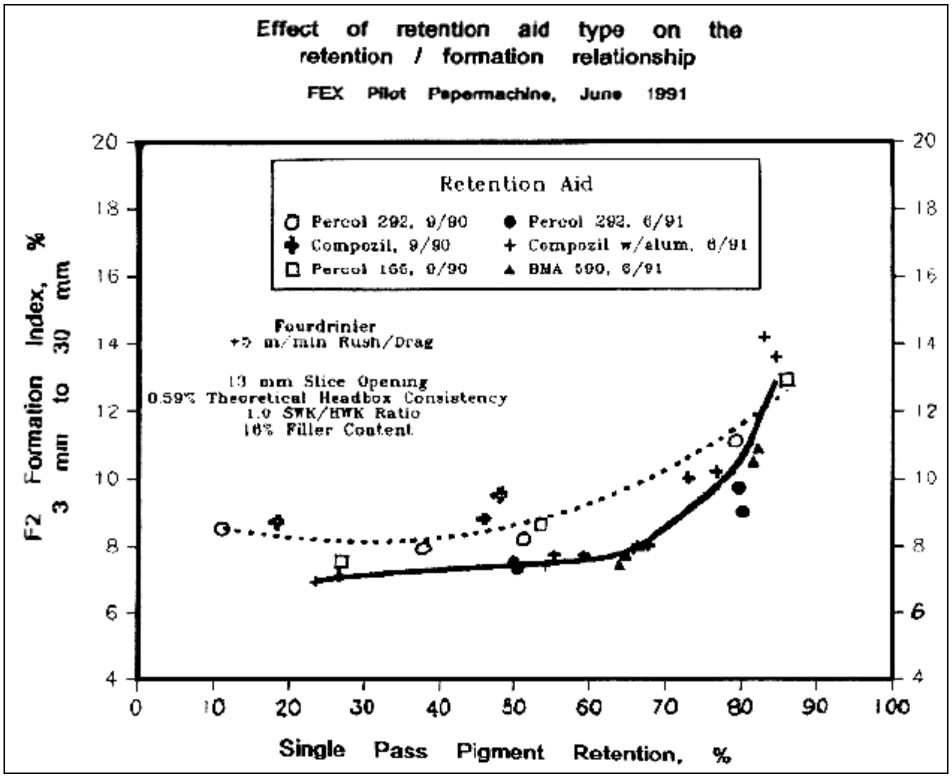

Figure 6. Unpublished data showing the (non)effect of retention aid type on formation. (Source: Wayne Robbins, Institute of Paper Science and Technology.)

Since there is evidence that retention aid type plays a small role, if any, in the kinetics of flocculation, other retention aid parameters may have a greater affect on flocculation.

The Effect of Chemical Dosage on Floc Formation

There are very few sources in the literature that have investigated the effect of chemical dosage on the flocculation of a pulp slurry. One study by Lindström et al. (1977) studied the effects of varying C-PAM dosage on the flocculation level. Flocculation level was measured using a turbidity technique. Results showed that flocculation is affected by polymer dosage and that the relationship may not be a simple one. One interesting trend in the data was that the time for initial quick flocculation was the same at all dosages.

Since not much kinetic flocculation data exists for chemical dosage in the pulp and paper literature, it may be helpful to examine other literature sources outside the industry to gain some knowledge about other kinetic models. One such area is the biological reactor literature which concerns itself with the kinetics of processes such as in biological fluidized-bed reactors, and activated sludge reactors. Even though the processes are vastly different, there are some conceptual similarities between the two that might allow the use of biological reactor kinetics models as a *starting point* for finding the important chemical variables that affect the kinetics of the flocculation process.

Work by Shahalam et al. (1996) looked at the kinetics of an aerobic fluidized-bed biofilm process. Shahalam's work focused on using fluidized-beds in the processing of sewage. In fluidized-beds, particles are suspended in the flow of a gas or liquid to take advantage of the vast surface area for purposes of the reaction. Sometimes the particles are used as a substrate, and in other variations the particles are used for catalytic purposes. Sand was used as the fluidized particle in Shahalam's work. In this type of fluidized-bed, a biofilm is formed on the sand particles. The biofilm is then sheared off the sand particles via hydraulic forces and collected as sludge. Shahalam concluded that, among other variables, influent substrate concentration, the quantity and size of the media used, the ambient temperature, and the velocity of fluidization produced the biggest effects on biofilm thickness. To apply this to the flocculation situation of this project, biofilm thickness could be likened to the extent of flocculation (e.g. number and size of flocs). If Shahalam's work is used as a **general starting point** to explain the important chemical variables for flocculation, it becomes apparent that chemical concentration (i.e. dosage), and temperature are going to be the significant players. Other work on activated sludge reactors (Jacobsen and Arvin, 1996) produced results similar to that of Shahalam's.

MECHANICAL ENERGY EFFECTS ON FLOC FORMATION

So far, with respect to their effects on flocculation, only the physical properties of the fibers and the chemical properties of the fibers and aqueous environment in the wet end have been discussed. The physical properties of the aqueous environment or the hydrodynamic characteristics also play a major role in affecting fiber flocculation. Most of the literature reviewed states that the colloidal forces present are secondary in importance with respect to the hydrodynamic forces. Most authors agree that fiber flocculation is mechanical in nature (Mason, 1954; Kerekes et al. 1985), and that colloidal forces play a small role. As a result of this belief, there is far more literature available on the topic of mechanical energy effects on fiber flocculation than on chemical effects.

Fiber flocculation in a turbulent suspension has been termed a *dynamic equilibrium* (Mason, 1954). Because of the effects of turbulence, fibers will collide and form flocs, but these same flocs will disperse just as fast as they are formed. At a specific level of turbulence, and a specific point in the suspension, there is a flocculation equilibrium where a definite size distribution of flocs exists. According to Parker (1972), the local floc size distribution is independent of the flow regime existing further upstream and is only dependent on the local turbulence level. This fact is taken advantage of in headbox design where higher turbulence is used to attain a smaller mean floc size.

Many of the kinetic studies that have been done on flocculation have modeled the process as a combination of a floc dispersion rate and a floc aggregation rate. One such study was completed by Steen (1990) in which he developed a fiber flocculation concept (FFC). Flocculation in turbulence is a result of the interaction between fibers and the "turbulent energy cascade" that Steen describes. Important to the flocculation of fibers in turbulence is the *intensity* of the turbulent eddies and the *scale* of the eddies. Floc rupture was described as a process whereby the larger flocs in the system were broken up by the stretching of high energy turbulent eddies of the same length scale as the flocs. On a much smaller scale, dissipative eddies that reside between the large eddies serve to erode the outer surfaces of the flocs making rupture by the large scale eddy stretching more probable. Steen suggested that floc aggregation occurs as a result of small scale flocs being transported by large scale eddies. Inside these large eddies small flocs can collide and create larger ones. Since the FFC predicts that large flocs will tend to rupture, and the small flocs will tend to aggregate, at a constant turbulence level, an equilibrium floc scale will be created. This is similar to what Mason observed (1954); changing the turbulence level will change the equilibrium floc scale. Figure 7 is a graphic representation of this occurring. As fibers are passed through an obstruction, they are subjected to a certain level of turbulence. This turbulence decays as the distance from the obstruction increases. At a point downstream of the obstruction, a different level of turbulence exists, therefore resulting in a changed equilibrium floc scale.

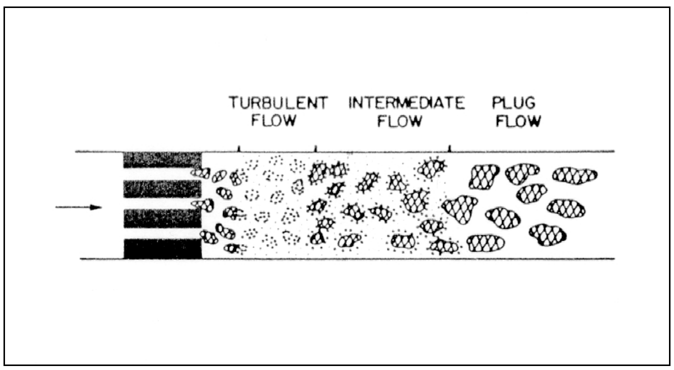

Figure 7. The effect of decaying turbulence on flocculation. (Source: Kerekes, R., R. Soszynski, and P. Tam Doo. "The Flocculation of Pulp Fibers." In *The Proceedings of the Papermaking Raw Materials Conference* edited by Punton, 1985.)

THESIS OBJECTIVES

The objective of this problem is to gain a better understanding of how mechanical energy input and retention chemical dosage affect the flocculation characteristics of flowing wood pulp suspensions. This will be accomplished by conducting experiments where measurements of floc formation are collected while mechanical energy and chemical dosage are varied. This is a plausible first step in a larger research program that is interested in how to improve formation to achieve better end-use properties.

EXPERIMENTAL METHODS AND MATERIALS

HYPOTHESIS

The influence of mechanical energy on fiber floc formation (or dissociation) is diminished by chemical retention aid dosage.

VARIABLES AND CONDITIONS

Only two independent variables are considered in this problem. This will allow the collection of data that is not confounded. Of interest in this problem are the variables mechanical energy input and chemical dosage. All of the other variables including fiber properties, retention aid type, pH, and temperature will be held constant.

Fiber Parameters and Preparation

As was apparent in the section about fiber effects, there are several important fiber properties that are important to flocculation. These properties have been held constant during this project. Because the fibers used must perform as intended with the retention aids, wood fiber was chosen to use in these experiments.

The fiber selected for this project was a softwood market pulp blend that was donated by Weyerhaeuser Company's Grande Prairie mill in Alberta, Canada. The pulp is a 55%/45% blend of spruce and pine. Since the fiber was in market pulp form, hornification was a concern. During hornification, which occurs during drying, the fiber closes up and leaves many of the anionic sites crucial to retention aid performance closed. In order to free up the anionic sites again, the fiber was processed with a Valley beater at 2.5% consistency for 10 minutes. Consistency was achieved using deionized water. No additional weight was added to the beater's diaphragm. After beating, the fiber was collected using a 500 mesh screen and was dewatered down to approximately 15% consistency. This 15% consistency pulp was kept in a cooler held at 37 °F until it was used in the experiments. Aging was not a concern because the pulp was used within days of processing. A summary of pertinent fiber data can be found in Table I.

Table I. Pertinent Fiber Data

Pulp Composition	Spruce/Pine 55%/45%
FQA Length-Weighted Fiber Length	2.28 mm
% Fines Content (length-weighted)	0.78
Average fiber coarseness	13.9 mg/100 m
Freeness	400 CSF

Compounds such as extractives and lignin, which have a highly anionic nature, interfere with retention aid performance by neutralizing charges. For this project, it was important to have a bleached fiber because many of these extraneous compounds would have been removed in the bleaching process. The market pulp obtained was a bleached fiber.

As witnessed by Kerekes' crowding factor (equation 2), the most important fiber characteristic that affects flocculation is the fiber length. The beaten pulp used in this project had a length-weighted average fiber length of 2.28 mm.

The last variable that was held constant during the experiments is the stock consistency. To choose a consistency, the crowding factor equation was visited again. Papermaking is typically done in a range of crowding factors from 50 up to 120. Choosing a crowding factor locks in a consistency because the properties of the fiber are fixed. For this project, a crowding factor of 60 was chosen. This translates into a mass consistency of 0.32%--very typical for papermaking conditions.

<u>Retention Aid</u>

In an effort to decrease the complexity of the experiments, retention aid type will be held constant. Looking at past work should be helpful in deciding which retention aid to use in the experiments. Of the past work that was reviewed, one retention aid type was common among all of them: cationic polyacrylamide. This is not a coincidence. Cationic polyacrylamide (C-PAM) is a very common retention aid used in the papermaking industry. Because of its high molecular weight, and low charge density, C-PAM works via the bridging mechanism. The length of a typical C-PAM is 1 μm for every 10^6 molecular weight (Mills, 1999). Various C-PAM retention aids used by Lindström et al. (1977) had a molecular weight in the range of 0.7 to 12.0 x 10^6 molecular weight. Combining both values, we see that the length of a C-PAM molecule could range anywhere from 0.7 to 12 μm. C-PAM was used in past work by the author (Weseman, 1999). Because of past work with C-PAM and the commonality of C-PAM in the industry today, it has been chosen as the retention aid to use in this project. Eka Chemicals donated the C-PAM used in this project.

A parameter that is one of the variables in the experiments is retention aid dosage. In order to obtain meaningful results, the range this variable takes on must be broad and it must bracket typical dosages found in the industry today. Past work by Robbins (Figure 29) used a dosage range of 0.02% to 0.15% polymer on dried fiber. A value of 1 pound/ton (0.05%) was recommended by Eka Chemicals. The range used in this experiment was 0.05% to 0.1%. In this study retention aid dosages are referred to in lb/ton, so the dosage range is 1 lb/ton to 2 lb/ton (0.5 kg/t to 1 kg/t).

Mechanical Energy Input

In the previous discussion on mechanical energy, it is apparent that not only is mechanical energy *intensity* important to flocculation, but the mechanical energy *scale* is important too. Eddy scale depends on a number of parameters including the Reynolds number, the viscosity, and the geometry of the flow channel. The maximum size of eddies for a particular system is more dependent on the flow geometry, whereas the minimum size is more dependent on the Reynolds number and the viscosity of the fluid

(Park, 1999). Scale will not be an experimental variable and is not a focus of study in this experiment.

Mechanical energy input was varied by changing the volumetric flow rate inside the flow loop. Four different flow rates were used during the experiments. Table II outlines the Reynolds numbers associated with these flow rates.

Table II. Reynolds Number Summary

Flow Rate (LPM)	Reynolds Number (N_{Re})	Linear Velocity (m/s)
100	20488	0.87
133	27249	1.16
166	34009	1.45
200	40975	1.75

FLOCCULATION DETECTION EQUIPMENT

Remembering that the goal of the experiments is to study the effect of chemical dosage and mechanical energy input on the kinetics of flocculation, it becomes apparent that a detector must be chosen that will measure floc size versus time.

Several detection techniques and associated equipment were considered for this project. An acceptable detector should be able to distinguish between flocs and the water medium that is present. Floc detection equipment used for dry sheets, such as the beta radiographic method discussed earlier, would not be appropriate because they directly measure mass variations. In a sheet of paper, there is very good contrast because the test is carried out in air. The density of air is much lower than the density of cellulose, so the beta radiograph will pick up flocs in a sheet. In a water environment, the beta radiograph would not produce acceptable results because both water and cellulose have densities at or near 1.0 g/cm^3. For this same reason, a flash X-ray technique that was considered would not work as intended.

Another promising technique was first developed by Wågberg (1985). The detection principle is based on the backward scattering of laser light. The instrument directly measures the intensity of backward scattered laser light over a range of wavelengths. Because of the complexity and cost of the equipment, this detection method was considered, but not used in the current research.

The method of floc size detection that was chosen for this project employs an image analysis technique. Image analysis was chosen because of the availability of pertinent equipment at the Institute and because of promising results from other workers. With advances in computing power and technology, it is no longer cost-prohibitive to construct a powerful image analysis system with off-the-shelf components. The system constructed for this project was inspired by a similar system first described by Beghello et al. in 1996. Figure 8 displays the system used by Beghello and his co-workers.

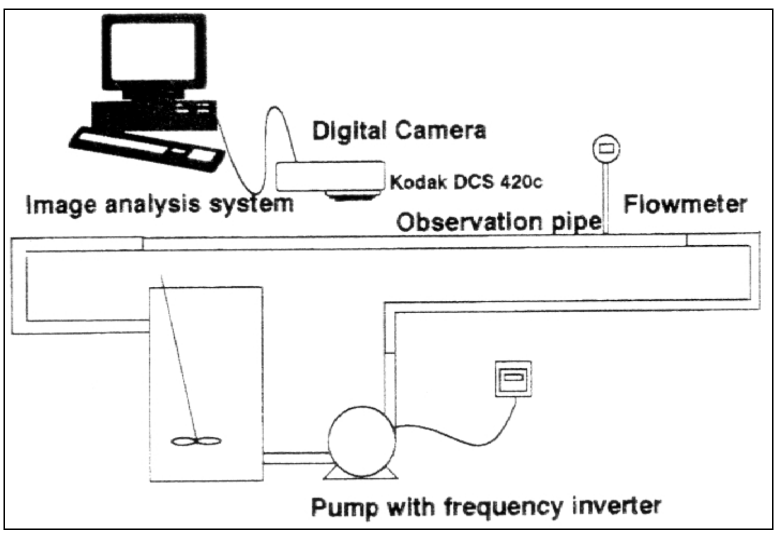

Figure 8. Floc size detection system. (Source: Beghello, M., and M. Toivakka, and D. Eklund. "A Device for Measuring Fiber floc Sizes in Highly Turbulent Fiber Suspensions." Nordic Pulp and Paper Research Journal 11, no. 4 (December 1996): 249-253.)

The general idea of Beghello's equipment was used as a framework for the construction of the flow loop and imaging channel at IPST. An existing flow loop at IPST already had most of the essential equipment, so it was only necessary to construct the specialized flow channel.

Flow Loop

The flow loop used in this project existed before the project began and it contained most of the needed equipment. Comprising the flow loop are a 100 gallon stock tank, a large mixer, a 100 GPM centrifugal pump, a magnetic flow meter, and two 50 gallon secondary tanks. The flow loop is constructed of 2” schedule 80 PVC pipe. In order to incorporate the current project, pipes and valves were added to branch off the existing loop. Flow was diverted to these new pipes and through the imaging channel. An image of the flow loop can be found in Figure 9 and a diagram in Figure 10.

Figure 9. Flow loop: stock tank, mixer, and centrifugal pump.

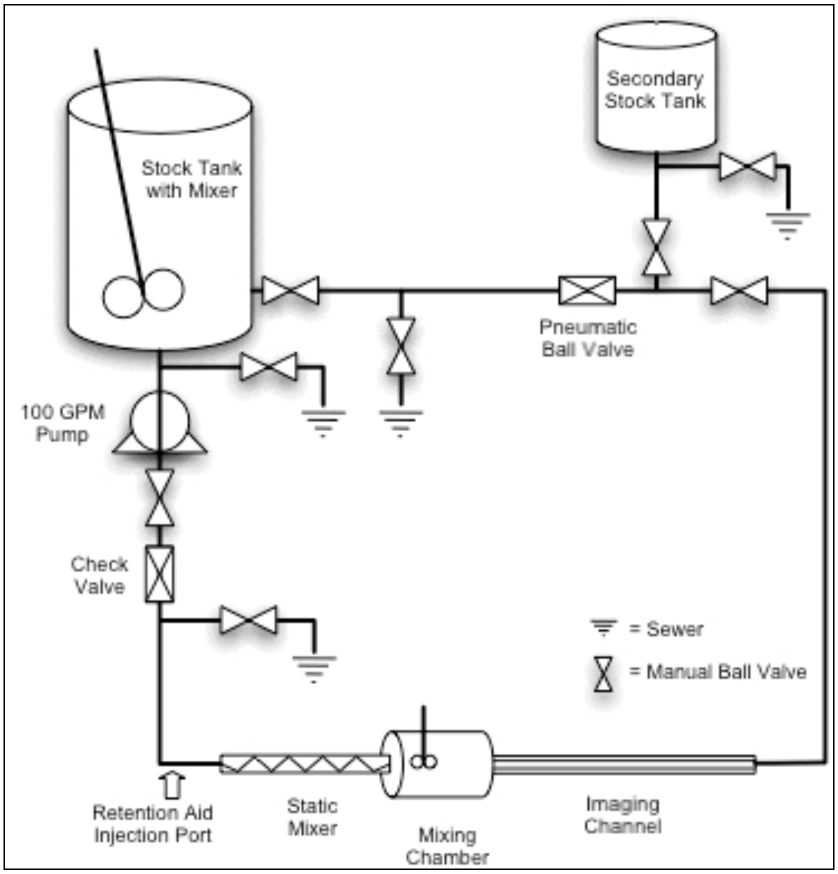

Figure 10. Flow loop diagram.

Controlling the centrifugal pump is a Baldor power inverter that allows adjustment of the pump speed via frequency. This was the primary control for adjusting the turbulence level in the experiments. Flow was monitored using the magnetic flow meter and an ABB digital readout positioned next to the Baldor drive control.

Several additions were incorporated into the flow loop to accommodate retention aid injection. The most important addition was a pneumatically-actuated ball valve (Figure 11). This valve was strategically positioned so that when it was actuated, flow was diverted to one of the secondary stock tanks. Diverting the flow while injecting retention aid was necessary because retention aid concentration would change over time if the flow loop was allowed to function normally. The actuation switch for the valve was centrally placed near the pump and computer controls.

An injection port for retention aid was placed ahead of the imaging channel. The injection port incorporated a mini-check valve so pulp would not flow into the injection line. To facilitate an appropriate level of retention aid mixing, a static in-line mixer was added between the injection port and the imaging channel. A check valve was added to stop back flow once the pump was shut off (Figure 12). This valve was placed upstream of the retention aid injection port and assured that pulp which had been “contaminated” with retention aid did not flow backward and mix with the “clean” pulp.

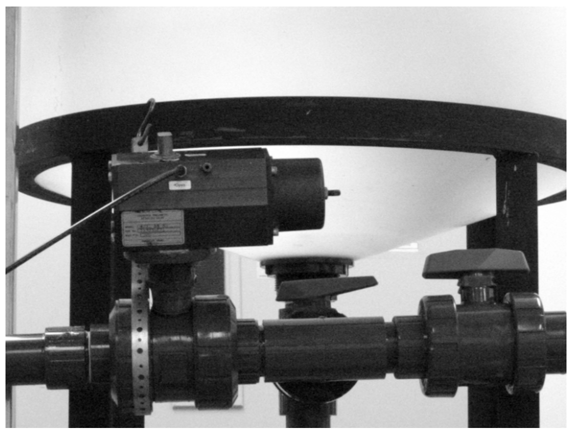

Figure 11. Pneumatically-actuated ball valve.

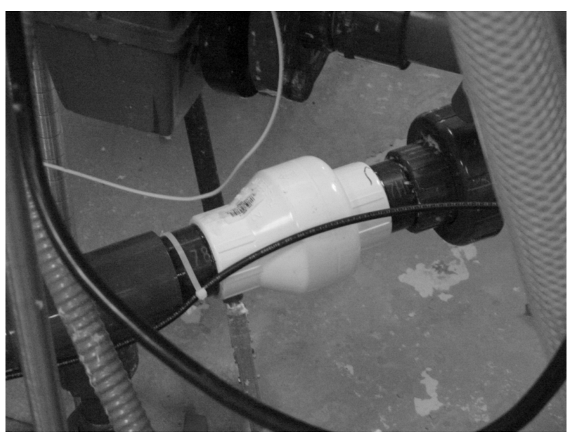

Figure 12. Check valve.

Imaging Channel

The purpose of the imaging channel is to facilitate the acquisition of satisfactory images of fiber flocs that can be eventually analyzed for floc size and floc size distribution.

As mentioned earlier, a channel design based on previous work by Beghello et al. was used to construct the current channel (Figure 13). Inside dimensions of the channel are 12.7 mm high by 150 mm wide. The majority of the channel was constructed using 0.5" thick plexiglass.

The pulp flow had to transition from a circular cross-sectional pipe to a rectangular cross-sectional pipe (the imaging channel). The first attempt at this transition (Figure 14) produced very undesirable flow patterns which consisted of large eddies forming in the imaging channel. The eddies were caused by the very abrupt transition from circular to rectangular flow.

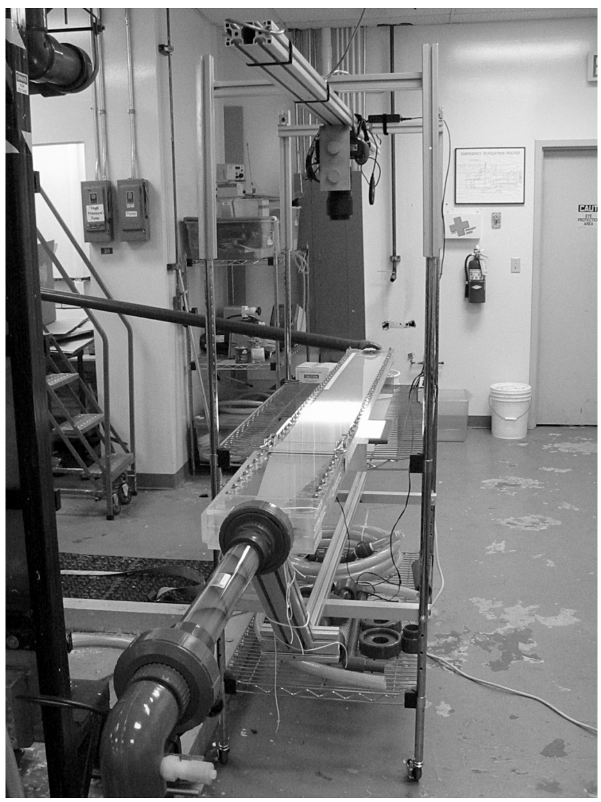

Figure 13. Initial imaging channel and support structure.

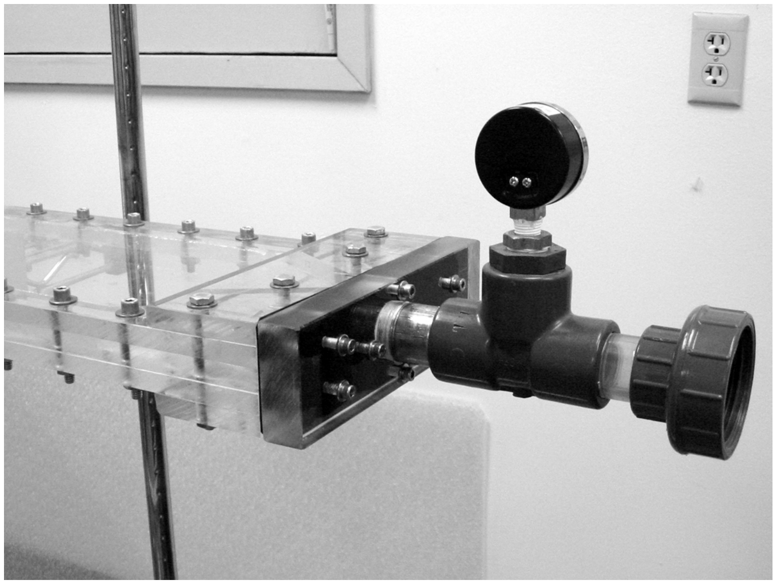

Figure 14. Original flow transition adapter.

Another transitional flow piece for the channel inlet was constructed to alleviate the eddies. In order to accomplish this, a diverging inlet angle of 6° was used. A closeup of the diverging transitional flow piece can be found in Figure 15.

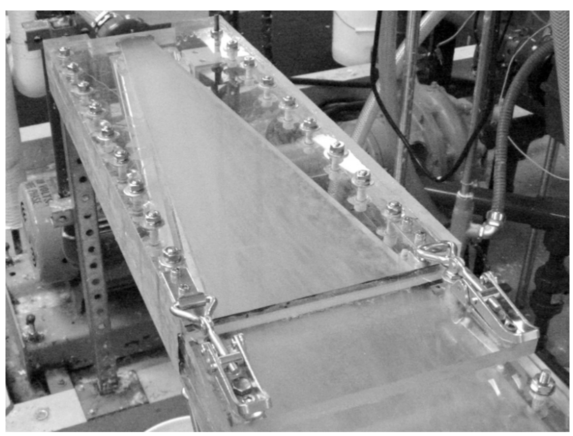

Figure 15. Transitional flow piece.

For the majority of the studies, a different inlet scheme was used. In order to capture floc formation in just the constant width section of the channel (as opposed to the diverging section) a flanged mixing chamber was employed. Instead of transitioning a 2″ pipe to a 6″ wide channel, a 12″ length of 7″ diameter acrylic pipe was used as a mixing chamber prior to the imaging channel. This mixing chamber is displayed in Figure 16. A flange connection allowed the chamber exit to be exactly the inside dimensions of the imaging channel. Since the chamber was constructed of optically clear acrylic, it was possible to evaluate the mixing efficiency of the chamber visually.

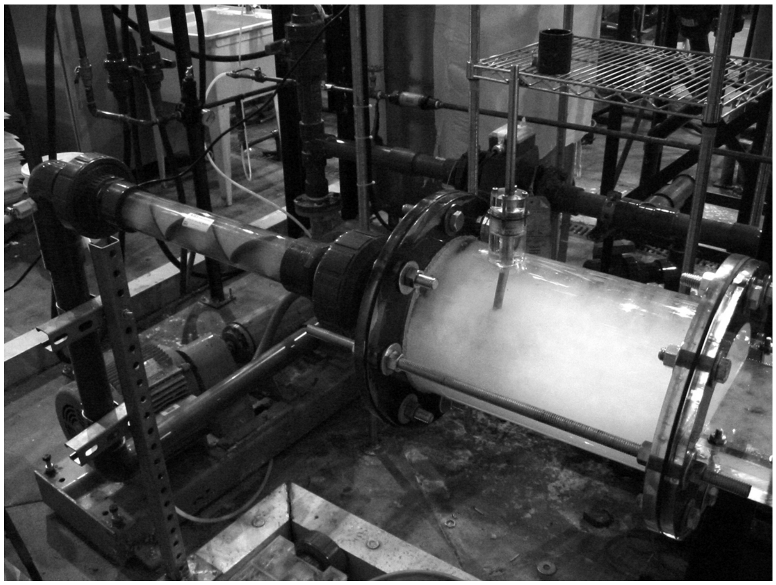

Figure 16. Inline static mixer and mixing chamber.

Inside the mixing chamber, the flow was tangential and rotating. Transitioning this flow into the 150 mm wide imaging channel slot created some random flow patterns that were undesirable. Initially, a high torque air mixer was attached to the mixing chamber to agitate the pulp slurry. The mixing shaft was attached via an adapted pump shaft seal enclosure that allowed mixing inside the chamber without leakage. Upon inspection of the imaging channel flow patterns while using the air mixer, it was determined that running the mixer was detrimental to the flow evenness. Operating without a mixer shaft inside the chamber produced similar, undesirable results. It was discovered that by just placing the mixing shaft (with the impeller) inside the chamber with no rotation, most of the undesirable flow patterns disappeared. This worked best if the impeller was aligned with the inlet pipe to the mixing chamber. All of the experiments were run in this manner.

Retention Aid Injection

Retention aid injection was performed by a high flow rate syringe pump from Harvard Apparatus (Figure 17). The syringes were attached to the injection port using 1/4″ ID flexible polyethylene hose and hose clamps. 140 mL Sherwood Monoject syringes were used. Table III summarizes the syringe pump specifications.

Figure 17. Syringe pump and injection port.

Table III. Pertinent Syringe Pump Technical Specifications

Syringe Pump Make:	Harvard Apparatus
Syringe Pump Model:	PHD 20/2000 Hi-force
Maximum pusher travel rate:	190.676 mm/min.
Maximum pusher linear force:	66 lb.
Maximum pressure achievable with 140 mL syringe:	36.8 psi
Maximum flow rate achievable with 140 mL syringe:	220.83 mL/min.

Adsorption time for the cationic polyacrylamide retention aid was a concern. Care was taken to make sure enough time between the injection point and the imaging channel elapsed so that polymer adsorption could occur. Past work by Ödberg (1995) showed that cationic polyacrylamide adsorption onto cellulose fibers in turbulent conditions occurred in less than 1 second. Earlier, Van de Ven (1989) conducted similar research and found that polymer adsorption onto cellulose fibers in turbulent flow occurred in a fraction of a second. Past work has shown that polymer adsorption is almost instantaneous. The experimental setup of this study contained both a 1.913" ID static mixer that was 19" long and a 7" ID mixing chamber that was 12" long between the polymer injection point and the imaging channel. Accounting for additional length with fittings, the total volume of pipe from the injection point to the imaging channel was approximately 8604 cm^3. At the highest flow rate used in the study (200 L/min), an elapsed time of 2.58 seconds occurs from the point of injection to the beginning of the imaging channel. At the lowest flow rate (100 L/min) this elapsed time increases to 5.16 seconds.

Image Acquisition System

In order to accurately measure a moving subject, it is necessary to "freeze" the movement as much as possible. The ability of a camera to "freeze" motion is a function of the camera's shutter speed. Shutter speed is a misnomer as it is not a measure of speed, but a measure of time. It is the time the camera takes to open and close its light shutter. For example, a subject moving at 2 m/s will have traveled 20 mm in the time it takes a camera with a shutter speed of 1/100th of a second to acquire an image. The resulting image would make the subject appear to be 20 mm longer than it actually is. Of course the relative magnitude of this error depends on the length scale of the subject and is inversely proportional to it. Relative to the length scale of a typical softwood fiber (say 3 mm), the extra 20 mm results in an error of more than 600%. However, if the length scale is of a 10' car (traveling at 4.5 mph), the error is only 0.66%. This example begins to show how important the choices in image acquisition equipment are and the importance of shutter speed to the accuracy of measurements.

Another important aspect when considering imaging equipment is acquiring speed or frame rate, as it is more commonly referred to. Frame rate is different from shutter speed in that it is how many images can be acquired over a specified amount of time. The typical unit for frame rate is frames per second (fps). Choosing a suitable frame rate depends on what properties of the subject are of interest. For example, if the imaging equipment will be following the subject over a trajectory, it is important to have a high acquiring speed as this will ensure that large portions of the subject's movement will not go unrecorded. To put this into perspective, most commercial video cameras operate in the 30 fps range, whereas video cameras used in ballistics testing can achieve frame rates exceeding 10,000 fps.

As with any measurement, resolution is important. If a subject has a length scale of microns, but the instrument used to measure it has a resolution of only 1 mm, the accuracy of that measurement is going to be low. The same holds true for imaging equipment. Digital images are made up of several million discrete elements (pixels). The size of each pixel is the resolution of the image and is usually measured in pixels per inch (ppi); when referring to printed images the measurement is dots per inch (dpi). It is important to consider the desired accuracy for measuring the length of an object, as this will help determine a suitable resolution for the imaging equipment. For example, if a measurement resolution of 0.1 mm is desired, a suitable image resolution may be 300 ppi. At 300 ppi, each pixel has a length of 0.085 mm.

Another crucial consideration for imaging systems is lighting. Without light illuminating the subject, there are no photons for the camera to record. Subject illumination can occur via reflected light, transmitted light, or a combination of both. Regardless of which lighting method is used, when using images for measurement, evenness and consistency of the lighting over the imaging area is paramount. Much better results can be achieved if even lighting is used during image acquisition than if software-based techniques are used to correct for the unevenness later. Another reason lighting is important is that higher shutter speeds require elevated light intensities. Holding light intensity constant while increasing shutter speed (decreasing the time) will result in progressively darker images because there is less time to allow light past the shutter. When choosing a lighting solution, it is important to take into account the shutter speed at which the system will be operating. As discussed earlier, shutter speed will depend heavily on the velocity and length scale of the subject of interest.

The image analysis considerations just discussed were used to select an appropriate image acquisition system for the current project. The subject of interest in the experiments is a moving pulp slurry viewed through a plexiglass imaging channel. During the experiments the pulp slurry experiences a maximum flowrate of 200 L/min which translates into a linear velocity of approximately 1.75 m/s. Table IV summarizes the absolute measurement error associated with several shutter speeds for this situation.

Table IV. Measurement Error Attributed To Shutter Speed

Shutter Speed (s)	Absolute Error (mm)
1/100	17.50
1/1000	1.75
1/5000	0.35
1/10,000	0.17
1/13,000	0.13
1/16,000	0.11
1/22,000	0.08

This project was not concerned with the movement of flocs—just the size of them. As a result, high frame rates were not a necessary capability of the chosen imaging system. Frame rates even as high as a standard commercial video camera (30 fps) were not necessary. The main use of frame rates in the chosen imaging system was to provide an adequate number of frames over a small amount of time to achieve a suitable statistical population.

Resolution, like shutter speed, was an important consideration in this project. Accuracy of 0.1 mm was desired so image resolutions greater than 254 ppi were necessary. Image magnification was taken into account because it increases the resolution of the camera by changing the area over which the fixed number of pixels are laid.

Based on the three considerations of shutter speed, frame rate, and resolution (and price), the Nikon D1H professional digital SLR camera was chosen as the image acquisition tool for this project. The D1H offered a balance of high shutter speed, acceptable frame rate and medium resolution at a price point that other cameras could not match. Table V displays the pertinent technical specifications of the D1H. Attached to the D1H was a Nikkor 70-180 mm AF micro lens with an aperture of f/4.5-32. This lens was developed for photomicrography purposes. The camera and lens can be seen in Figures 18 and 19. The camera was attached to the imaging channel support structure as shown in Figure 20.

Table V. Pertinent Nikon D1H Technical Specifications

Make of camera:	Nikon
Model of camera:	D1H
Type of Camera:	Lens-interchangeable digital SLR
Lens:	Nikkor 70-180 mm AF micro; f/4.5-32
Resolution:	~300 ppi (depends on magnification)
ISO Sensitivity:	1600
Maximum Frame Rate:	5 fps (up to 40 frames)
Computer Interface:	IEEE 1394 (Firewire)
Shutter speed:	30 to 1/16000th second

Figure 18. Nikon D1H digital SLR camera.

Figure 19. Nikkor 70-180 mm AF micro lens.

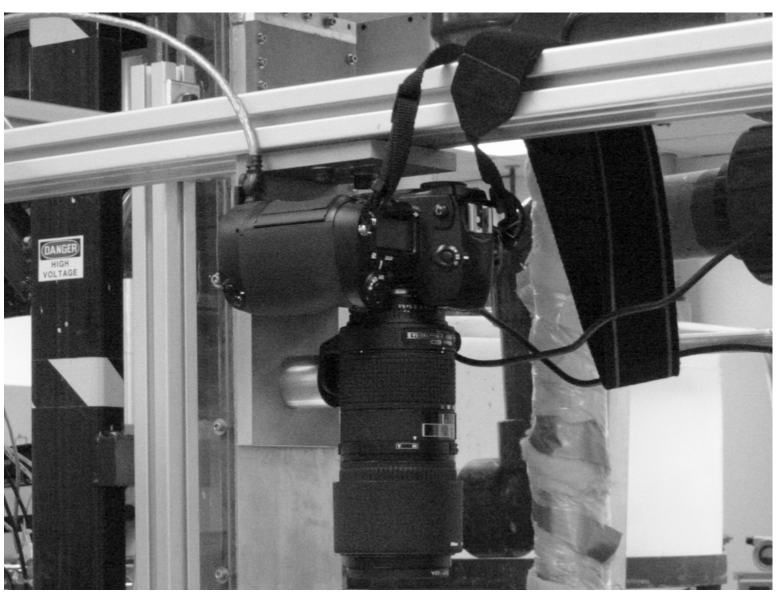

Figure 20. Camera attachment to support structure.

The most important aspects of the lighting in this project were the evenness over the area of the image and the intensity. As discussed earlier, lighting evenness is important when measuring features of images. It is necessary to have the same background intensity to compare different areas of the images. In addition, since the experiments were carried out at elevated shutter speeds, a high enough light intensity was necessary.

Several lighting sources were tested for this project. Initially, it was believed that a high-power halogen lamp would perform adequately. The 500 W halogen light delivered more than enough intensity for the shutter speed, but the evenness was very poor. Figure 21 shows the typical lighting the halogen light delivered. To help alleviate the unevenness, sheets of plastic were placed between the lamp and the imaging channel to diffuse the light. This did not work satisfactorily. The light source that was eventually chosen was a Stocker-Yale Slimline fluorescent light panel (much like the ones used to view x-ray photographs and photographic negatives. Figure 22 shows the evenness achieved with the fluorescent light panel and Table VI summarizes the fluorescent light specifications.

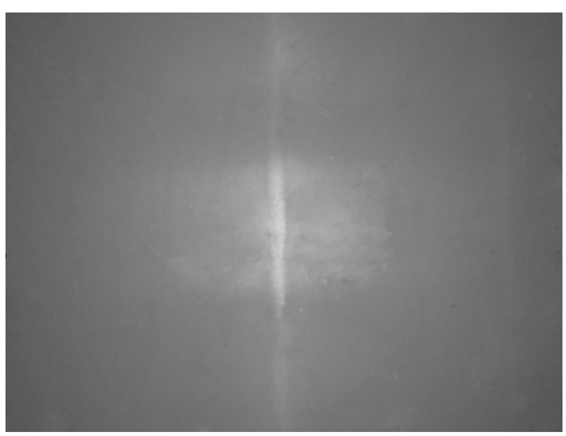

Figure 21. Halogen backlight unevenness.

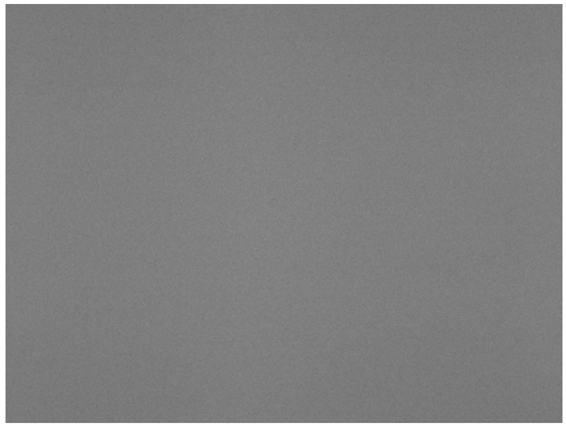

Figure 22. Fluorescent light has better evenness.

Table VI. Pertinent Light Source Technical Specifications

Make of light:	Stocker-Yale
Model of light:	Slimline CL5000M
Light type:	Fluorescent light panel
Input power:	10 Watts
Input voltage:	100-240 VAC
Operating frequency:	90 kHz
Light output:	1400 cd/m2 (± 300)

Image acquisition was carried out by an Apple PowerBook G3 laptop computer which controlled every aspect of the camera. While the camera does achieve 5 fps, after approximately 8 seconds when its 40 image buffer fills, the D1H must transfer all collected images to the computer. The computer, D1H, and a 120 GB external hard drive communicated via the Firewire interface. Firewire, which has a bandwith more than 20 times that of standard USB, allowed fast transfer of the images for a particular experiment. Figure 23 displays the computer setup used in the project.

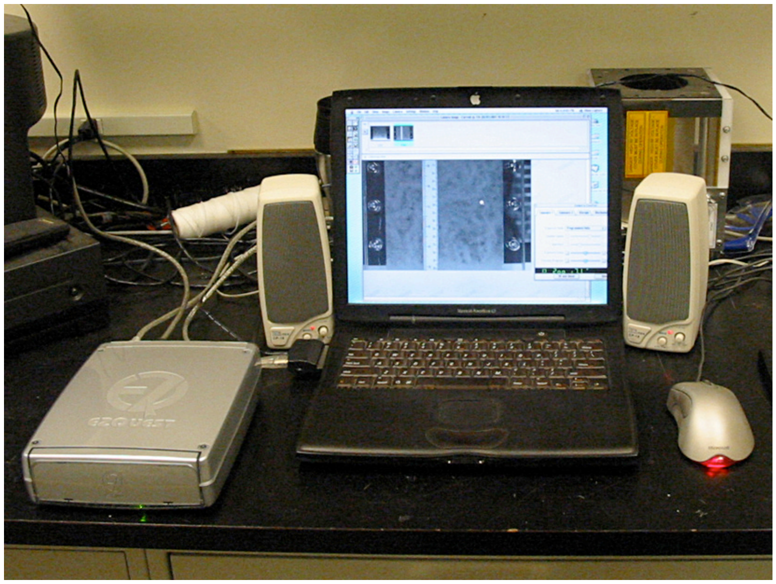

Figure 23. Image acquisition computer

The software used for image acquisition was Nikon Capture 2.0. Capture's function was twofold. First, Capture controlled every aspect of the D1H remotely. This meant that once the camera was communicating with the computer, the computer (on the other side of the lab) could control everything without physical interaction with the camera. Second, Capture coordinated the acquiring of thousands of images with batch features that allowed detailed naming conventions of the images. The naming conventions helped with organizing the images and distinguishing between experimental runs.

It was important to consider image format for this experiment. There are many image formats available for use that offer differing levels of compression, quality, and portability. The images in this experiment were being scientifically analyzed so quality had to remain high during processing. Deciding which format to use was simple as the D1H produced images in only three formats: JPEG (Joint Photographers Expert Group), TIFF (Tagged Image File Format), and RAW. The JPEG format was easy to eliminate because it does not use lossless compression, thereby making quality degradation of the images a factor. The D1H designated the TIFF and RAW formats as the high quality formats because of their ability to output uncompressed images. The TIFF format also offered two color spaces: YCbCr and RGB. The YCbCr color space describes the color of each pixel with two chrominance channels (CbCr) and one luminance channel (Y). The RGB color space utilizes three channels (red, green, and blue) to describe each pixel. The camera outputs both 8-bit YcbCr and 8-bit RGB images. This translates into 24 bit images because the 8 bit designation is for each channel. Portability of the image (the ability to open the image using several programs on different computing platforms) was important as well. After considering all of these parameters, the TIFF-RGB format was chosen as the format for images in this project. The RGB portion of the format was unimportant as the images were converted to grayscale upon post-processing.

Image Analysis System

Acquiring the images was the first step in a multi-step process. After acquiring the floc images it was necessary to analyze them to glean useful data from them. Since floc size was the important characteristic, a system was needed that could calibrate pixels based on known lengths and determine floc size by counting pixels in the floc image. The number of images being analyzed was in the thousands, so a system that could batch analyze would be a big time saver. Having to analyze each image one by one, would take much longer. Another consideration was the ability to enhance images based on certain criteria. Even the best lighting conditions could have small variations in intensity, and image enhancement could help to alleviate these variations. One last consideration was the compatibility with the image acquiring system. Although not necessary, it would be more efficient if all the image analysis could be done on the same computer.

Several image analysis solutions were tested based on the mentioned considerations. Many of the packages tested were capable of producing the desired data, but required a certain amount of programming to tailor the analysis to the project. Some programs were freeware (NIH Image) and some were commercial packages that did much more than what was needed (MATLAB). In the end, an off-the-shelf solution was chosen that was a combination of two software commercial products. These two products were Adobe Photoshop 7 and Reindeer Graphics Fovea Pro 3.

Photoshop is the standard in image processing on any computing platform, but it does not contain the scientific routines that were needed for this project. Fovea Pro is a set of third party Photoshop plugins that added the necessary scientific analysis routines that made floc measurement possible. Since thousands of images were being processed at once, automating the process was a key concern. Photoshop is a very mature program and comes with built-in automating and scripting tools that allowed the computer to analyze unattended.

Fovea Pro was made to be 100% compatible with Photoshop. As a result, all of the filters and routines included in Fovea Pro were accessible to the automation tools in Photoshop. Several of the routines found in Fovea Pro could also be found in Photoshop, but the advantage of using Fovea Pro is the greatly increased control over the details of the routines.

IMAGE ANALYSIS PROCEDURES

Three separate techniques were used to analyze the images collected in the research: direct size measurement of flocs using what is known as morphological operations to process the images, a formation number analysis using mean pixel brightness and standard deviation, and size measurement using a Fourier transform analysis of the images. Each method used the same images for the analysis.

Images are acquired in landscape format across the channel such that the flow of the pulp suspension is in the direction from the bottom of the image to the top of the image. Since flocculation is occurring even over the height of one image, each image is broken down further into regions of interest. The location of each region of interest relative to the entrance of the channel is carefully measured and recorded.

Figure 24 displays a typical untouched image directly from the camera. The size of the images are 2000 X 1312 and the magnification of the camera is adjusted to achieve a resolution of 0.1 mm/pixel (i.e. 130 mm over the 1312 pixels). Shutter speed is set at the camera's maximum 1/16000th second to freeze the motion of the flocs as much as possible and an aperture of f4.5 is used.

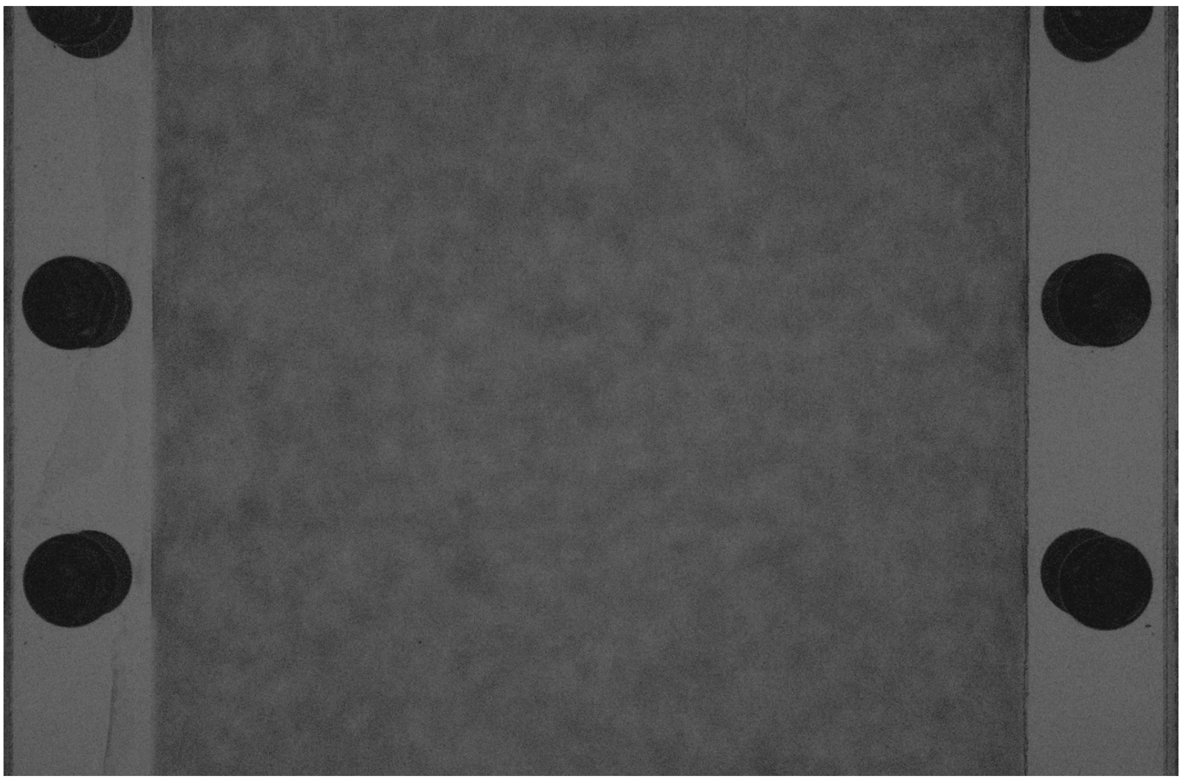

Figure 24. Untouched raw image of flowing pulp suspension.

Morphological Operations

Photoshop and Fovea Pro working together can enhance and adjust images so that useful data can be gathered on images such as Figure 24. The first step is to crop the image so that uninteresting features are discarded (Figure 25a). The next page displays several images which outline the image analysis processing for this project.

Since color is not necessary in this processing, the image is converted to grayscale which describes each pixel with a brightness value from 0 to 255 (black is 0). The next step is to adjust the contrast. At first glance it appears that this image would not yield useful data, due to its poor contrast. Adjusting the contrast is a process that does change the pixel values, but it does not change the *relative* values of the pixels. The AutoLevel Contrast routine divides the image up into a 9x9 grid of rectangles and forms the histogram of each in order to find the brightest and darkest values in each one. The result is two lists of 81 points whose X, Y, and Brightness values are tabulated. With these values, two third order polynomials can be constructed that express brightness as a power function of location. Each pixel is then scaled linearly between the limits that are calculated at each location. Figure 25b displays the appearance of the image after running the AutoLevel Contrast routine. Darker regions are where light is transmitted less (a floc).

The next step is to segment the image into the features of interest (the flocs). This is done via binary thresholding. Thresholding is a process whereby a brightness level (or range) is chosen and every pixel with a value lower than the threshold value is considered part of a feature, and every pixel with a value higher than the threshold value is considered part of the background. This process can become quite subjective as the researcher often adjusts the threshold value and watches the image in real time to see which value gives the "best" fit. In an effort to alleviate the subjectiveness, the Auto Bi-Level Threshold routine in Fovea Pro was used. This Auto Bi-Level Threshold routine has a feature that chooses a default threshold value that is unique for each image.

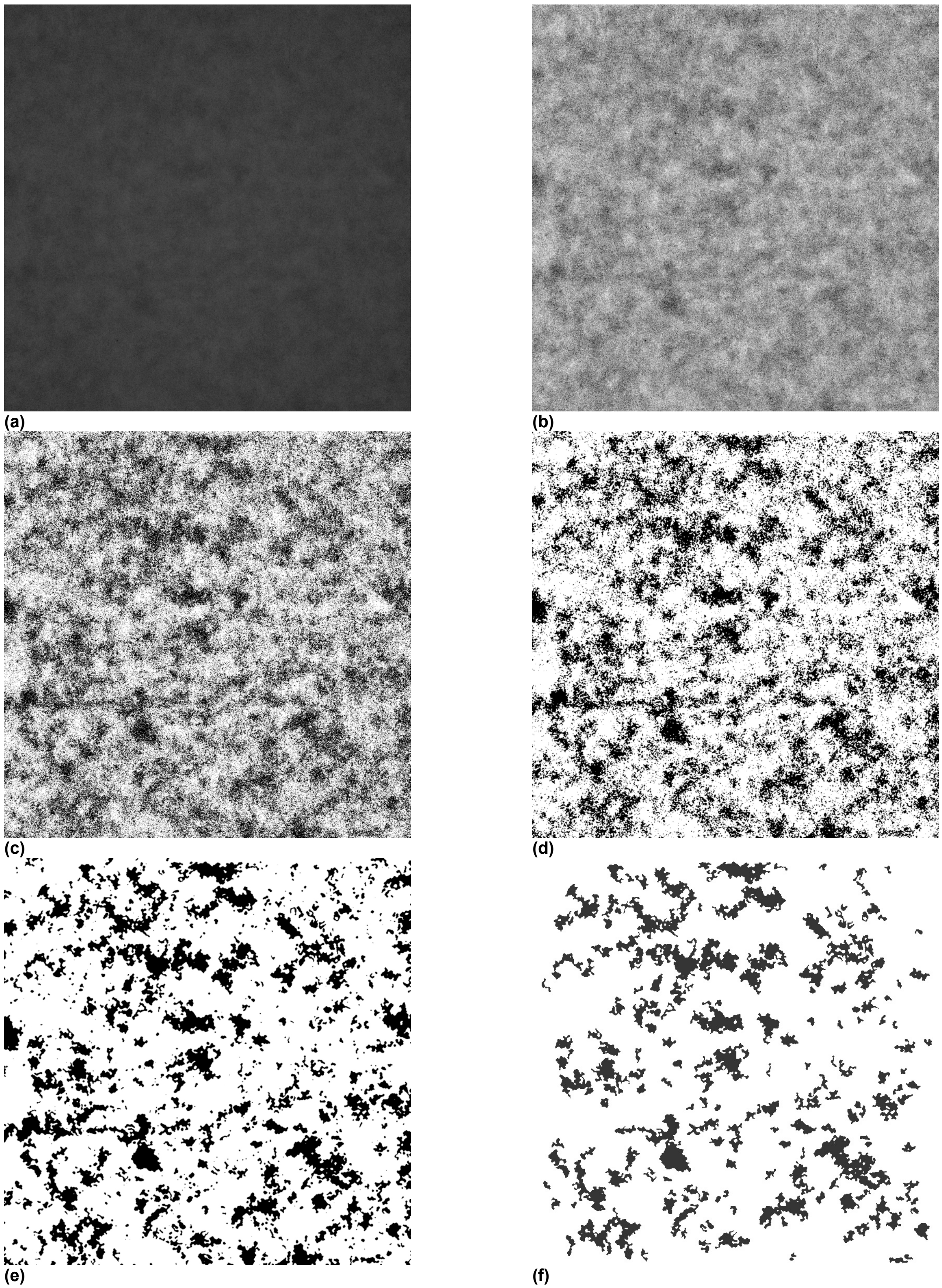

Figure 25. Examples of image analysis routine: (a) cropped raw image, (b) result of AutoLevel Contrast routine, (c) result of Auto Bi-level thresholding, (d) result of first open iteration, (e) result of the open iterations, (f) result of removing edge features and anything smaller than 0.785 mm^2 in area.

The value is chosen independently of user input, and is based on the point at which a statistical t-test of the brightness values associated with each portion of the segmented image gives the highest probability of significant difference. Figure 25c displays what the image looks like after the thresholding routine.

After thresholding, the image still contains a good deal of extraneous noise which will be necessary to remove to define the individual flocs. The method used to remove this noise is called *morphological operations*. Entire books have been written which describe morphological operations, so a full discussion about the topic will not be conducted here. What will be described are the exact operations used on the images in this project.

According to Russ (2002), morphological "…operations can be described simply in terms of adding or removing pixels from the binary image according to certain rules, which depend on the pattern of neighboring pixels." The operations are referred to as erosion (removing pixels) and dilation (adding pixels). There are also operations consisting of sets of erosions and dilations. An "opening" is an erosion followed by a dilation. A "closing" is a dilation followed by an erosion. Each opening and closing has a specified depth as well. A depth of three indicates an opening that consists of three erosions followed by three dilations. The rules these operations are guided by are based on the status of the neighboring pixels. Each pixel has eight neighbors. In the case of erosion, a pixel is turned off (becomes a background pixel) if enough of its neighbors are background pixels. In the case of dilation, a pixel is turned on (becomes part of a feature) if enough of its neighbors are feature pixels.

Since the objective in this analysis is to remove noise (which consists of many isolated pixels) and reveal individual flocs, then the appropriate operation is an opening. An opening will initially remove any isolated pixels while at the same time removing some pixels from valid flocs. In the second part of the opening, the dilation will add back pixels to the valid flocs that were turned off by the erosion. No pixels will be added to the removed pixels because they are not there anymore. The open routine is set at a coefficient of 3 (three or more neighbors have to be of the opposite color for the central pixel to change) and a depth of 1 (only one erosion followed by one dilation will be performed). This "3-1" open is one iteration of the 20 iteration open routine that was performed on the images in this analysis. Figure 25e displays what the image looks like after the 10^{th} iteration.

Inspection of figure 25e reveals issues about the image analysis technique that needed to be addressed. First, it is apparent that flocs lying on the edge of the image would be counted incorrectly because a portion of those flocs lie outside of the image and are not visible. This issue was resolved by telling Fovea Pro to remove all features touching any edge of the image. Figure 25f displays the effect of removing the edge features. Removing the edge features is necessary to achieve accurate measurement of particle size and distribution.

Figure 25f also brings to light the necessity of defining what a floc was in this study. It became apparent during the initial attempts to optimize the image analysis routines that the software was including very small features in the analysis. The small features were single, stray pixels and slightly larger features that were not meaningful. A single pixel at the magnification used had a side length of 0.1 mm and an area of 0.01 mm^2. Stray pixels most definitely do not represent a fiber or meaningful feature in the image. To make the software more accurate in measuring flocs sizes, it was necessary to apply some type of filter that would remove the smaller features.

Utilizing a filter required defining what a floc was with respect to size. Past work in the literature has been varied in what has been defined as a floc. In work by Beghello (1997), an image analysis technique was used to measure the floc size of a turbulent flowing fiber suspension through a horizontal imaging channel much like the one employed in the current study. The fiber used in the study was from a commercial bleached sulfate softwood pulp. After beating, the pulp was separated into three fiber fractions: one with an arithmetic mean fiber length of 0.40 mm, and two fractions with length-weighted average fiber lengths of 1.33 mm and 1.51 mm (all three were measured by a Kajaani FS-200 analyzer). Beghello's image analysis technique was based on previously published work by Norman and Wahren (1972). Although the method used a fast Fourier transform (FFT) analysis instead of morphological operations to measure floc size, a cutoff point for floc size inclusion was used. To be counted, a floc needed to be 1 mm or larger.

Steen (1990) also used an FFT technique to measure floc size of a turbulent flowing fiber suspension. Both hardwood and softwood bleached kraft fibers were used in the study. Since only the graphical fiber length distributions were given, arithmetic mean fiber lengths were estimated to be approximately 0.8 mm for the hardwood species, and 2.1 mm for the softwood species. The FFT technique that Steen used was similar to the technique employed by Beghello, but a cutoff point of 0.4 mm (as opposed to 1 mm) was chosen.

In yet another FFT technique, Wågberg and Eriksson (2000) used a flow loop and imaging channel to measure floc size in turbulent conditions. Three pulps were used in that study: an unbleached thermomechanical pulp, an elemental chlorine free bleached chemical softwood pulp, and an unbleached chemical softwood pulp. No length data was given for the pulp used. For purposes of that analysis it was determined that flocs smaller than 0.25 mm were not meaningful. Past work has shown that size cutoffs are important, but are unique to the specific study. The size cutoff should reflect and serve the objectives of the research.

When referring to floc sizes in this study, the equivalent floc diameter was used. Length of the floc (the distance between the two furthest points on the floc) was measured, but determined to provide misleading results. A feature (floc) that was classified, for example, as 5 mm in length could conceivably be a 5 mm long row of pixels. Using length to classify flocs may have resulted in single fibers being counted as flocs and this was not acceptable. For a more realistic measure of floc size, the equivalent floc diameter was used. The equivalent floc diameter is the diameter of a circle whose area is the same as the floc in question. Using equivalent floc diameter made the counting of single fibers much less likely and kept the classification of flocs related to the area of flocs (i.e. a variable used elsewhere in the study).

To determine a floc size cutoff, we start with the FQA length-weighted average fiber length of the pulp used in the study. That value is 2.28 mm. Since the resolution of the imaging equipment was 0.1 mm, for the purposes of this exercise the fiber length is 2.3 mm. In an acquired image a straight fiber will be a row of single pixels. For the case of this pulp, it is a row of 23 pixels. Each pixel has an area of 0.01 mm^2 so a complete fiber will have a total area of 0.23 mm^2. As said before, a single fiber does not represent a floc. It can also be argued that two fibers do not make a floc as this, at its simplest form, is just two fibers crossing at one point. What can be considered a floc is three fibers in some type of network configuration (e.g. two fibers crossing one fiber, a triangular network with three contact points, etc.). Three fibers have a total of 0.69 mm^2 which translates to an equivalent diameter of 0.94 mm. Rounding up because of the resolution of the equipment, we see that for the situation of three fibers, an equivalent diameter of 1 mm should describe the lower end of possible floc sizes seen in the flowing suspension. A cutoff of 1 mm equivalent floc diameter was chosen for this study. This is less than the general rule put forth by Wrist (1961) that flocs are usually one to three fiber lengths in diameter, but what is important is that we are attempting to describe the lower end of a distribution, not what the mean floc size is. Using the filter resulted in all flocs smaller than 0.785 mm^2 not being counted. In addition to showing what happens when edge flocs are discarded, figure 25f also shows what happens when flocs of less than 1 mm equivalent floc diameter are discarded.

At this point (Figure 25f) each image was analyzed by Fovea Pro for particle size. Before any measuring was performed, the length scale was set via the "calibrate magnification" selection. Figure 26 displays a typical image that was used for such purposes. The calibration was a persistent parameter, so it only had to be performed once. The "measure all" routine in Fovea Pro uses the calibration data and performs a battery of tests on an image. This data was outputted to a tab-delimited text file that could be read into almost any spreadsheet or statistical program. In this case, Microsoft Excel was used for calculations done with the data exported by Fovea Pro.

What has just been described are the routines performed on one image. During normal analysis, several hundred and sometimes over 1000 images are analyzed in succession. This batch analysis is separated into a "preparation" batch and a "measurement" batch. During the preparation batch, all images from every experimental setting are subjected to the crop, AutoLevel Contrast, Auto Bi-level Threshold, and open routines. The measurement batches are conducted on sets of images from a single experimental run so raw data are not mixed between runs.

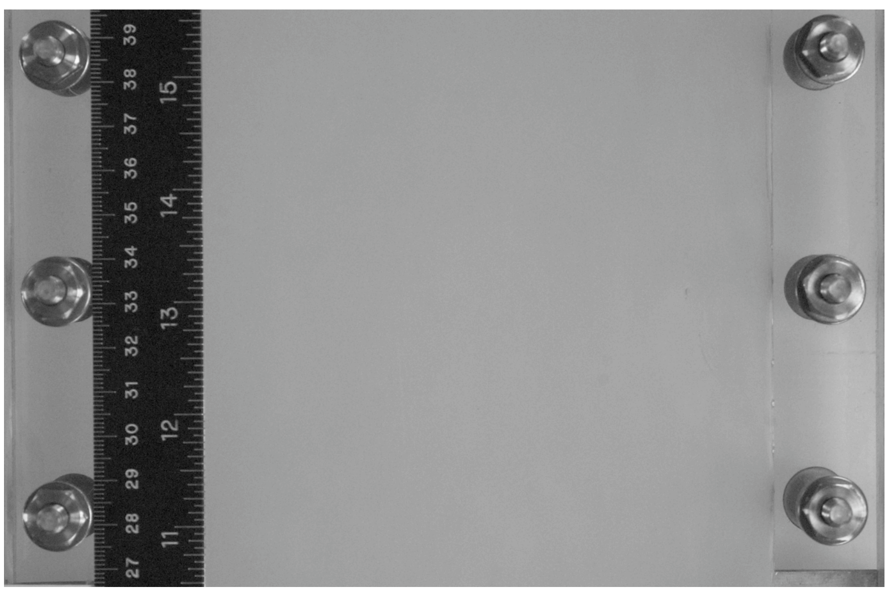

Figure 26. Alignment image showing length scale.

Imaging Locations

Beginning at the imaging channel entrance, there were four locations where image capture was completed. It can be seen in Figure 26 that the images were captured in landscape mode across the channel. In addition, it can be seen that each image is capturing a scene that is 130 mm in length along the direction of flow. Flow occurs from the bottom of the image to the top of the image.

Each image was further divided into three analysis sectors. The cross-channel direction was split into three equal parts so that wall effects were minimized. Figure 27 displays the area in each image that was analyzed. The middle section of each image was further divided into three equal sections. The physical dimensions of each analysis sector was 50 mm in the cross channel direction and 43 mm in the flow direction.

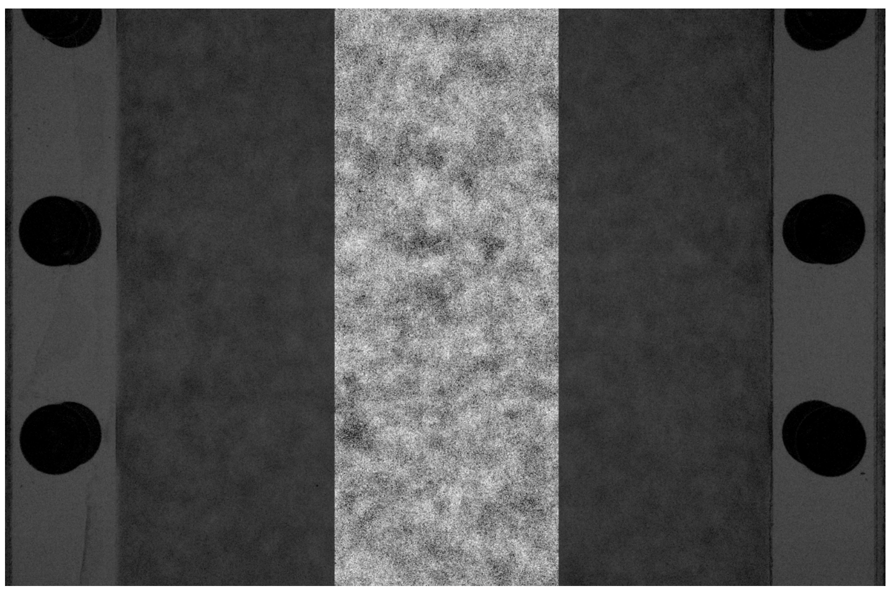

Figure 27. Portion of each image that was analyzed for floc size.

Formation Number Analysis

Past work in the literature (Norman and Wahren, 1972) has shown that one way to measure flocculation intensity is to calculate the coefficient of variation of basis weight. This is sometimes referred to as a formation number. What is being directly measured in this work is transmitted light intensity. Light intensity is proportional to the fiber mass distribution of the moving slurry so variations in the fiber mass distribution will cause corresponding variations in the intensity of the transmitted light.

The same images (and cropping routines) used in the morphological operations technique were used to analyze formation number, but different post processing was used. After running the AutoLevel Contrast routine (see figure 25), Photoshop was used to calculate the mean brightness and brightness standard deviation of all the pixels in an image. The standard deviation and the mean brightness were used to calculate a formation number such that:

$$F^2 = \frac{\sigma^2}{\bar{b}^2} \qquad \textbf{(11)}$$

F^2 = formation number
σ = standard deviation of pixel brightness
$\bar{b}$ = mean of pixel brightness

Each experimental condition, again, consisted of 40 images. The formation number for each image was calculated and a mean formation number for the set of 40 images was obtained.

Fourier Transform Analysis

Fourier transform analysis is frequently used to measure mass distribution of sheets and can be used to calculate actual sizes of floc structures in paper (Norman and Wahren, 1972; Beghello et al, 1996).

In this work the same raw images were used in the Fourier transform method, however different cropping and processing techniques were used. Photoshop was used to crop the areas of interest to 512 X 512 pixels. The AutoLevel Contrast routine was performed on each of the cropped images and images were then saved for further processing.

The Fourier transform of the images (actually a fast Fourier transform, or FFT) was completed inside the software application MATLAB. Output from MATLAB consisted of a "power" value at each of the "n" frequencies (in this case n=512 for the image size). The power value P(n) is the square of the magnitude of the FFT value which has a real portion and an imaginary portion. Plotting power versus frequency (Figure 28) gives what is known as a power spectrum.

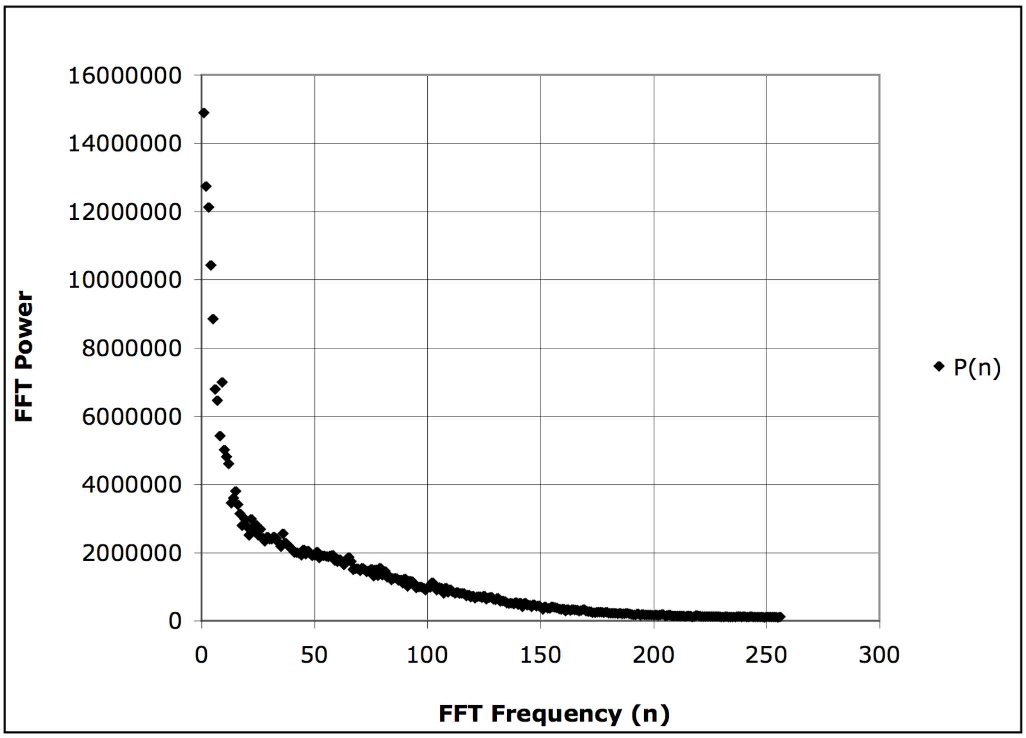

Figure 28. Example power spectrum obtained from an FFT.

The power spectrum can be converted into a wavelength spectrum so length scales can be calculated. This is done by knowing something about the physical size of what was analyzed. In this case, each image was 50.7 mm in length. Using that knowledge, the frequencies can be converted into wavelength and the analogous spectrum can be plotted (Figure 29). The wavelength spectrum is also referred to as the spectral density curve.

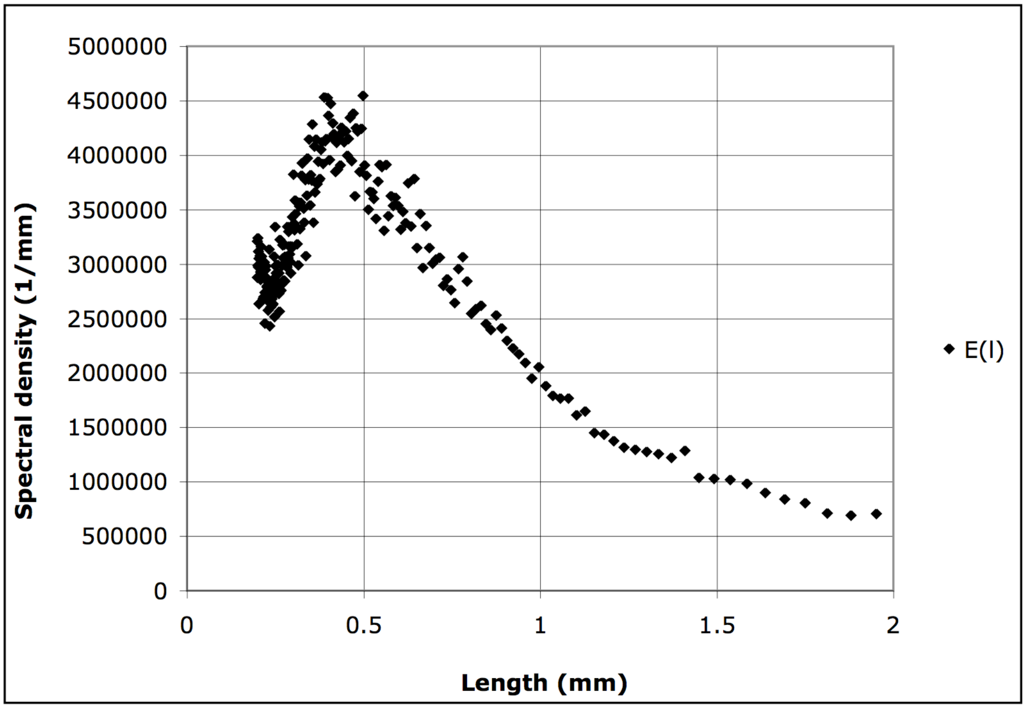

Figure 29. Example wavelength spectrum obtained from an FFT.

To calculate average floc length from the curve in Figure 29, the area under the curve is calculated. The average floc length is the length at which half of the area of the curve falls below it.

Experimental Run Order

Because of limitations in positioning the camera, it was difficult to randomize the entire run order for the experiments. At each imaging location, flow rate and retention aid dosage was randomized, but each imaging location was shot in order. Refer to Appendix II for the run order of the experiments.

DIFFERENTIAL PRESSURE MEASUREMENT

To allow calculation of the rate of mechanical energy transformation (or dissipation) in the fluid, differential pressure along the imaging channel was measured. This energy transformation happens as a result of friction along the walls of the channel and is a conversion from mechanical energy to thermal energy. It is the amount of this energy conversion that was used to relate mechanical energy input to flocculation characteristics in this project. High dissipation rates are associated with high turbulence levels and a tendency to impede formation of large flocs.

Differential pressure was measured using an Omega model PX2300-5DI differential pressure transducer. The Omega transducer had a range of 0-5 PSID and a 4-20 mA signal that was output to the Omega DP41-E digital display. The transducer measured the differential pressure between two pressure taps located on the imaging channel. The upstream pressure tap was located 20 mm downstream from the imaging channel inlet, and the downstream tap was positioned 1617 mm downstream of the imaging channel inlet. Analogue pressure gauges were also used to help calibrate and confirm readings from the transducer.

It has been reported in the literature (Norman et al., 1977; McCabe et al., 1993; Xu, 2003) that at turbulent flow rates, the presence of pulp fibers in flowing water imparts a drag reduction effect that lowers the friction factor and the pressure drop of the flowing suspension. In stark contrast, at low flow rates in the laminar regime, fibers increase the pressure drop due to the plug flow of the fibers. The current research was completed in the turbulent regime at flow rates well above the plug flow scenario.

The drag reduction phenomena made it necessary to collect the differential pressure data with pulp fibers present because the pressure drop data for just water would have yielded less applicable results. For comparison purposes, and to confirm past results in the literature, measurements of differential pressure of both water and water with fiber were completed. The differential pressure was measured at twelve flow rates. Raw data for differential pressure can be found in Appendix V. Figure 30 displays how pressure drop varies with Reynolds number and figure 31 shows how friction factor varies with Reynolds number.

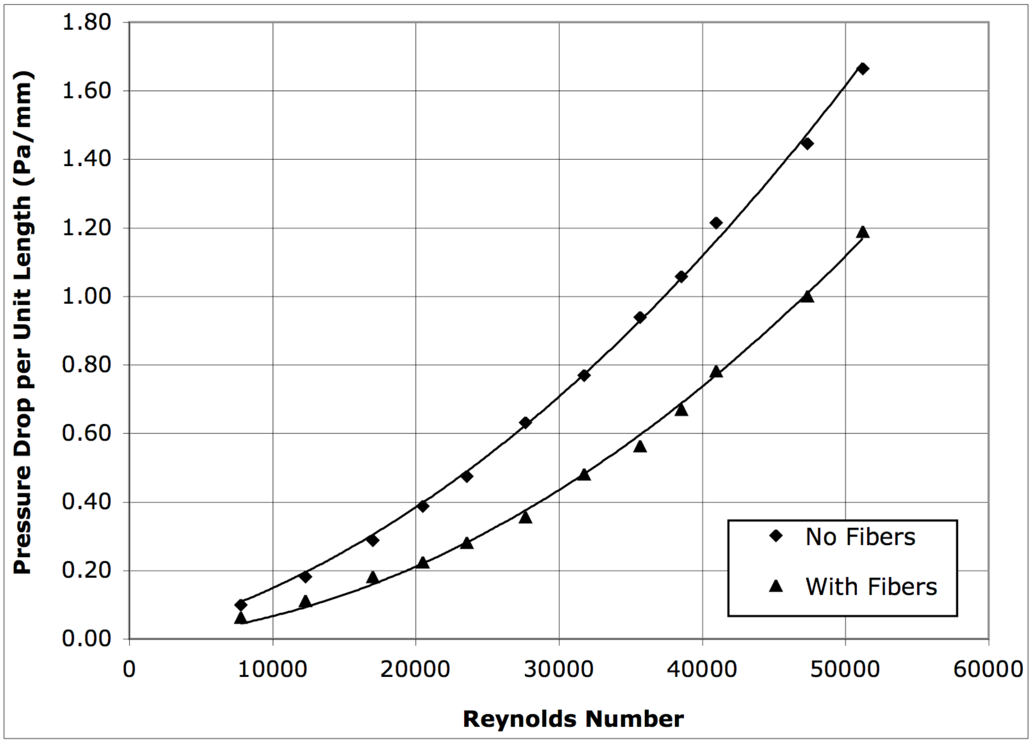

Figure 30. Pressure drop per unit length versus N_{Re} for flow with and without fiber.

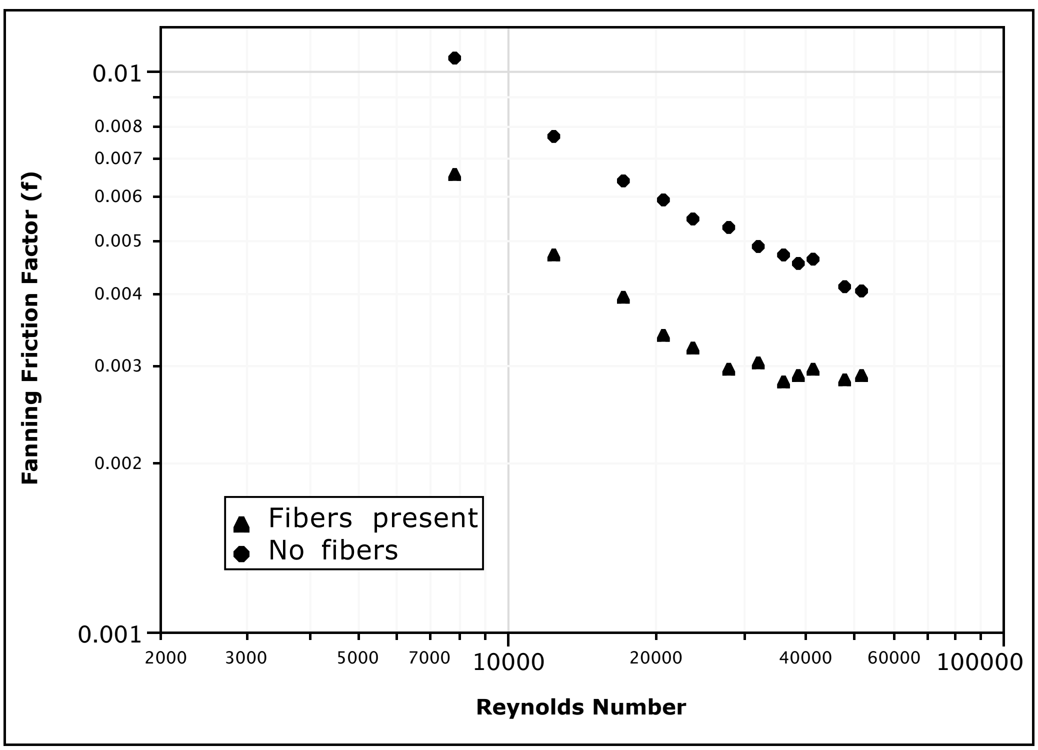

Figure 31. Fanning friction factor as a function of Reynolds number (logarithmic scale).

Figures 30 and 31 confirm the past work cited by showing that the presence of fibers in water lowers the pressure drop, and by definition, the friction factor. Figure 31 also displays the behavior of fiber suspensions seen in past work where after a certain flow rate, the friction factor becomes almost constant.

The energy being calculated is a result of skin friction between the walls of the channel and the fluid. This value is calculated knowing the pressure drop and the constant density of the fluid (McCabe, 1993) and assuming that there is no change in fluid velocity and potential energy along the length of the channel. Equation 12 outlines this calculation.

$$h_f = \frac{\Delta p}{\rho} = \frac{4}{\rho}\frac{\tau_W}{D}\Delta L [=] \frac{\text{J}}{\text{kg}} \qquad \textbf{(12)}$$

$h_f =$ energy dissipation due to skin friction
$\Delta p =$ pressure drop over a known length
$\rho =$ density of the fluid
$\tau_W =$ shear stress at the wall of the conduit
$D =$ diameter of the pipe
$\Delta L =$ length of pipe over which pressure drops

One concern in this work was the lowering of the viscosity of the fluid as retention aid was injected. Since h_f is proportional to the viscosity of the fluid, lowering the viscosity will lower the energy dissipation and will defeat the purpose of calculating h_f based on known pressure drops. In order to ascertain the degree of viscosity change, a viscometer was used to measure the viscosity of a solution of retention aid at the same concentration as that of the flow loop. The highest concentration experienced, 0.0003%, was used. At a 0.0003% concentration the viscometer could not distinguish between pure water and the polymer solution. Injecting retention aid into the flow loop should not appreciably affect the calculation of h_f.

What is of interest in this study is a rate of energy dissipation, or more specifically, a rate of energy dissipation per unit length. Using the Bernoulli equation, the following equation can be derived to give that value:

$$\frac{\dot{W}}{L} = \frac{\dot{Q}\Delta p}{L} \qquad \textbf{(13)}$$

$\dot{W} =$ power
$\dot{Q} =$ volumetric flow rate
$\Delta p =$ pressure drop
$L =$ length between pressure taps

Figure 32 displays the energy dissipation rate values calculated with equation 13 as a function of flow rate.

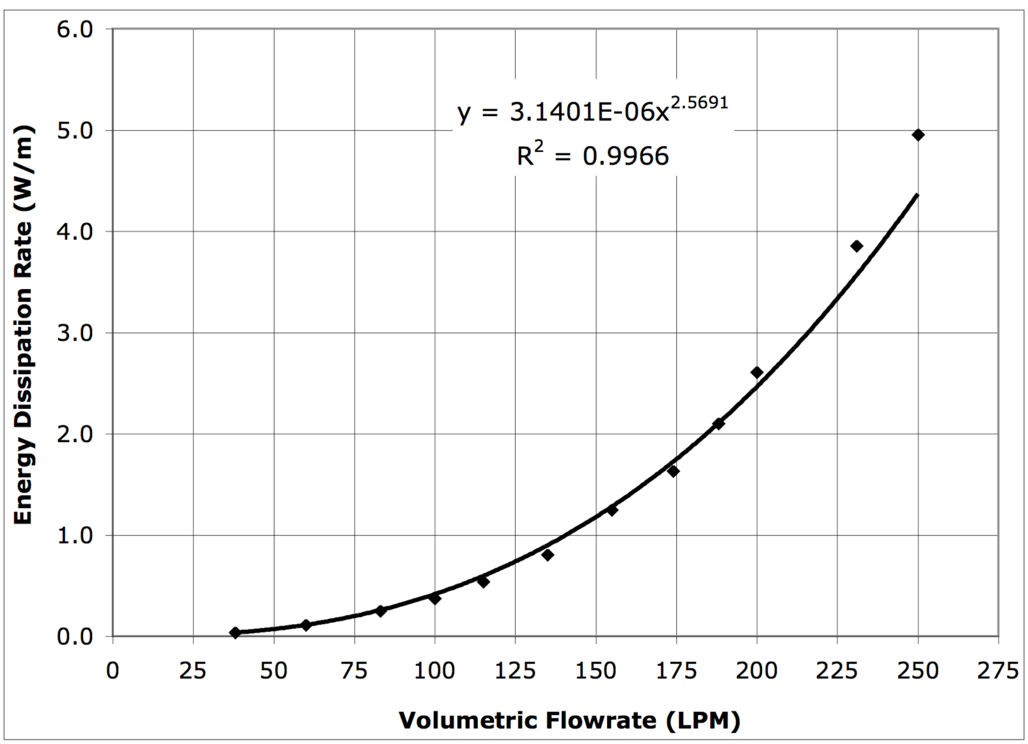

Figure 32. Energy dissipation rate as a function of volumetric flow rate.

Using the best fit equation in figure 32, energy dissipation rate values for the four flow settings in the experiments were calculated. These values can be found in Table VII.

Table VII. Energy Dissipation Rate Values

Flow Rate (LPM)	Fluid Velocity (m/s)	N_{Re}	Energy Dissipation Rate (W/m)	Energy Dissipation Rate (W/m^3)
100	0.88	20488	0.432	226.6
133	1.16	27248	0.898	471.5
166	1.45	34009	1.587	833.2
200	1.75	40975	2.562	1344.7

Although analysis in this study used an energy dissipation rate (W/m) on a unit length basis, a more applicable and fundamental property may be the volumetric energy dissipation rate (W/m^3). The linear energy dissipation value used in this study is only applicable to the specific geometry of the imaging channel used. Using the volumetric energy dissipation rate would allow comparison to other geometries of flow channels.

Compared to the Reynolds numbers experienced on an actual paper machine, the Reynolds numbers inside the flow channel are much smaller. Assuming a machine width of 300 inches, a machine speed of 3000 feet/minute and a slice opening of 1 inch, the calculated Reynolds number at the slice is approximately 770,000.

RESULTS

CONFIRMATION OF IMAGE ANALYSIS ACCURACY

It is important to know whether the image analysis routine described previously measures particle sizes correctly. In order to confirm this, a test was devised that allowed measurement of "particles" of different shapes and known areas.

To begin, data from an actual imaging channel image was inspected for prevalent floc sizes. Several flocs sizes (four in all) were selected from the image's data. Each floc size was assigned a shape and quantity that would appear in the test image. The quantity for each shape was determined by the relative percent that appeared in the original image. Particle data for the test image can be found in Table VIII.

Table VIII. Test Image Particle Parameters

Shape	Area (mm^2)	Pertinent Dimensions (mm)	Quantity in test image
Large Ellipse	147.80	A = 19.40 B = 9.70	1
Circle	11.10	R = 1.88	5
Square	7.40	L = 2.72	8
Small Ellipse	3.73	A = 3.08 B = 1.54	31

The data in Table VIII were used to create a repeating test pattern with the aid of a drawing program (Figure 33). This pattern was then printed out and overlaid on the imaging channel (Figure 34). The same method used to capture floc images in the experiments was then used to capture an image of the overlaid printout (this included light source, camera settings, and data analysis).

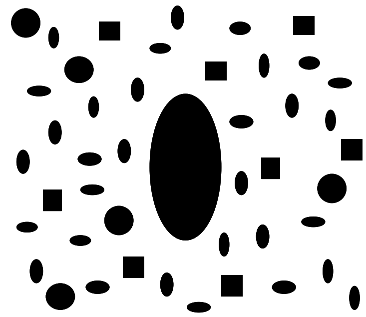

Figure 33. Repeating pattern used in test image.

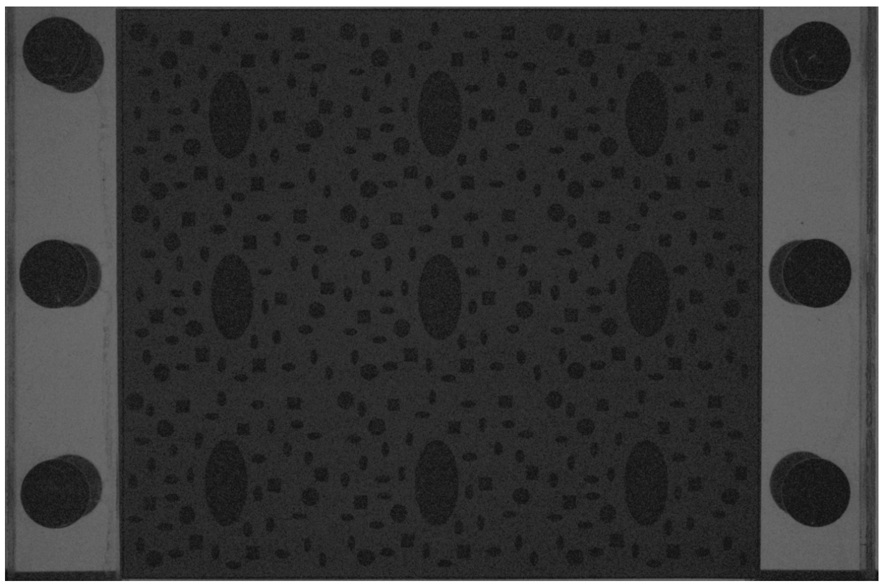

Figure 34. Image of test printout overlaid on the imaging channel.

Figure 34 was analyzed in the same manner as all of the images in the experiments and the results were compared with the known areas of the particles. Table VIII displays these results.

Table IX. Test Image Accuracy

Shape	Known Area (mm^2)	Test Image Area (mm^2)	Test Image % Error	Known Quantity	Quantity in Test Image
Large Ellipse	147.80	145.09	1.8	1	1
Circle	11.10	11.22	1.1	5	5
Square	7.40	7.46	0.9	8	8
Small Ellipse	3.73	4.0	7.2	31	31

As shown by Table VIII, the routine run in Fovea Pro to measure floc size performs very well with low error. These results support the validity of the morphological image analysis procedure used in these experiments.

FLOCCULATION RESULTS

Three separate methods were used to analyze the images acquired in this study: direct measurement of floc size and number through the use of morphological operations; calculation of the formation number to understand the intensity of the flocculation; and FFT analysis as a second way to understand floc size. The results here are given from two perspectives that correspond to the two main variables in the research: retention aid dosage and mechanical energy dissipation.

Morphological Operations

Experimental runs consisted of 40 images which were analyzed by the computer for floc area and floc number using morphological image operations. For each experimental run, the data from each of the 40 images were combined into one large data set. Each data set consisted of thousands of "features" or possible flocs that were measured. A significant amount of the features that were recorded were single pixels or particles too small to be meaningful. In order for the software to calculate floc properties (area and number) using only the features that were most likely flocs, a low pass filter was performed on the data. The combined list of features for all 40 images at each experimental run was sorted according to feature area. All features with an equivalent diameter of 1 mm or less (i.e. an area less than 0.785 mm^2) was removed from further analysis. Filtering based on equivalent diameter was preferred over filtering by feature length because feature length would yield undesirable results. For example, if features with a length less than 1 mm were removed, it is conceivable that some remaining features could be, for instance, a feature of length greater than 1 mm , but of one pixel in width (0.1 mm or 100 μm). The method of filtering by length would allow features with a width of two to three times that of a fiber to be counted which in this study was not considered to be a floc. It is for this reason, that filtering by equivalent diameter was chosen. A complete listing of all the averaged, filtered data can be found in Appendix I.

One measure of the level of flocculation in a pulp suspension is the number of distinct flocs present. The number of flocs does not give information about the size of the flocs, but it does allow understanding of what is happening, to a degree, inside the suspension. Figures 35 through 38 display results for number of flocs per unit area as a function of distance from the channel inlet. For each experimental setting, the number of flocs from all images was totaled and converted to a per area basis. Where applicable, power law curves have been fit to the data. The purpose of these curves is to provide a general guide to the trend of the data—not to imply knowledge of a continuous set of points for the data.

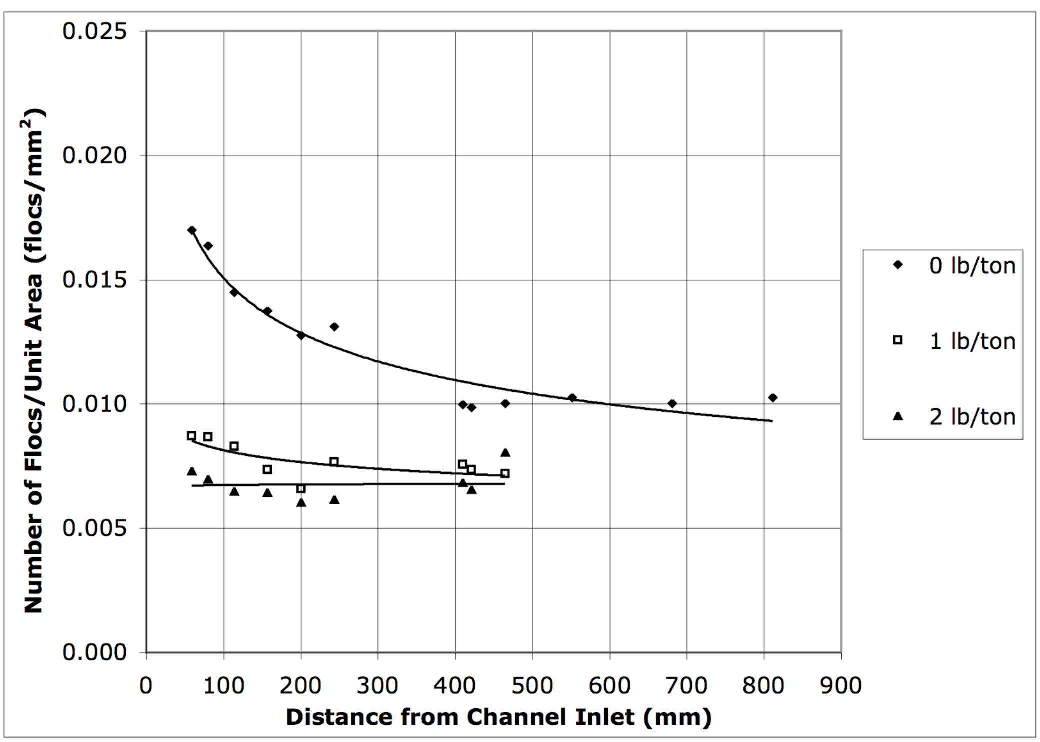

Figure 35. Number of flocs per unit area versus distance from channel inlet at 0.432 W/m energy dissipation. Data for 0, 1, and 2 lb/ton retention aid dosage.

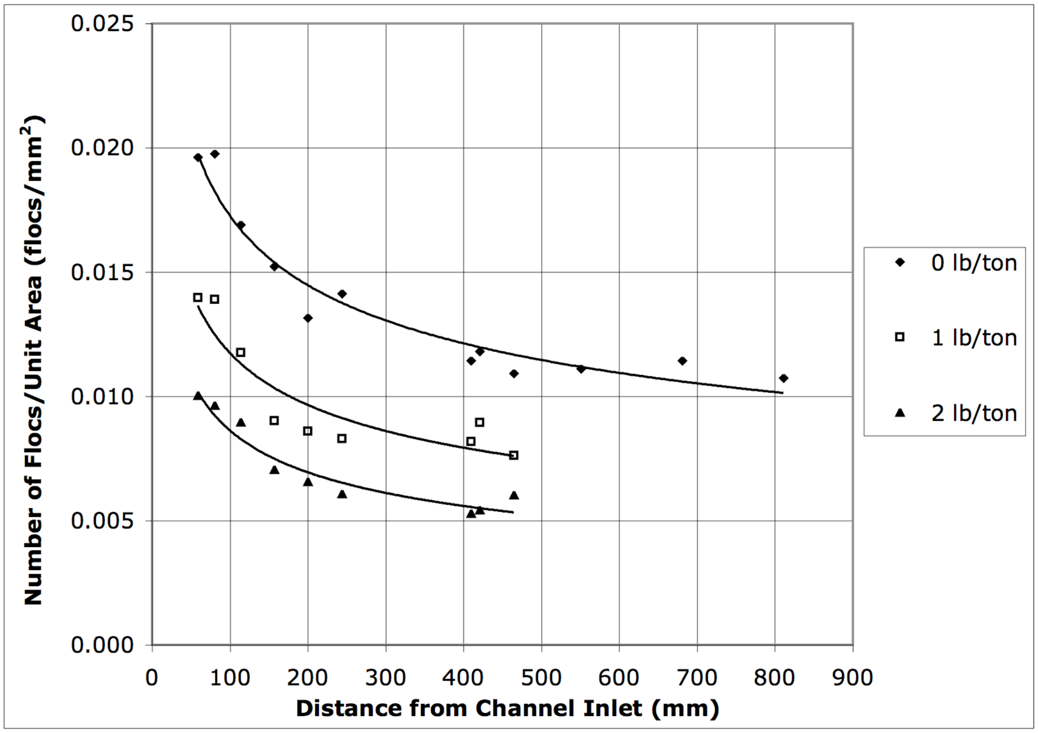

Figure 36. Number of flocs per unit area versus distance from channel inlet at 0.898 W/m energy dissipation. Data for 0, 1, and 2 lb/ton retention aid dosage.

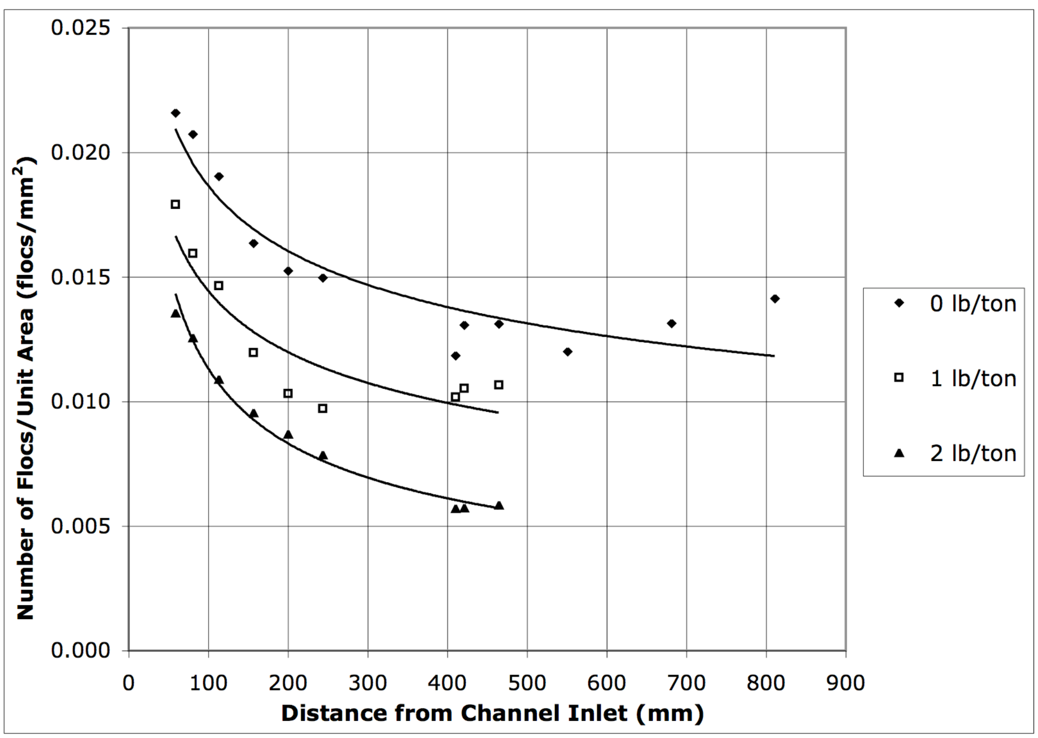

Figure 37. Number of flocs per unit area versus distance from channel inlet at 1.587 W/m energy dissipation. Data for 0, 1, and 2 lb/ton retention aid dosage.

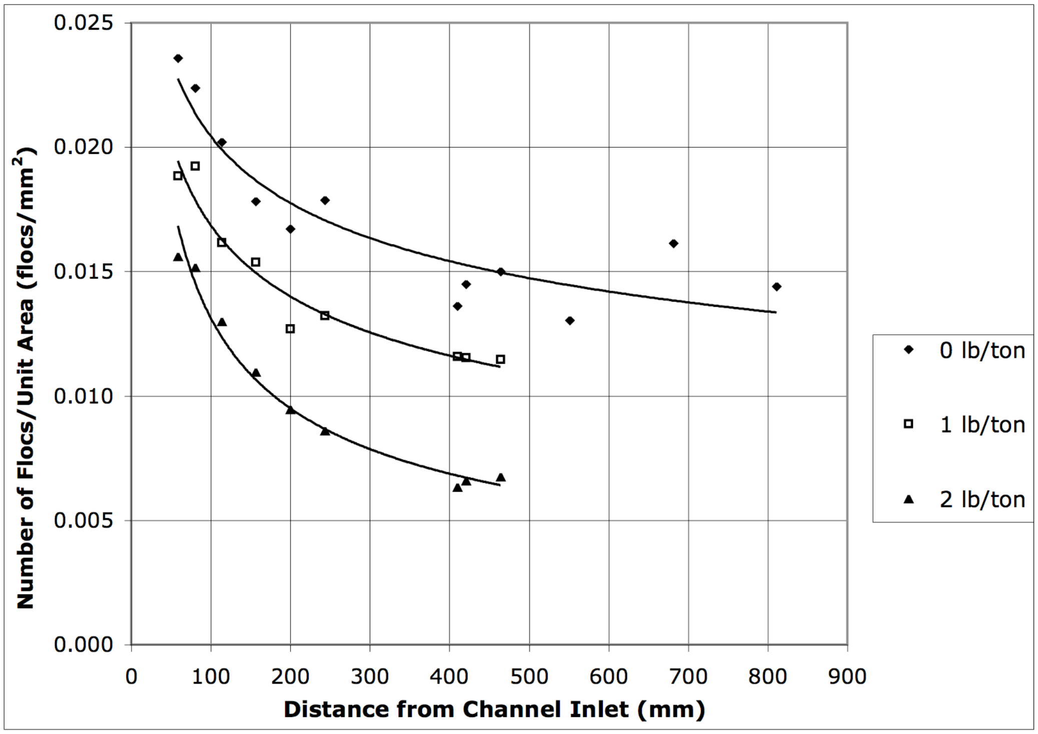

Figure 38. Number of flocs per unit area versus distance from channel inlet at 2.562 W/m energy dissipation. Data for 0, 1, and 2 lb/ton retention aid dosage.

In studying these figures, several features become apparent. Both retention aid dosage and energy dissipation level have an effect on the formation of flocs in the moving suspension. Notice that for all energy dissipation levels, as retention aid dosage is increased, the number of flocs is decreased significantly. The largest decrease in the number of flocs (from the equilibrium level) occurs at the highest energy dissipation level and is approximately a 50% decrease in floc number. It is also apparent that upon entering the imaging channel, the pulp suspension experiences a fast initial decrease in the number of flocs, followed by a gradual approach toward a quasi-equilibrium floc number. The decrease in number of flocs due to retention aid dosage can also be seen in figures 39 through 41 where data are grouped by retention aid dosage and the effect of energy dissipation is highlighted.

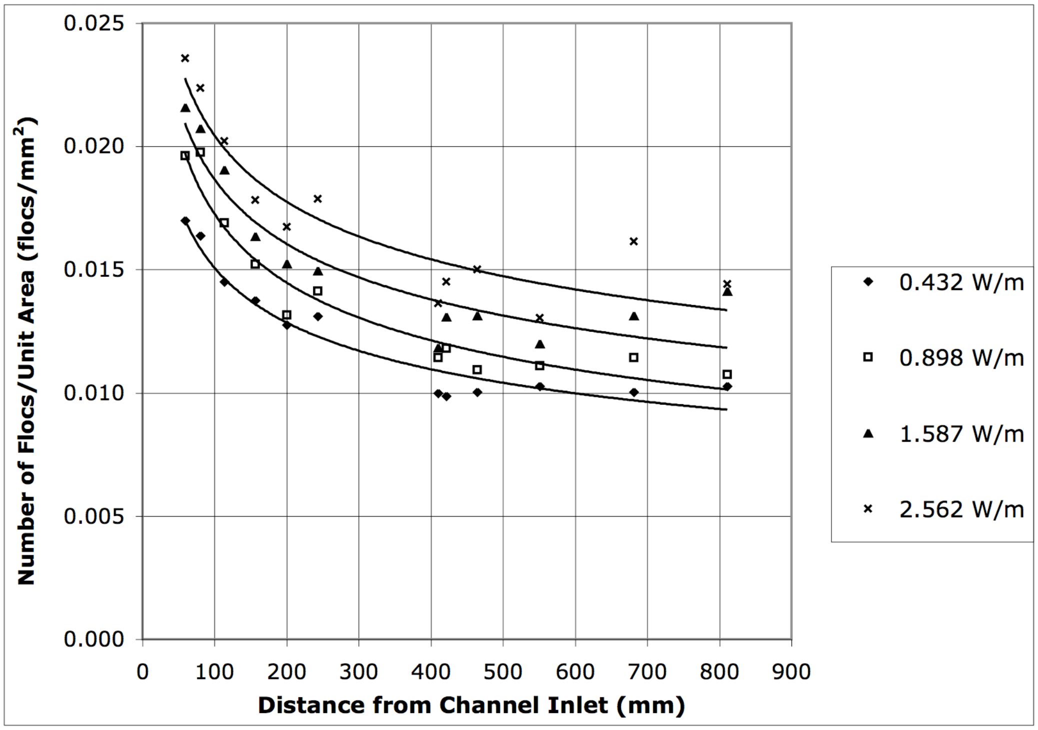

Figure 39. Number of flocs per unit area versus distance from channel inlet at 0 lb/ton retention aid dosage. Data for 0.432, 0.898, 1.587, 2.562 W/m energy dissipation.

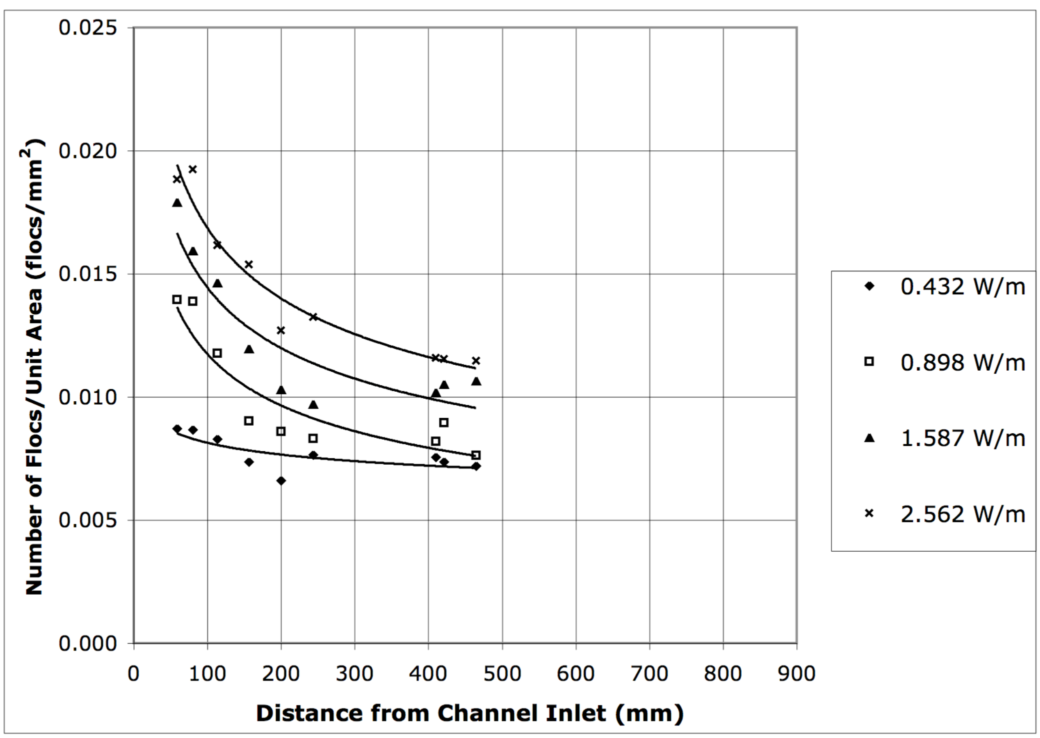

Figure 40. Number of flocs per unit area versus distance from channel inlet at 1 lb/ton retention aid dosage. Data for 0.432, 0.898, 1.587, 2.562 W/m energy dissipation.

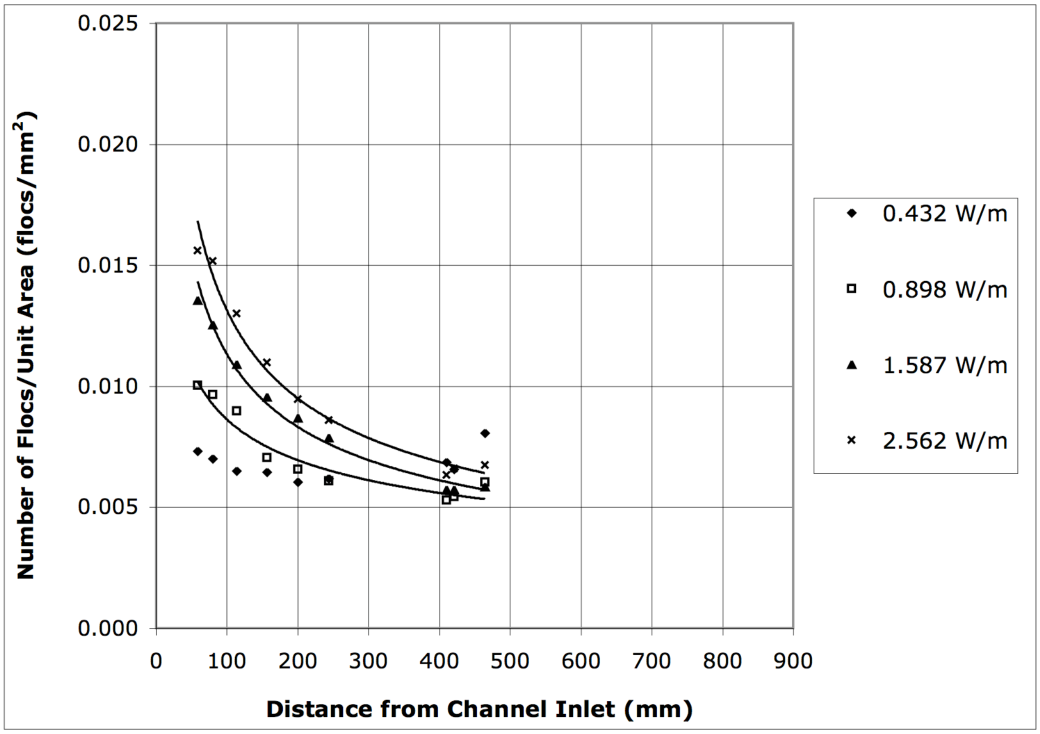

Figure 41. Number of flocs per unit area versus distance from channel inlet at 2 lb/ton retention aid dosage. Data for 0.432, 0.898, 1.587, 2.562 W/m energy dissipation.

Looking at the data as displayed in figures 39 through 41 allows other trends to stand out. In contrast to the decrease because of retention aid dosage, energy dissipation level appears to increase the number of flocs. This was evident for each retention aid dosage level. The effect of retention aid dosage was witnessed again because the data became grouped at lower and lower floc numbers as retention aid dosage was increased.

To understand how fast flocs are forming, it is necessary to take into account the flow rates and look at the data on a time basis. Figures 42 through 44 do this.

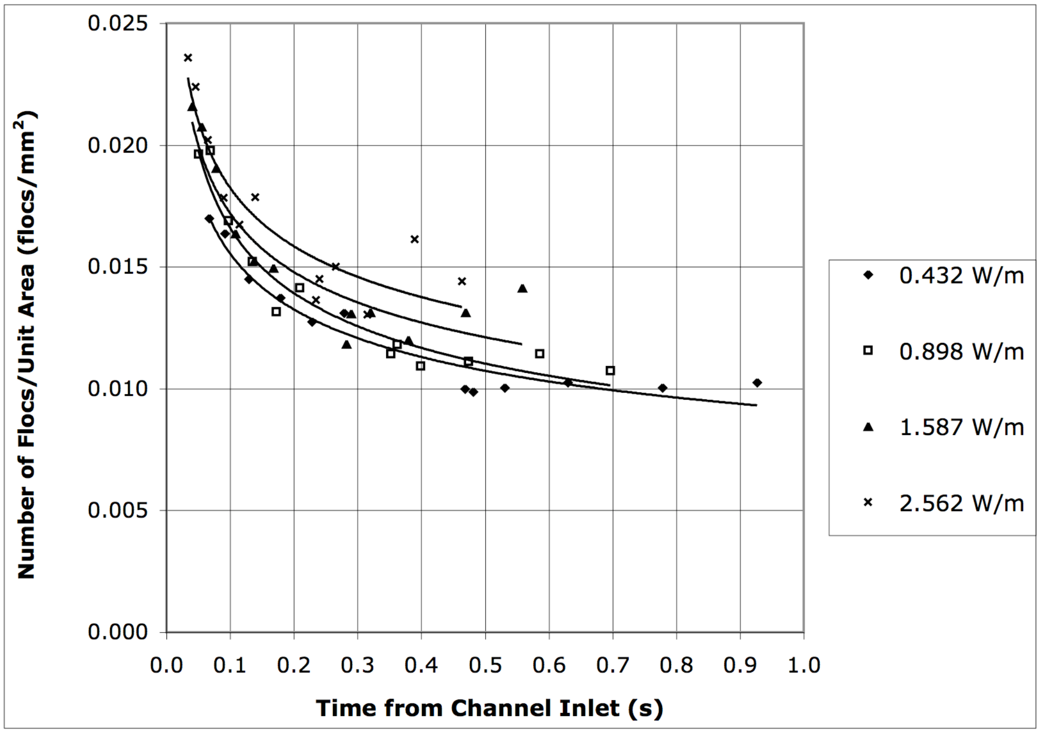

Figure 42. Number of flocs per unit area versus time from channel inlet at 0 lb/ton retention aid dosage. Data for 0.432, 0.898, 1.587, 2.562 W/m energy dissipation.

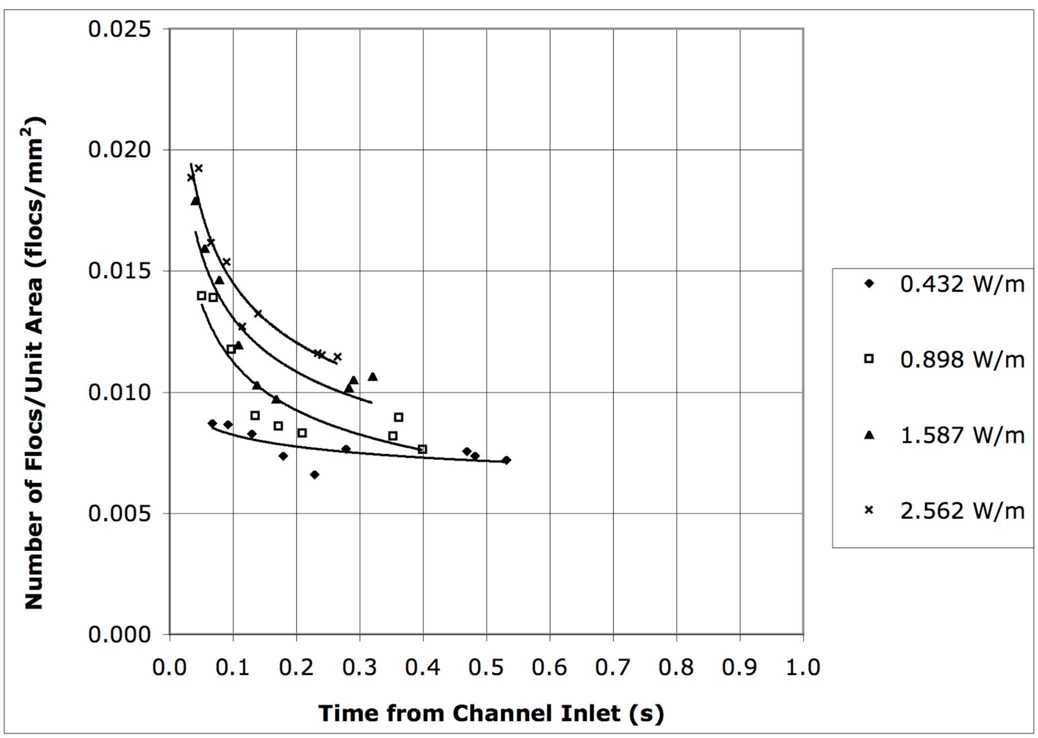

Figure 43. Number of flocs per unit area versus time from channel inlet at 1 lb/ton retention aid dosage. Data for 0.432, 0.898, 1.587, 2.562 W/m energy dissipation.

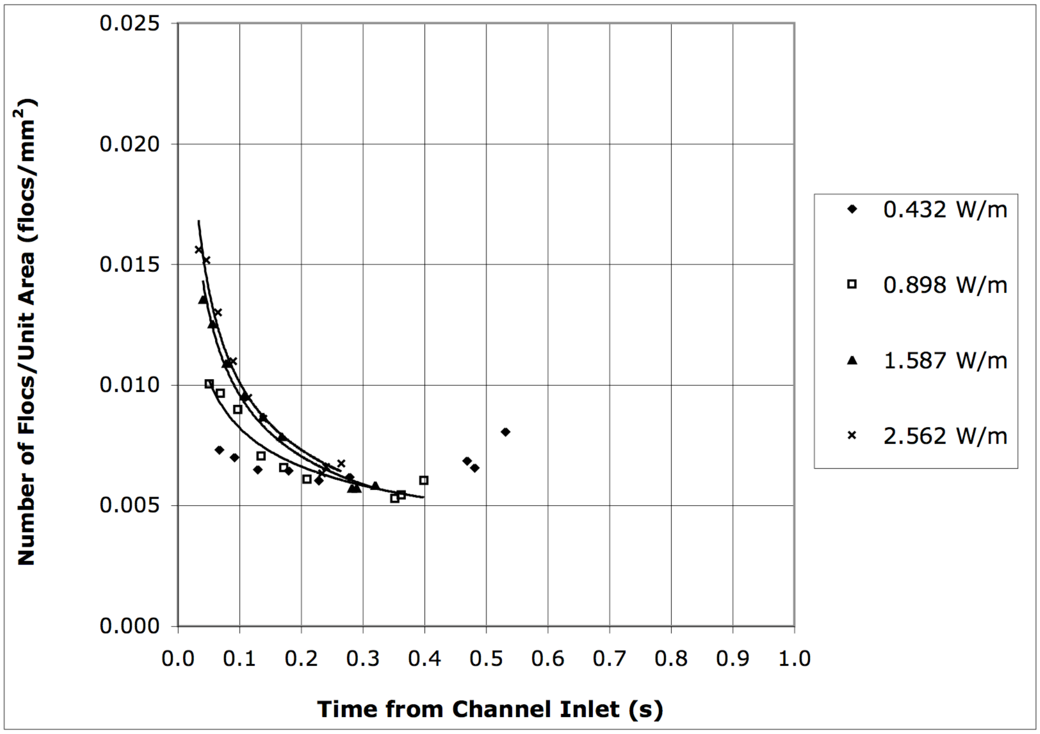

Figure 44. Number of flocs per unit area versus time from channel inlet at 2 lb/ton retention aid dosage. Data for 0.432, 0.898, 1.587, 2.562 W/m energy dissipation.

When looked at on a time basis, it becomes clear that increased retention aid dosage causes the suspension to reach the equilibrium number sooner than that experienced with lower dosage or no dosage at all. Increasing retention aid dosage also appears to magnify the differences between energy dissipation effects on flocculation. Notice how in figure 42 that, generally, each of the energy dissipation rate levels fall along the same curve. Figures 43 and 44 show deviation in the lower dissipation levels.

It is also important to look at how floc area varies with retention aid dosage and energy dissipation. In some ways, floc area is a more important measurement than floc number when considering the formation quality of paper. Floc number may vary, but if the size of the flocs are small it is not as big a concern as if the individual flocs were large in area. For presentation here, floc area is calculated as the area of flocs per unit area of the analyzed image. In other words the values are the fraction of area in an image that is a floc. Figures 45 through 51 display data for floc area.

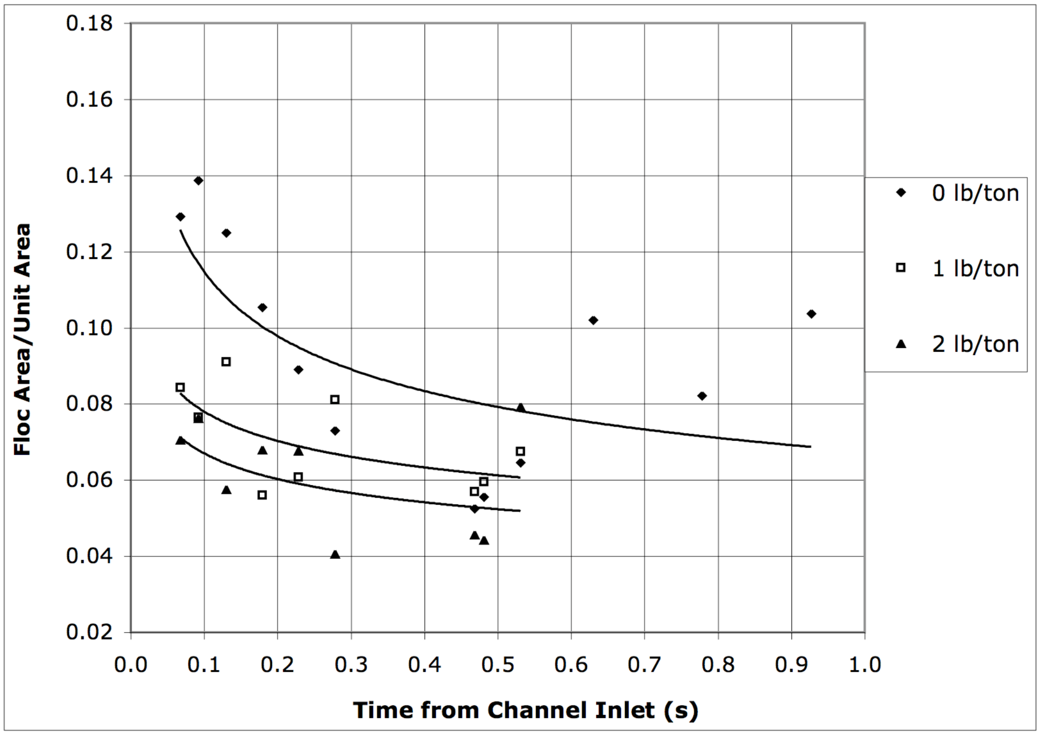

Figure 45. Floc area per unit area versus time from channel inlet at 0.432 W/m energy dissipation. Data for 0, 1, and 2 lb/ton retention aid dosage.

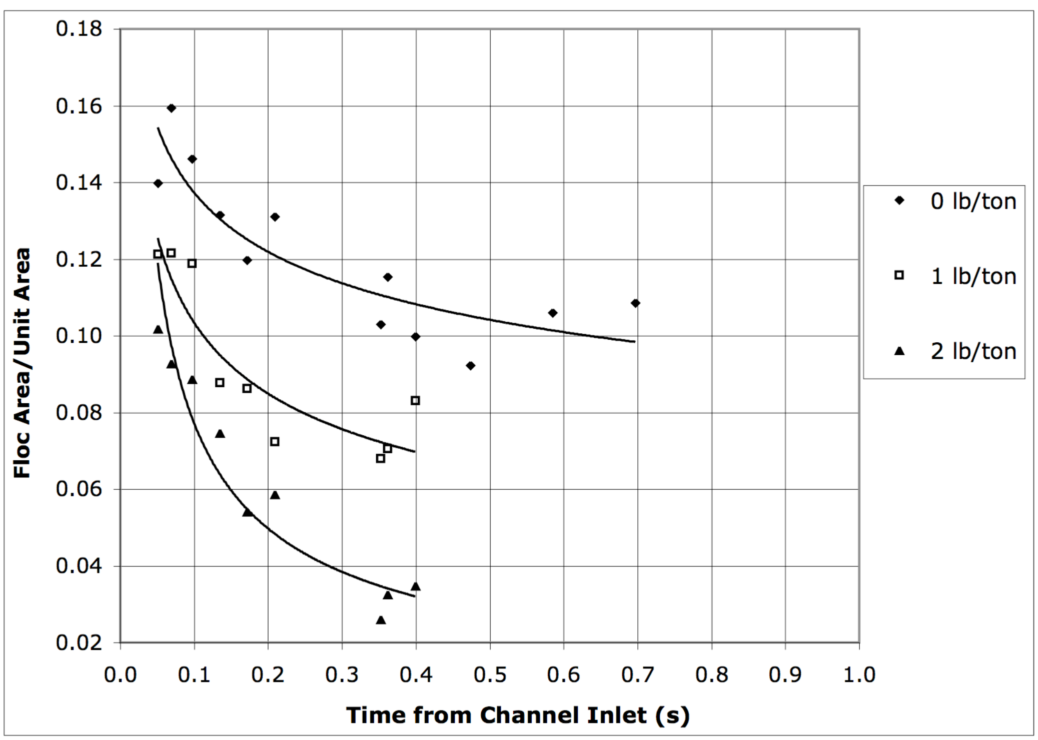

Figure 46. Floc area per unit area versus time from channel inlet at 0.898 W/m energy dissipation. Data for 0, 1, and 2 lb/ton retention aid dosage.

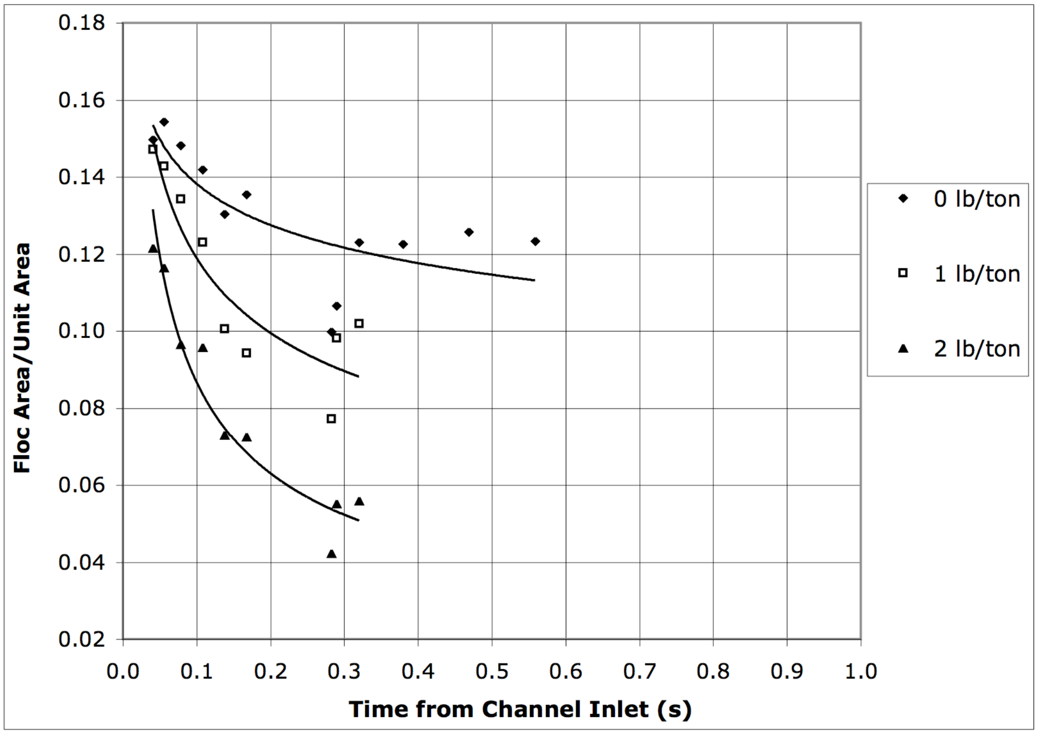

Figure 47. Floc area per unit area versus time from channel inlet at 1.587 W/m energy dissipation. Data for 0, 1, and 2 lb/ton retention aid dosage.

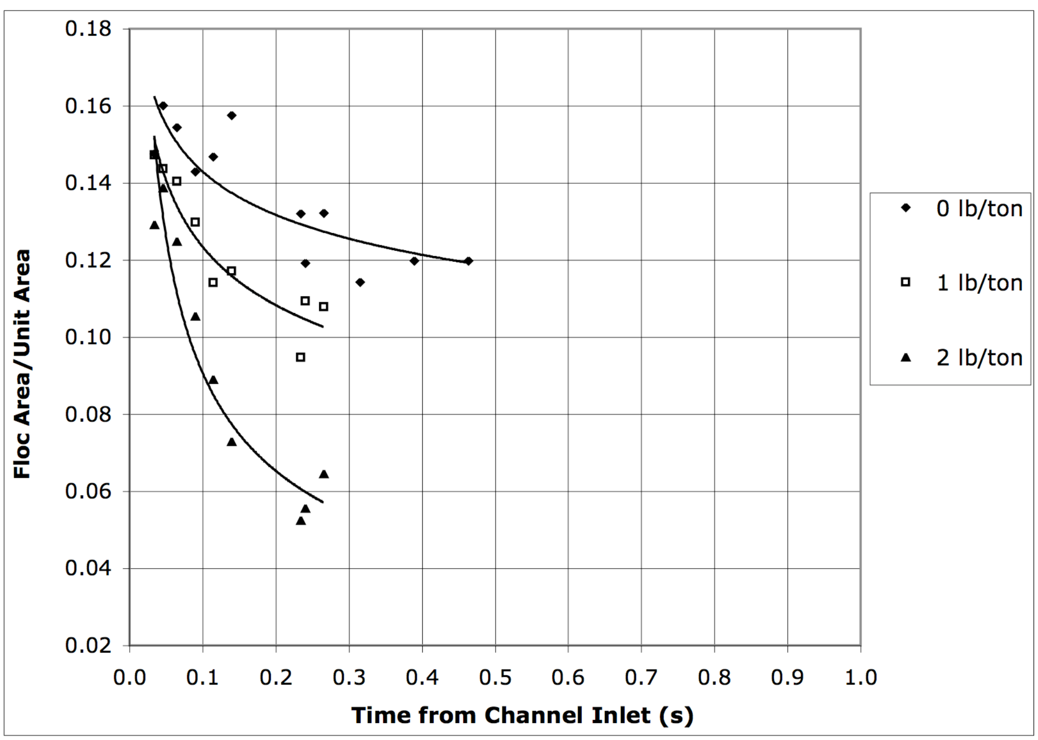

Figure 48. Floc area per unit area versus time from channel inlet at 2.562 W/m energy dissipation. Data for 0, 1, and 2 lb/ton retention aid dosage.

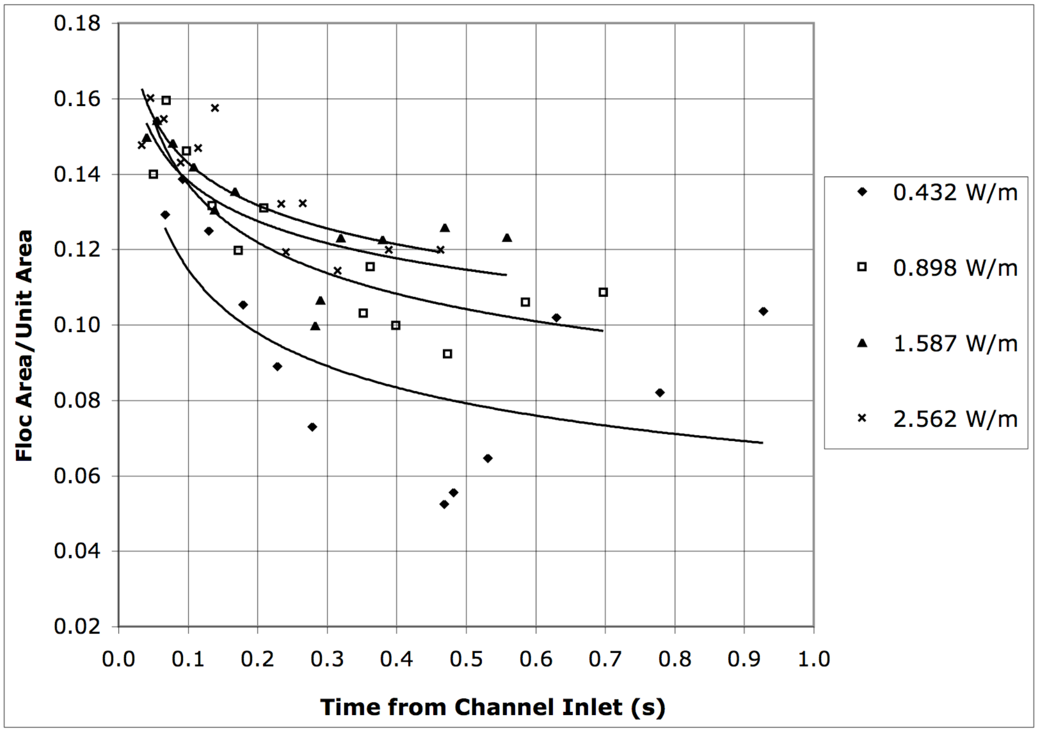

Figure 49. Floc area per unit area versus time from channel inlet at 0 lb/ton retention aid dosage. Data for 0.432, 0.898, 1.587, 2.562 W/m energy dissipation.

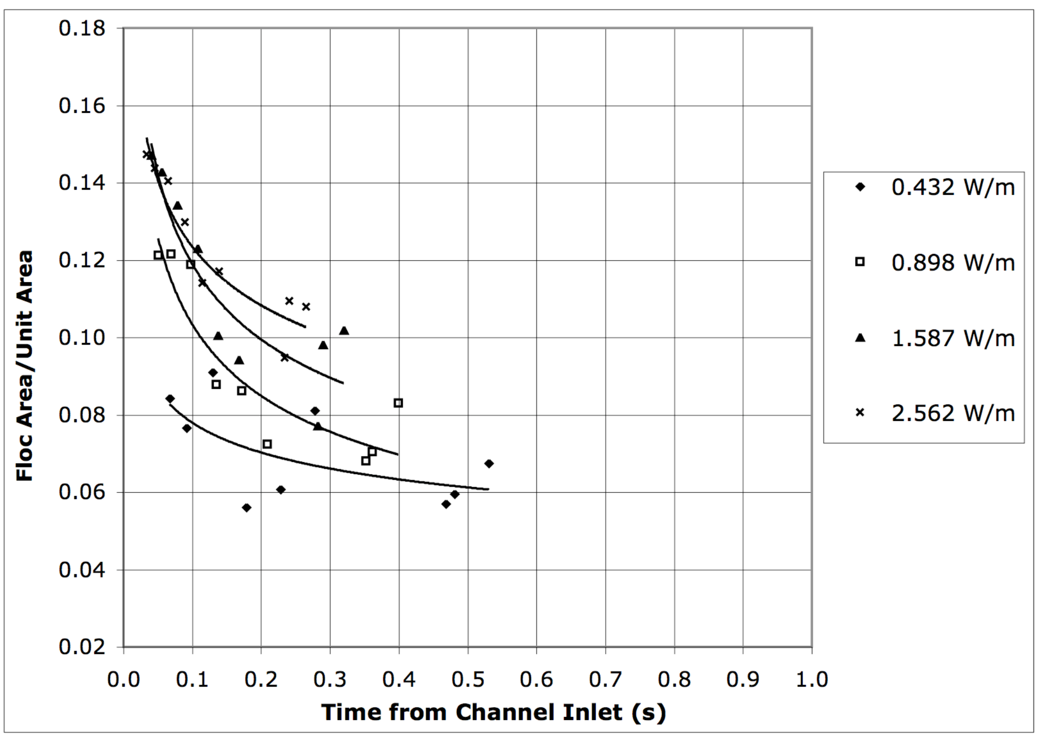

Figure 50. Floc area per unit area versus time from channel inlet at 1 lb/ton retention aid dosage. Data for 0.432, 0.898, 1.587, 2.562 W/m energy dissipation.

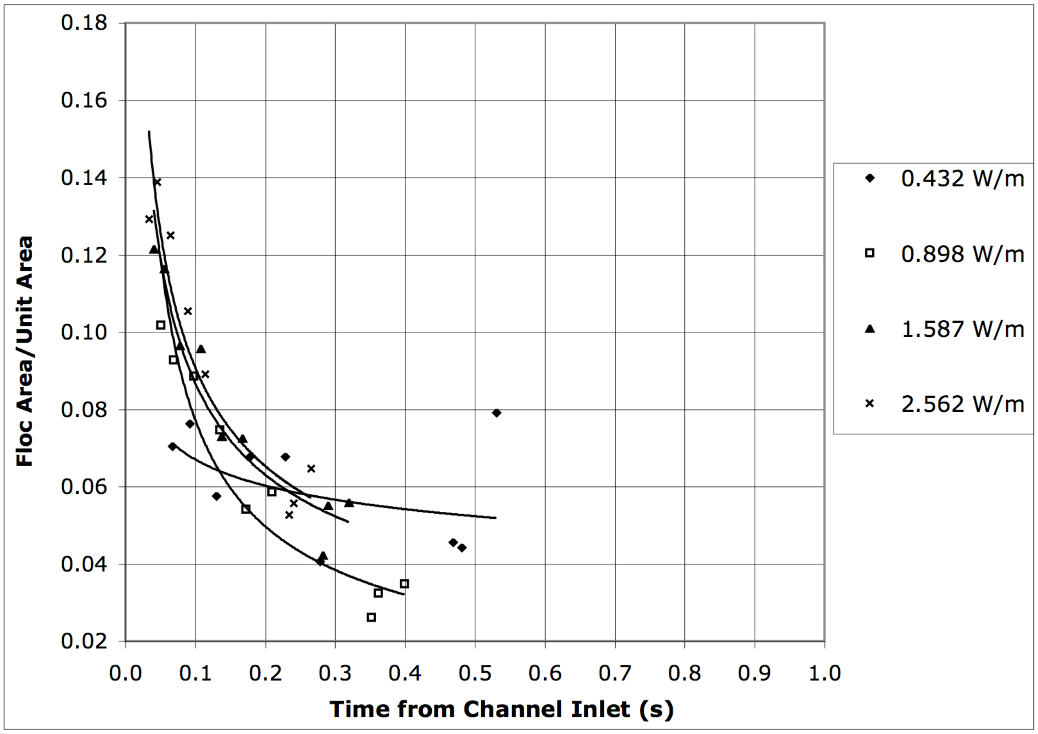

Figure 51. Floc area per unit area versus time from channel inlet at 2 lb/ton retention aid dosage. Data for 0.432, 0.898, 1.587, 2.562 W/m energy dissipation.

Upon inspection of the floc area data, a number of trends become apparent. Increasing retention aid dosage in all cases leads to significantly reduced floc area. Figures 43 and 44 show how retention aid dosage is more effective at lowering the floc area when it is used at lower energy dissipation levels. In all cases, increased energy dissipation levels resulted in increased floc area.

Figures 44 and 51 both displayed behavior in the 0.432 W/m energy dissipation level where both the area and the number reached a type of minimum and began to increase. This behavior did not occur in any of the other experimental settings. What may be happening in this situation might be turbulent eddy scale related. Recall the brief discussion about turbulent eddy scale on page 22. The point of that discussion was to highlight the theory that the relative size difference between floc size and turbulent eddy scale determines what happens to the floc (i.e. growth or decay). As mentioned on page

28 eddy scale was not controlled in this study. What we are seeing in figures 44 and 51 are increases in floc number and floc area per unit area. This translates into decreases in floc size (as measured by area per floc). A plausible explanation for this decay in floc size would be a decrease in eddy size. The suspension is flowing from a large mixing chamber to a rectangular flow channel with significantly decreased dimensions. At this low flow rate inside the mixing chamber the eddy scale is at a level that produces a certain size of floc (it may help to refer to figure 7 at this point). When that floc enters the imaging channel, the eddy scale decreases because of the decrease in dimensions of the flow channel. The decrease in eddy scale is enough to start tearing up the floc (as discussed earlier on page 22) because the eddy is now smaller or the same size as the floc. This is where the decrease in floc size comes from. The reason this is not seen at the lower retention aid levels is because, as we have seen, the lower the retention aid dosage, the lower the floc size. Eddy scale is still at the same level as in the high dosage case, but because the floc is smaller upon entering the channel, the floc is now allowed to grow instead of decay. The reason this may not be happening in the higher flow rates regardless of retention aid level, is that at the higher flow rates, smaller eddy scales already exist in the mixing chamber.

Although floc area is in no way controlled by the number of flocs present in the system (the two are most definitely related, but not controlled by each other), it would be interesting to see if there is a relationship that exists between the levels of each of the parameters. Figure 52 displays floc area as a function of the number of flocs regardless of the experimental setting.

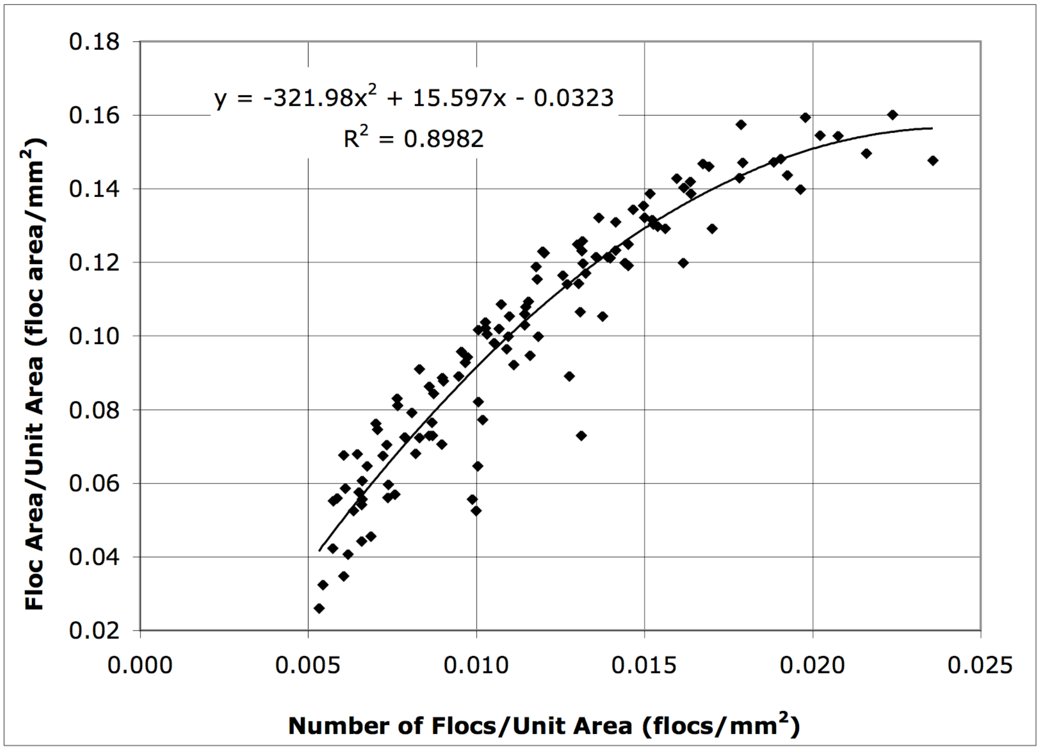

Figure 52. Floc area per unit area versus number of flocs per unit area.

Figures 53 and 54 are similar to figure 52, but the data are separated into the respective variables levels.

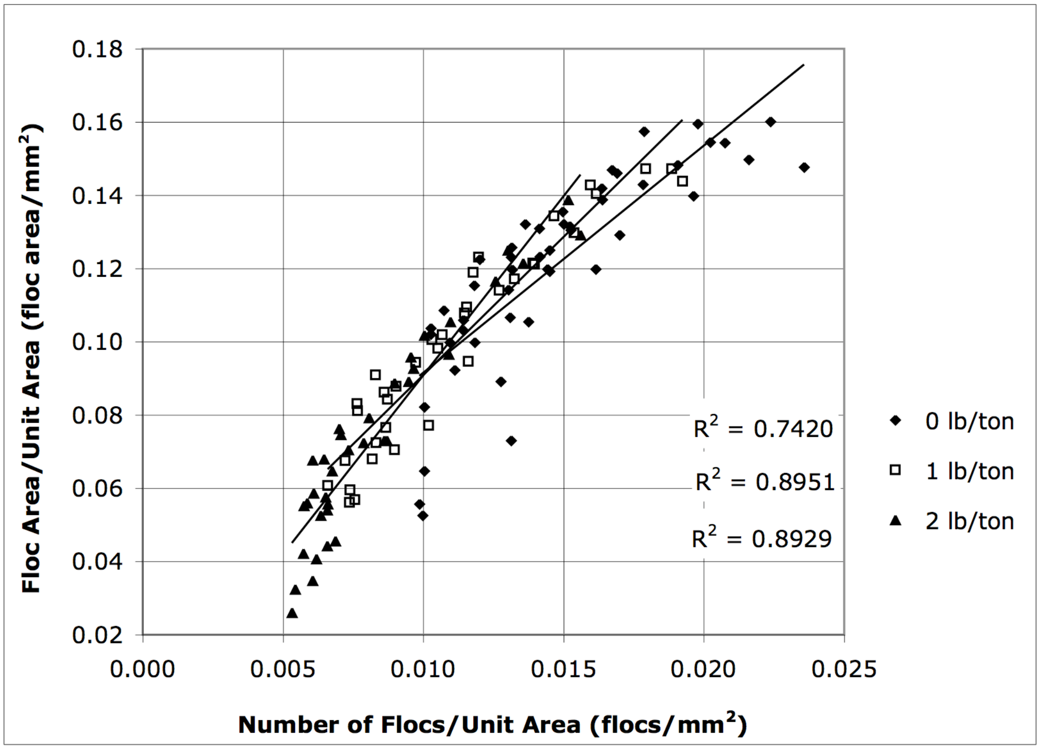

Figure 53. Floc area per unit area versus number of flocs per unit area. Retention aid effect.

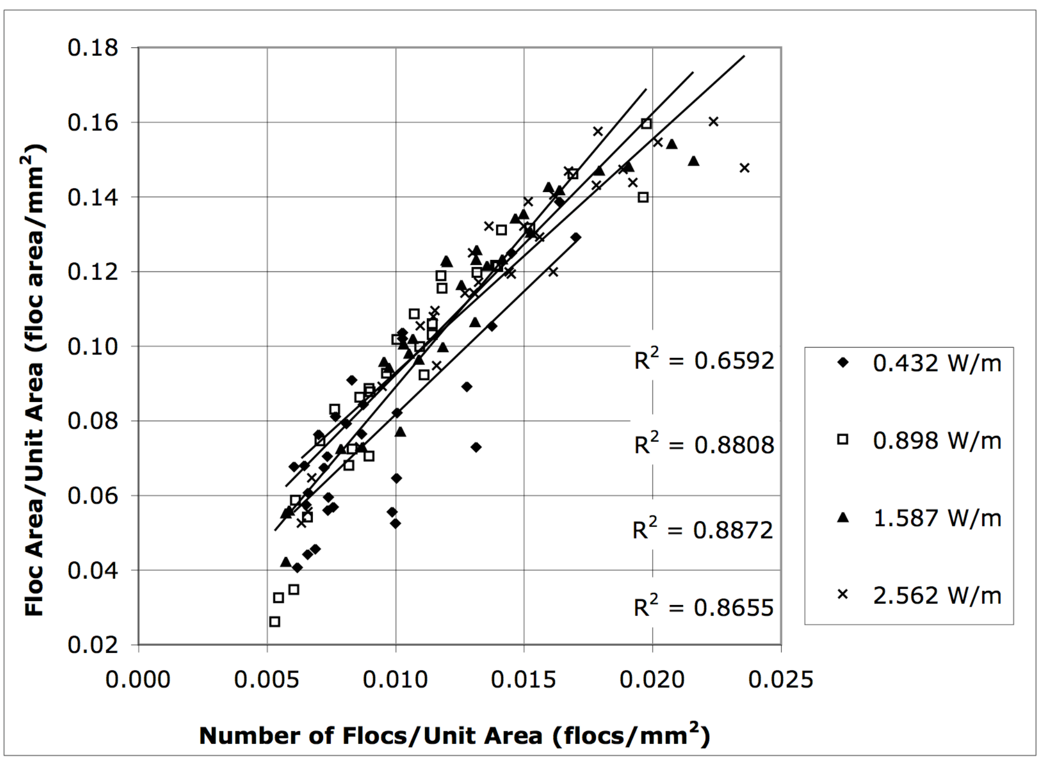

Figure 54. Floc area per unit area versus number of flocs per unit area. Energy dissipation effect.

Separating the experimental conditions out of the data in figures 53 and 54 illuminated more trends that were not apparent when all the data were taken as equivalent. Figure 53 clearly shows that differences exist between retention aid dosage levels. Each dosage level resides in its own portion of the graph. Fitted linear regressions of the data show an evenly spaced increase in the slope of the data as retention aid dosage is increased. The graph highlights the results already seen from the individual area and number graphs, but in a more efficient manner. The question that needs to be asked: is the data really three separate curves or one relationship across all experimental levels? As seen before, the energy dissipation level affects area and number to a lesser degree than retention aid. Figure 54 shows that the data for each energy level exists throughout the entire curve in contrast to the retention aid data being grouped in their own regions.

<u>Formation Number</u>

The images used to measure formation number were the same as the images used in the morphological operations. Post-processing of the images for formation number purposes was different from the morphological operations and was outlined in the experimental methods section.

Formation numbers do not describe size or numbers of flocs in a system. Instead, formation numbers describe the variability of the mass distribution in the system. If the mass distribution is highly variable (e.g. there are a lot of flocs) the formation number is going to be higher than if the mass distribution was very uniform (fewer or no flocs).

Figures 55 through 61 show how formation number varies with time elapsed from the inlet of the flow channel.

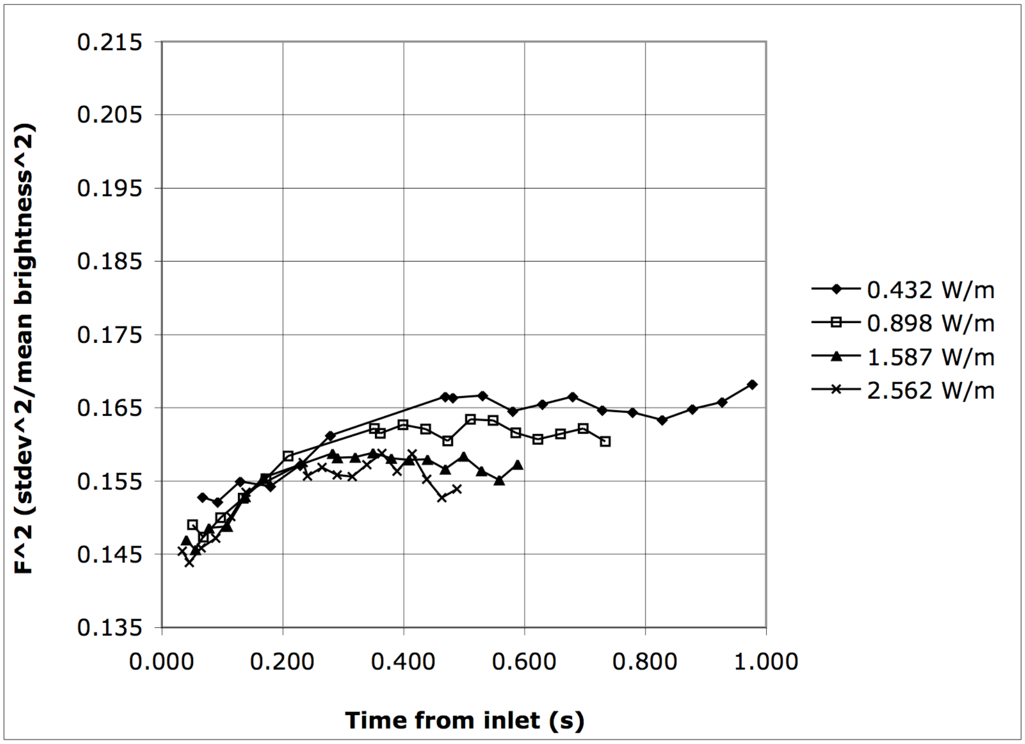

Figure 55. Formation number squared versus time from inlet as a function of energy dissipation at 0 lb/ton retention aid dosage.

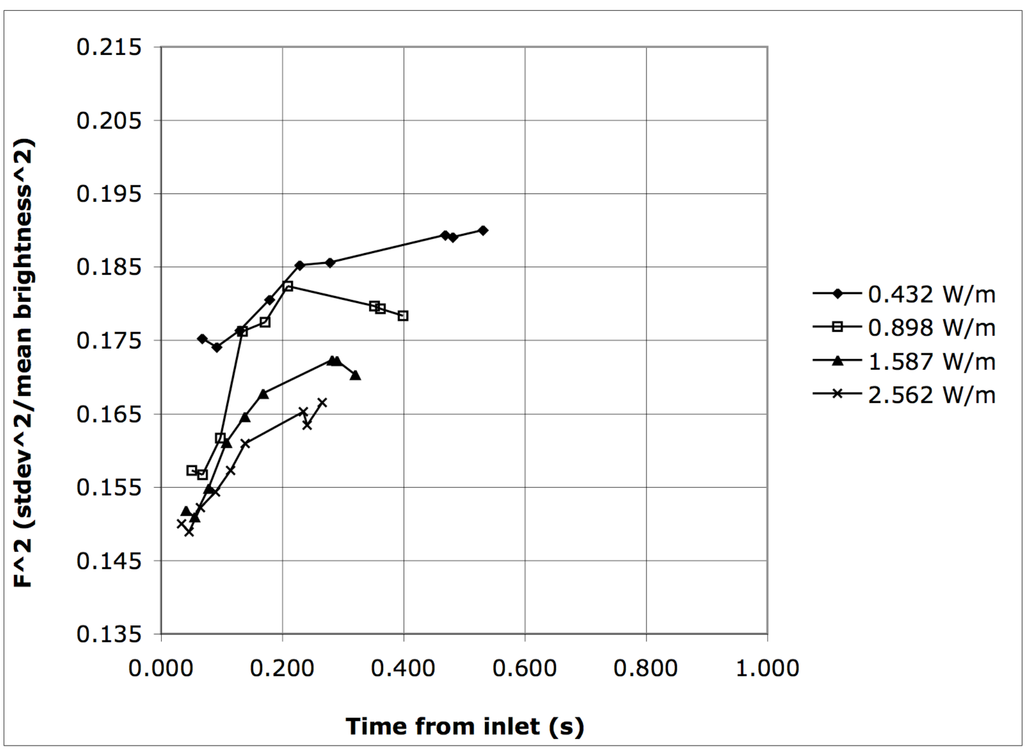

Figure 56. Formation number squared versus time from inlet as a function of energy dissipation at 1 lb/ton retention aid dosage.

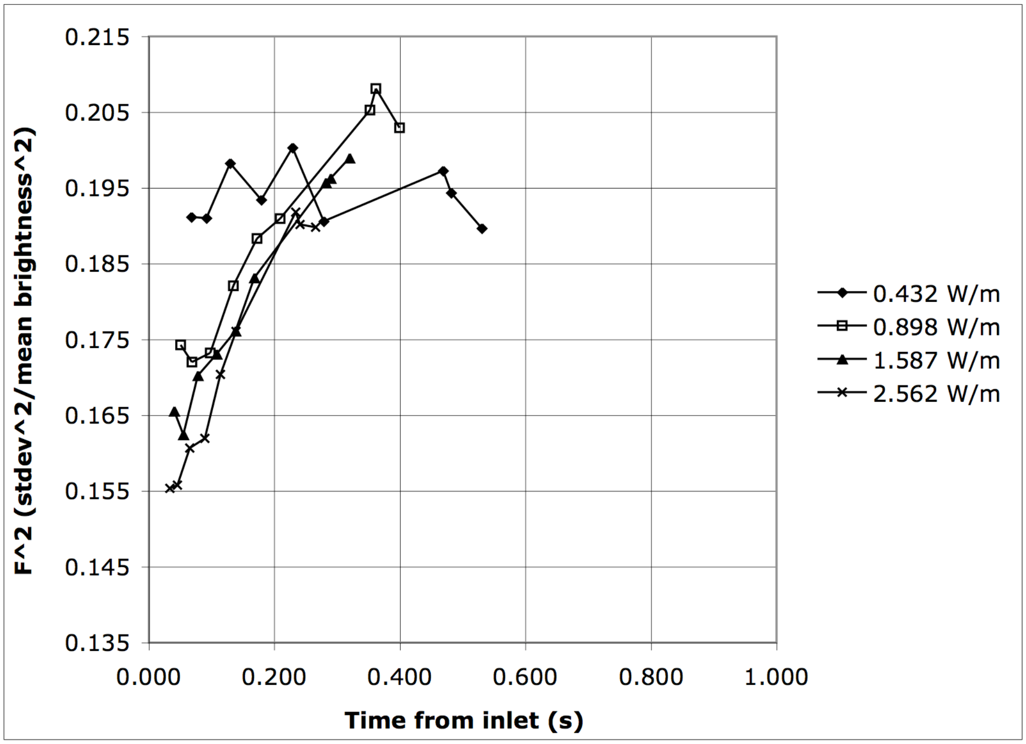

Figure 57. Formation number squared versus time from inlet as a function of energy dissipation at 2 lb/ton retention aid dosage.

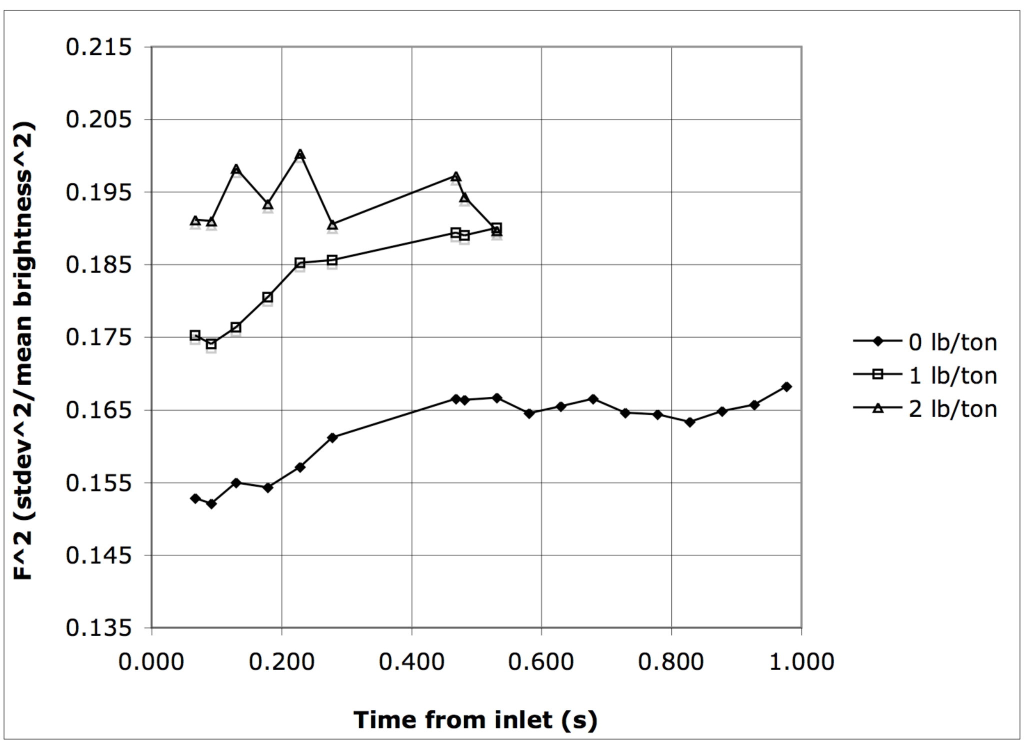

Figure 58. Formation number squared versus time from inlet as a function of retention aid dosage at 0.432 W/m energy dissipation.

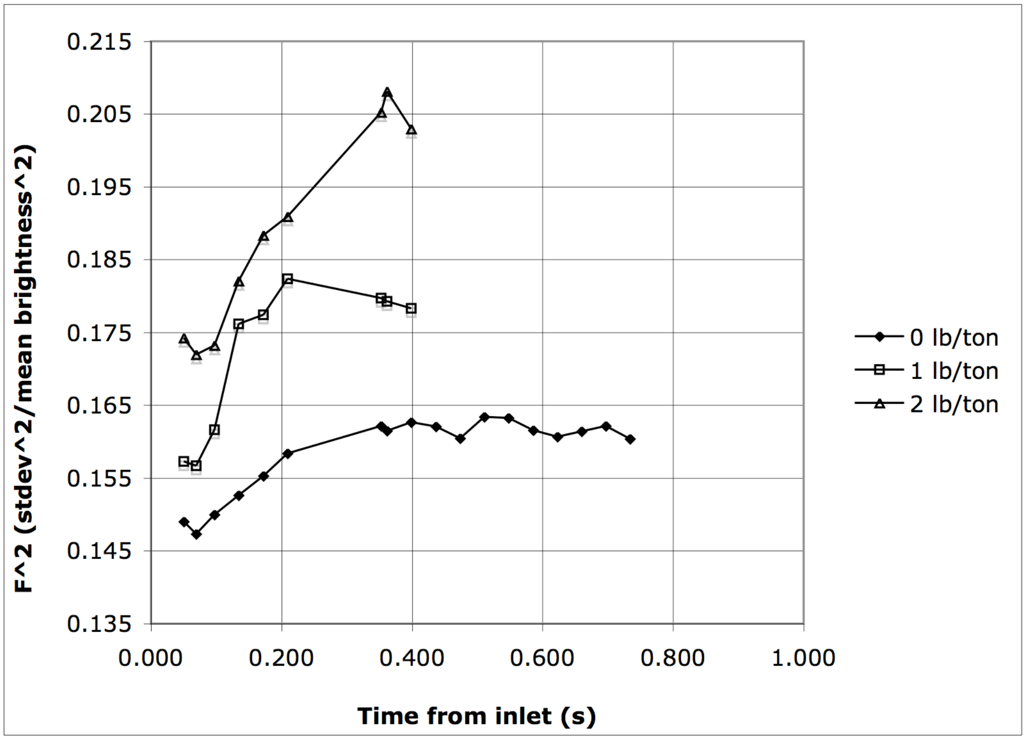

Figure 59. Formation number squared versus time from inlet as a function of retention aid dosage at 0.898 W/m energy dissipation.

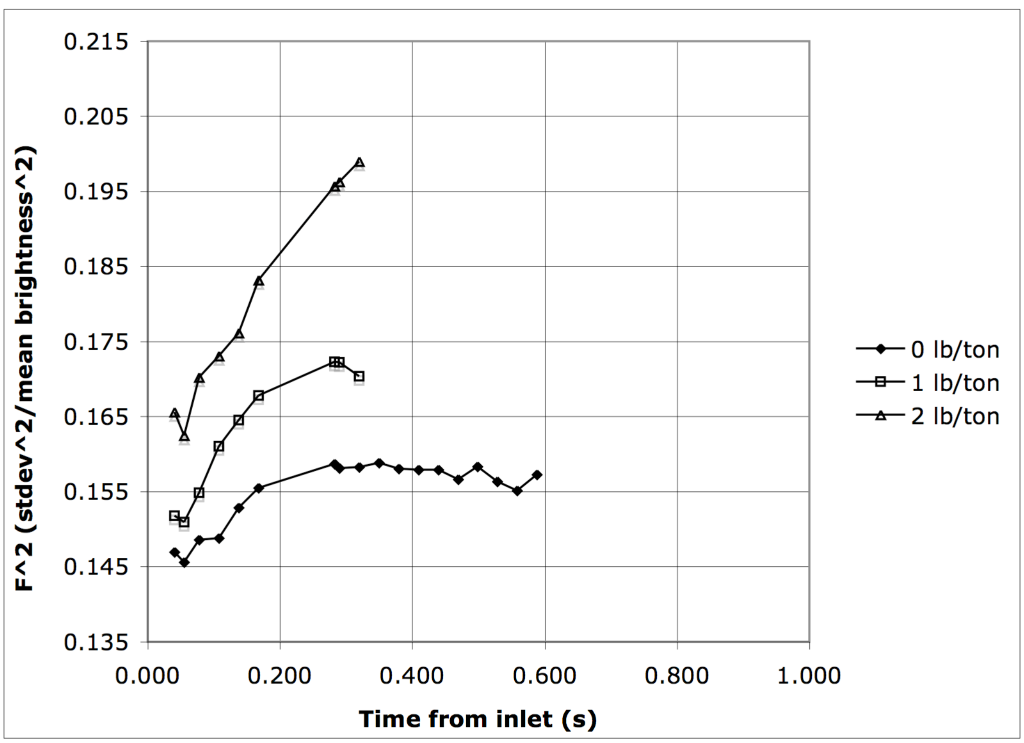

Figure 60. Formation number squared versus time from inlet as a function of retention aid dosage at 1.587 W/m energy dissipation.

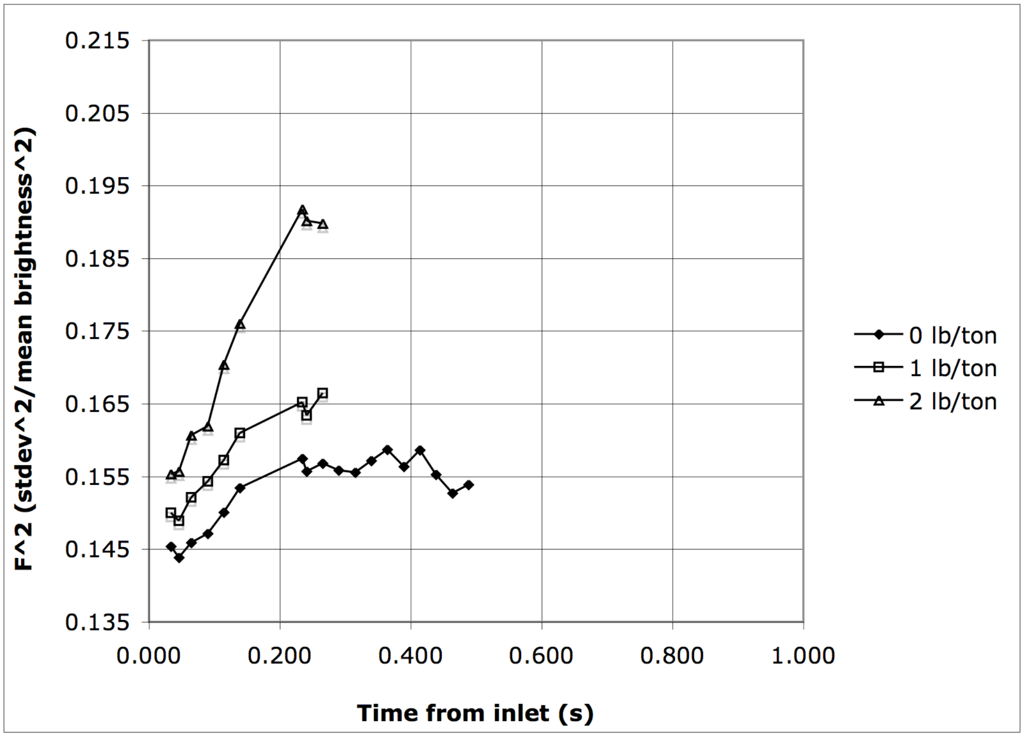

Figure 61. Formation number squared versus time from inlet as a function of retention aid dosage at 2.562 W/m energy dissipation.

Remembering that a lower formation number corresponds to a more uniform mass distribution, it can be seen that figures 55 through 61 displayed two reproducible, reasonable trends. First, higher mechanical energy dissipation results in a more uniform mass distribution. Second, lower retention aid dosage results in a more uniform mass distribution.

Relations Between Morphology and Formation Number

Two methods have been explored that serve to explain the flocculation level or uniformity of a mass distribution. It may be instructive to see how the two methods predict each other. Figures 62 through 67 look at the relationships between formation number, floc area, and floc number.

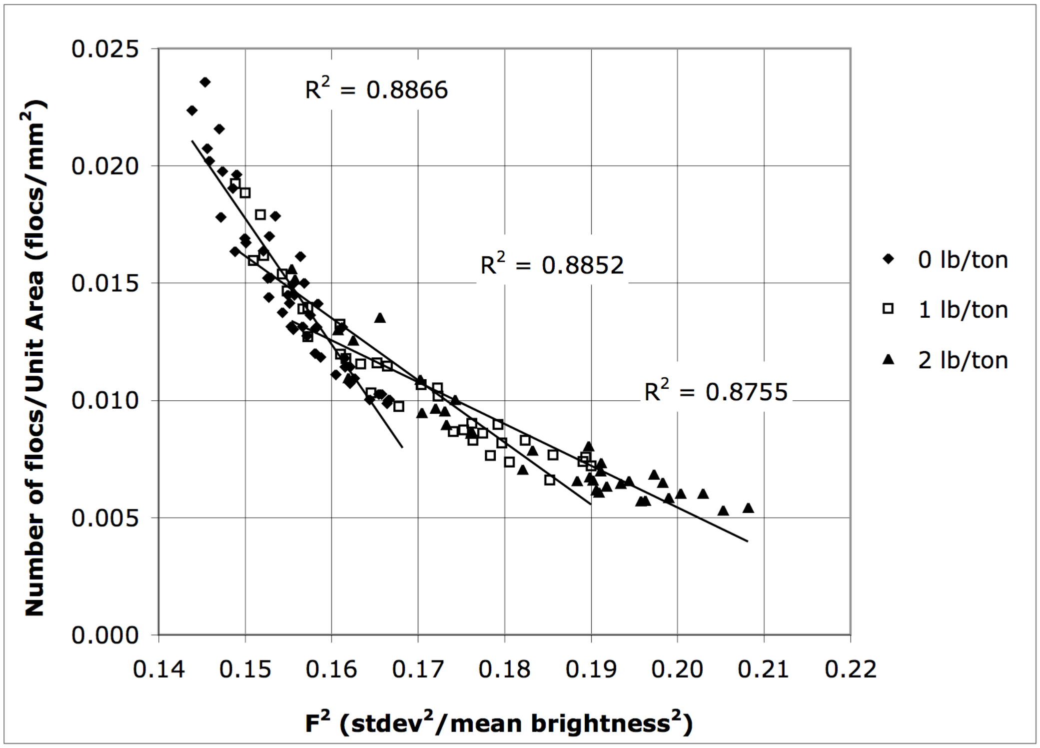

Figure 62. Number of flocs per unit area versus formation number squared as a function of retention aid dosage..

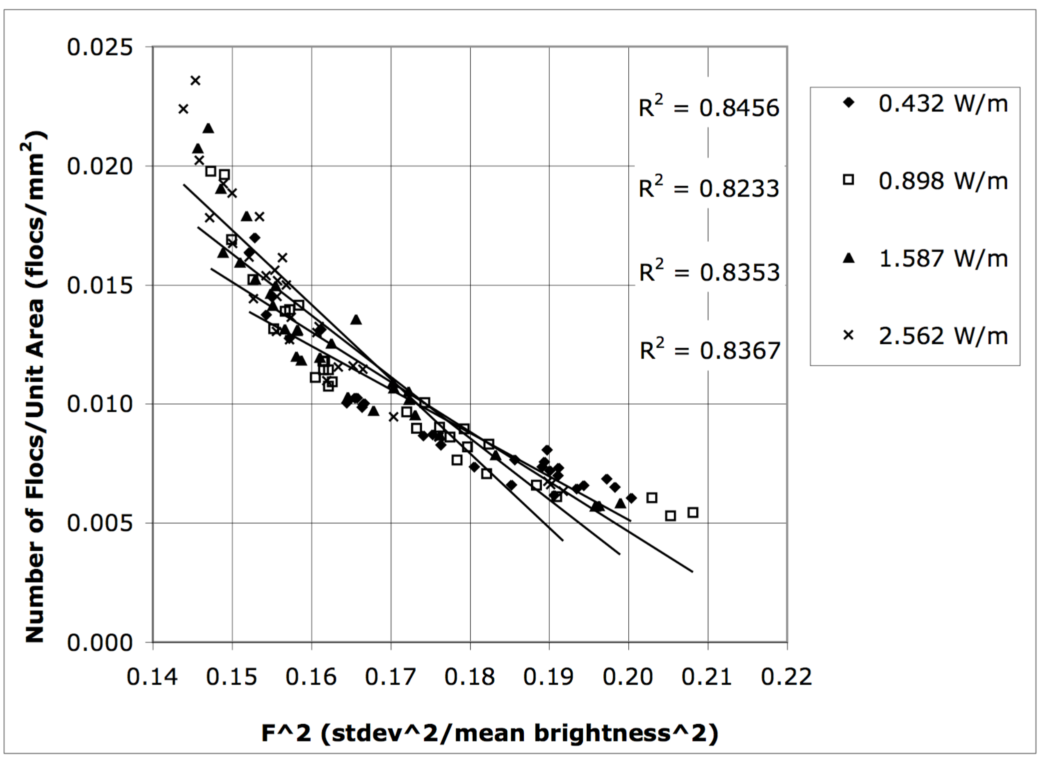

Figure 63. Number of flocs per unit area versus formation number squared as a function of energy dissipation.

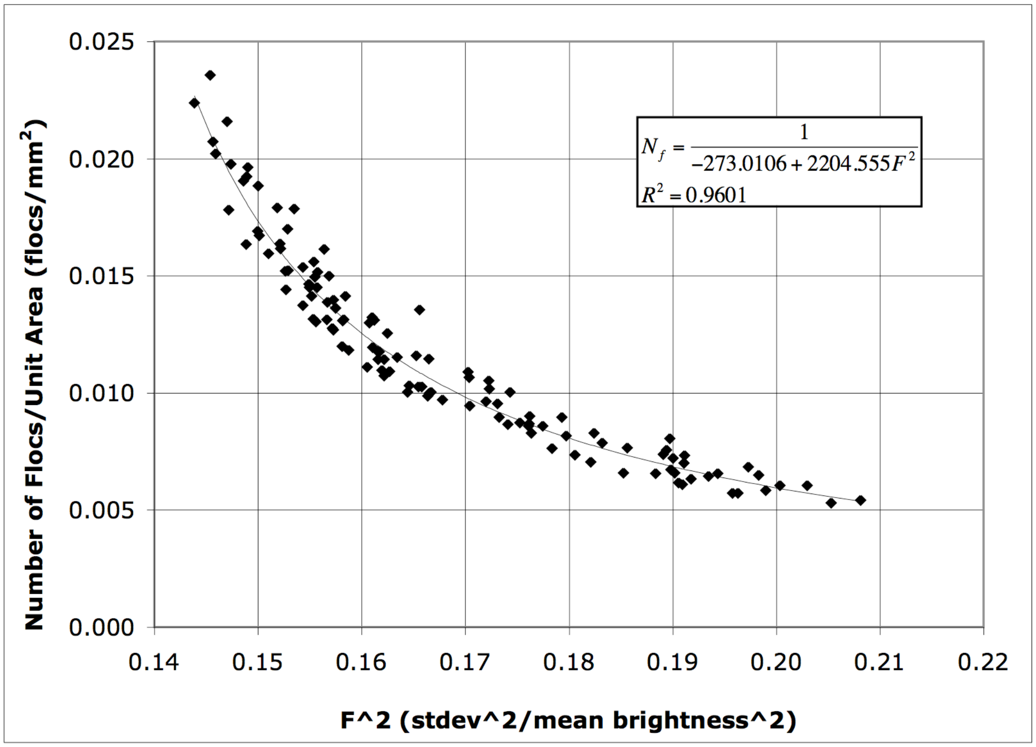

Figure 64. Number of flocs per unit area versus formation number squared. Composite of all experimental runs.

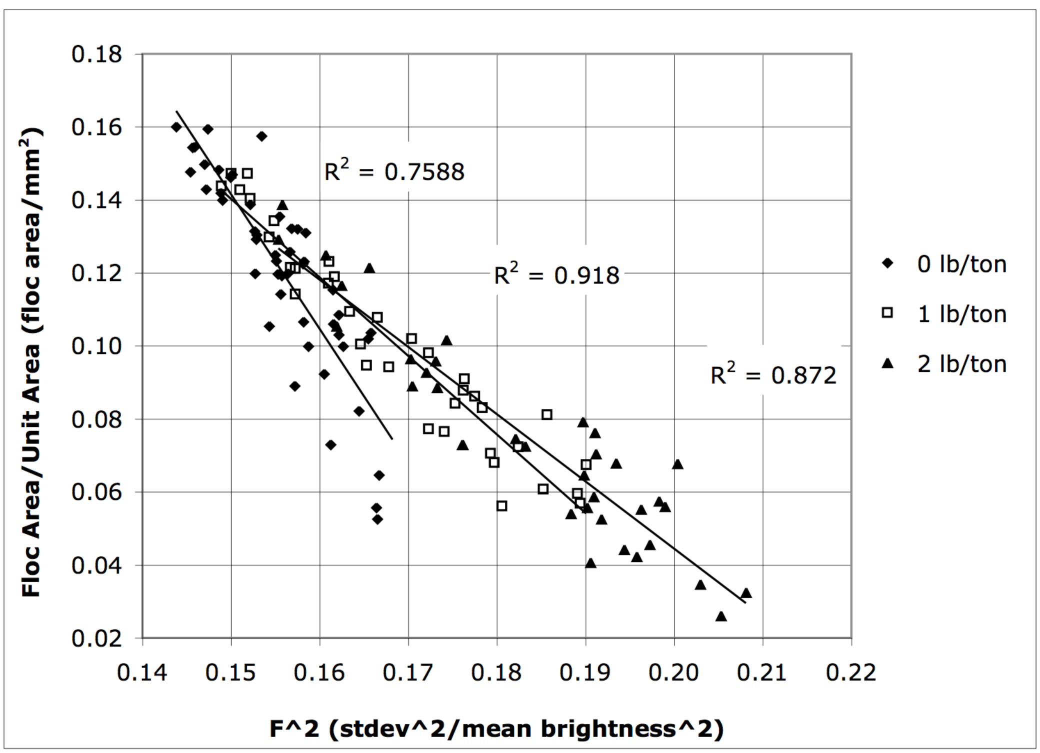

Figure 65. Floc area per unit area versus formation number squared as a function of retention aid dosage.

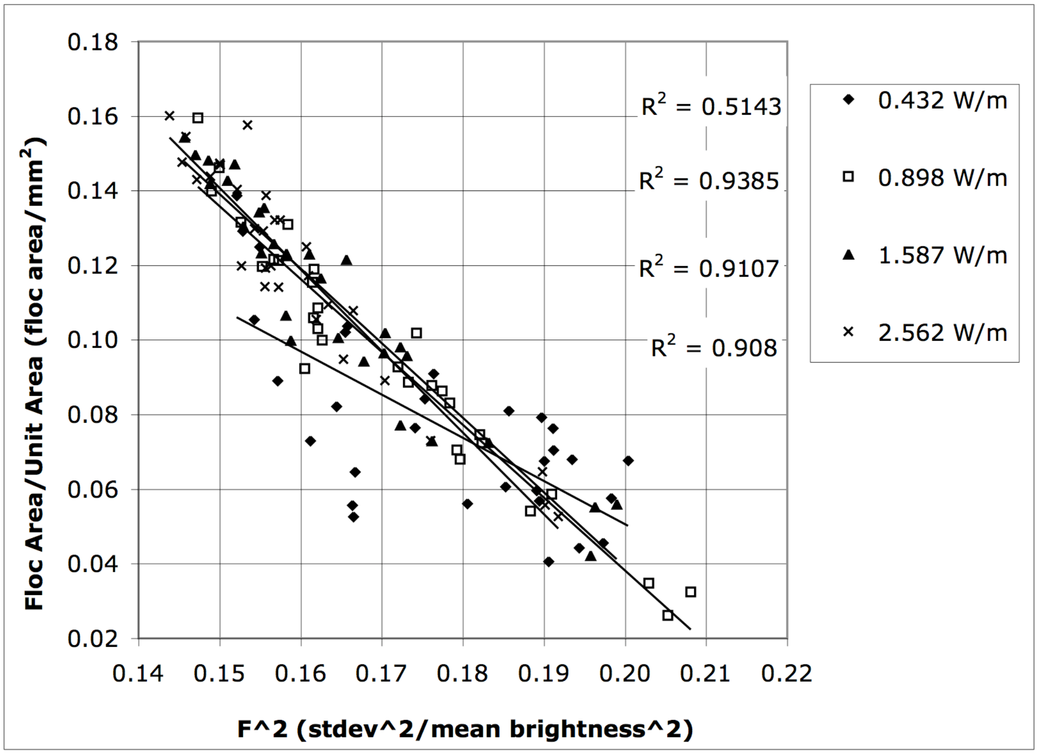

Figure 66. Floc area per unit area versus formation number squared as a function of energy dissipation.

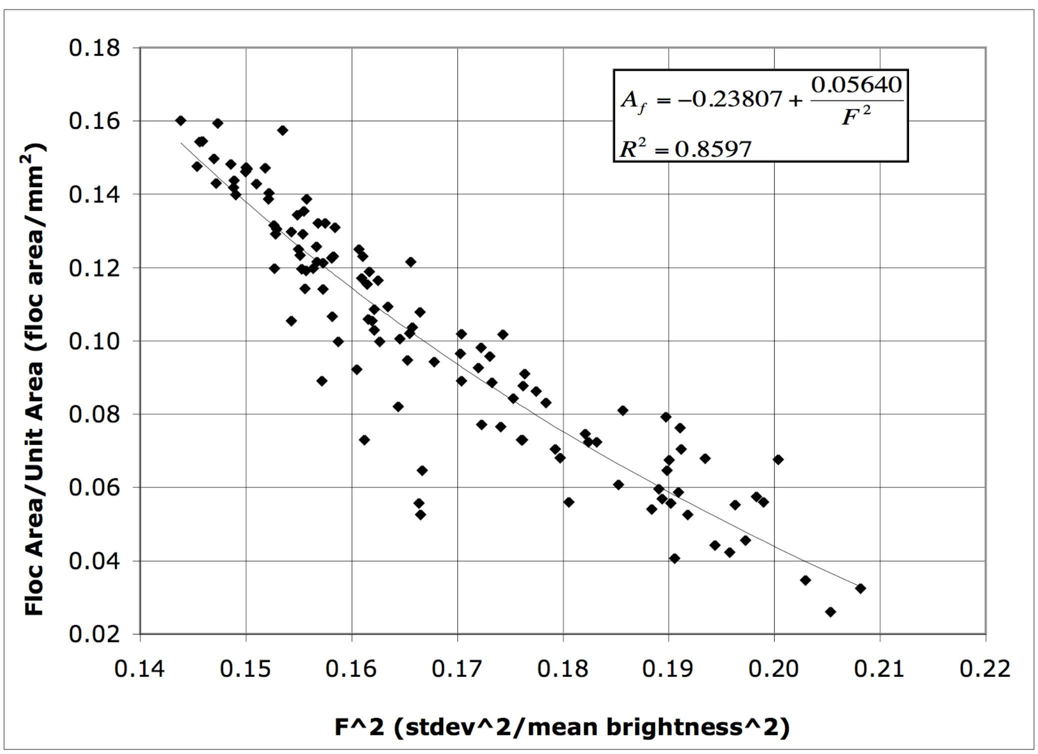

Figure 67. Floc area per unit area versus formation number squared. Composite of al experimental runs.

Formation number is a measure of the variability of mass distribution in the system. Because of this, it should come as no surprise that some type of relationship exists between formation number and the area and number of flocs. Here again, is the data a relationship that reaches across the different experimental levels (i.e. retention aid dosage and mechanical energy dissipation) or a composite of several different curves from each experimental setting?

Fourier Transform Analysis

The same raw images used in the preceding methods were used in the Fourier transform analysis. A few differences are worth noting though. First, because the images needed to be cropped differently, the exact images analyzed using the fast Fourier transform (FFT) were different from the cropped images in the morphological or formation number methods. Because of time constraints and the amount of time needed to analyze using FFT (e.g. no batch methods were available), it was decided that instead of averaging 40 images for each experimental setting, only five would be averaged. Using the FFT method allowed collection of average MD (flow direction in this case) floc length. Figures 68 through 74 summarize data collected using the FFT method.

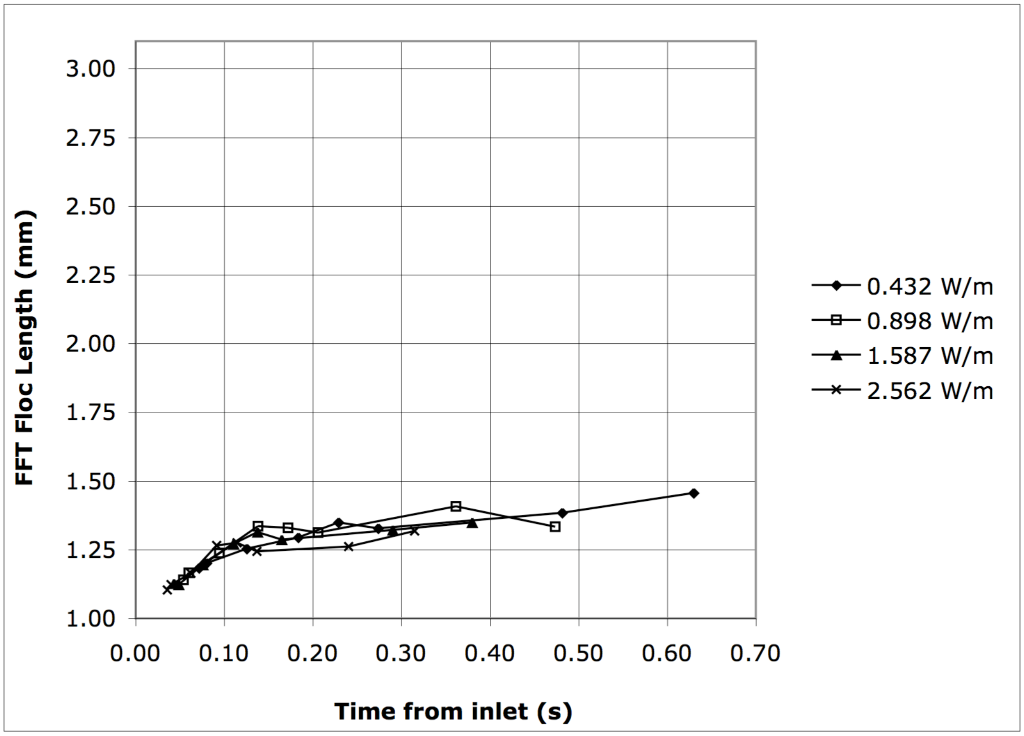

Figure 68. FFT floc length versus time from inlet as a function of energy dissipation at 0 lb/ton retention aid dosage.

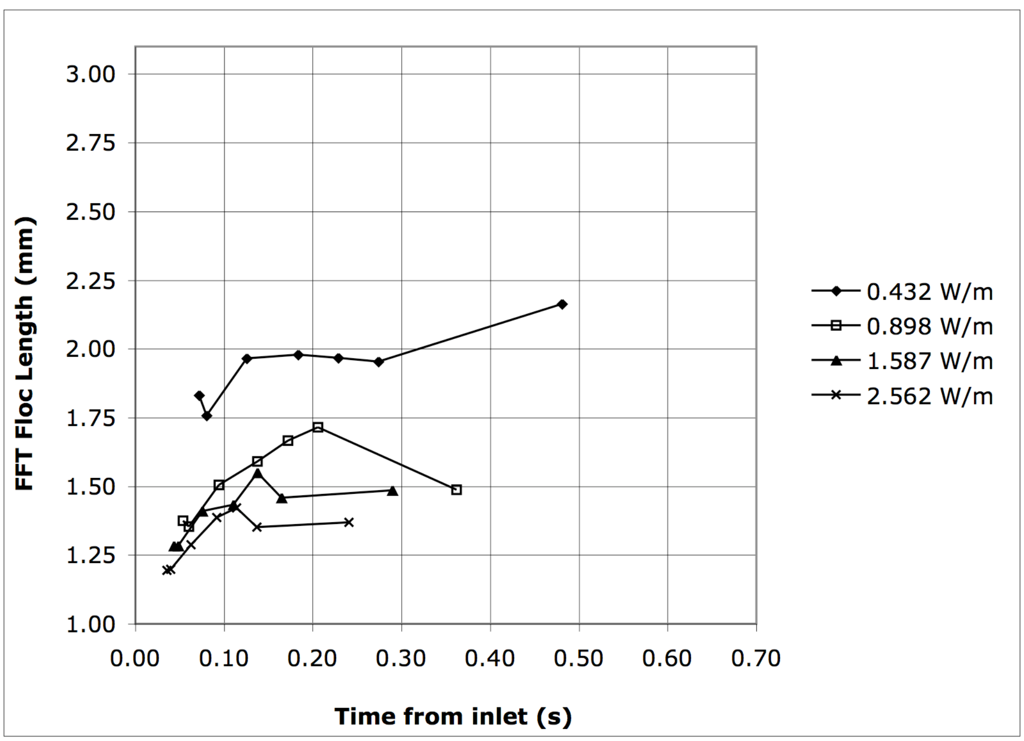

Figure 69. FFT floc length versus time from inlet as a function of energy dissipation at 1 lb/ton retention aid dosage.

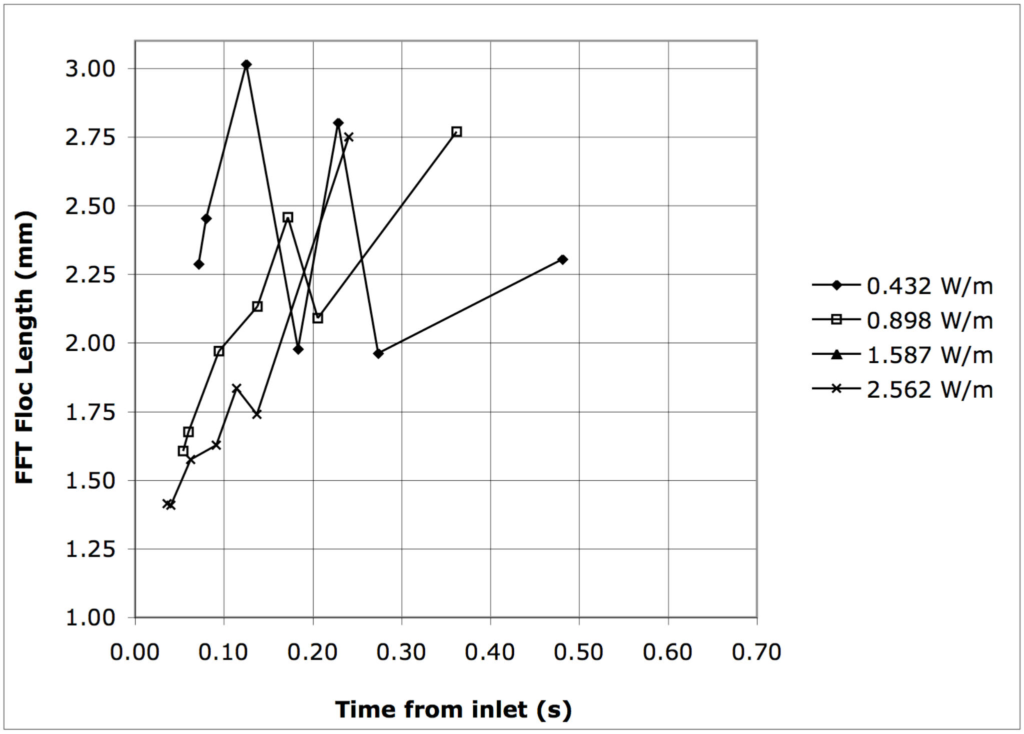

Figure 70. FFT floc length versus time from inlet as a function of energy dissipation at 2 lb/ton retention aid dosage.

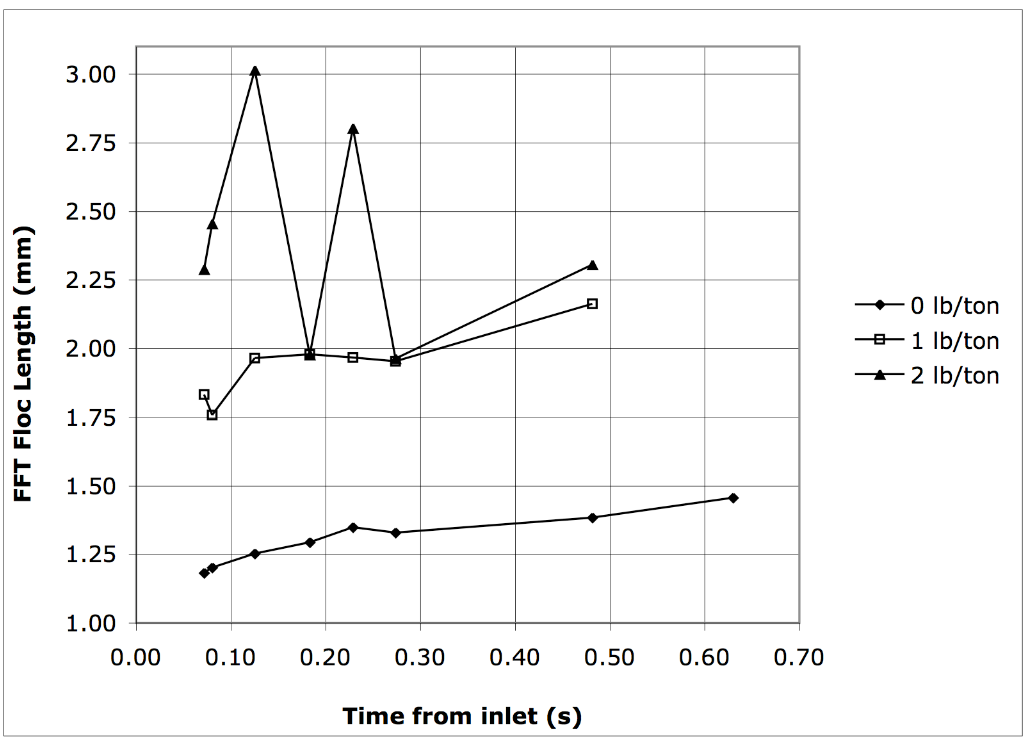

Figure 71. FFT floc length versus time from inlet as a function of retention aid dosage at 0.432 W/m energy dissipation.

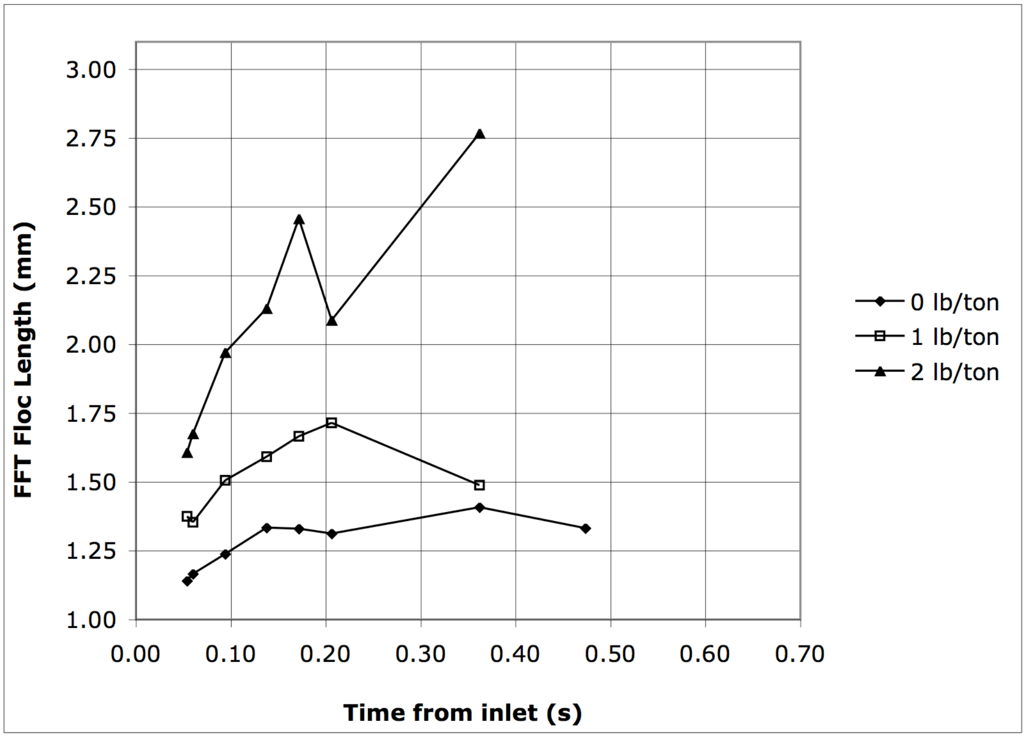

Figure 72. FFT floc length versus time from inlet as a function of retention aid dosage at 0.898 W/m energy dissipation.

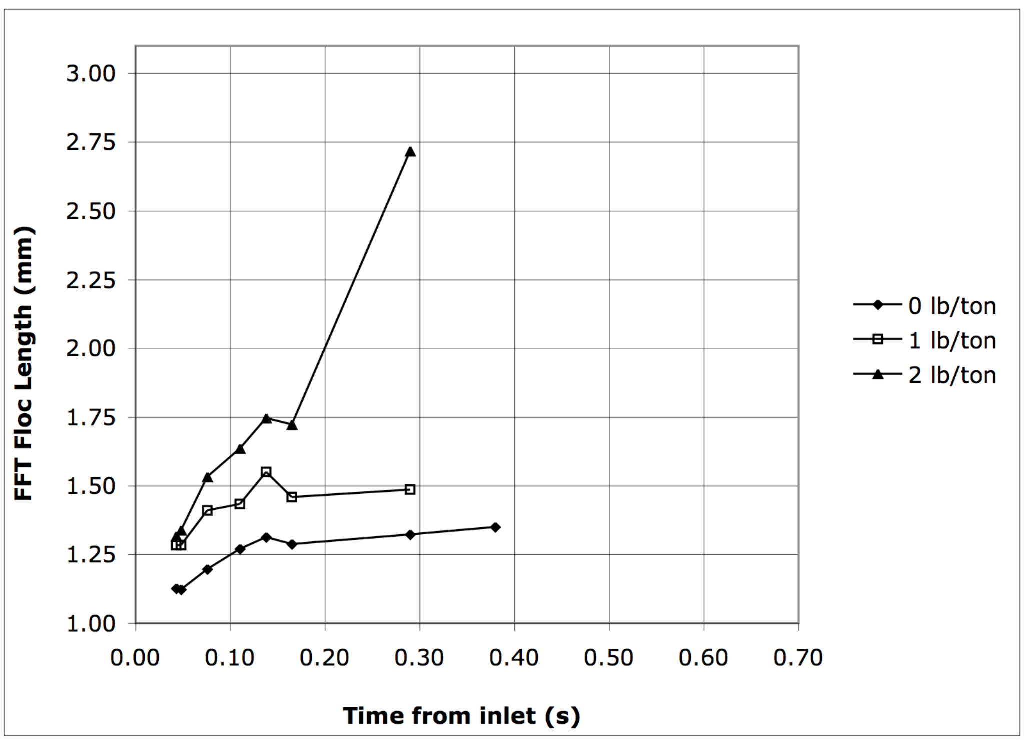

Figure 73. FFT floc length versus time from inlet as a function of retention aid dosage at 1.587 W/m energy dissipation.

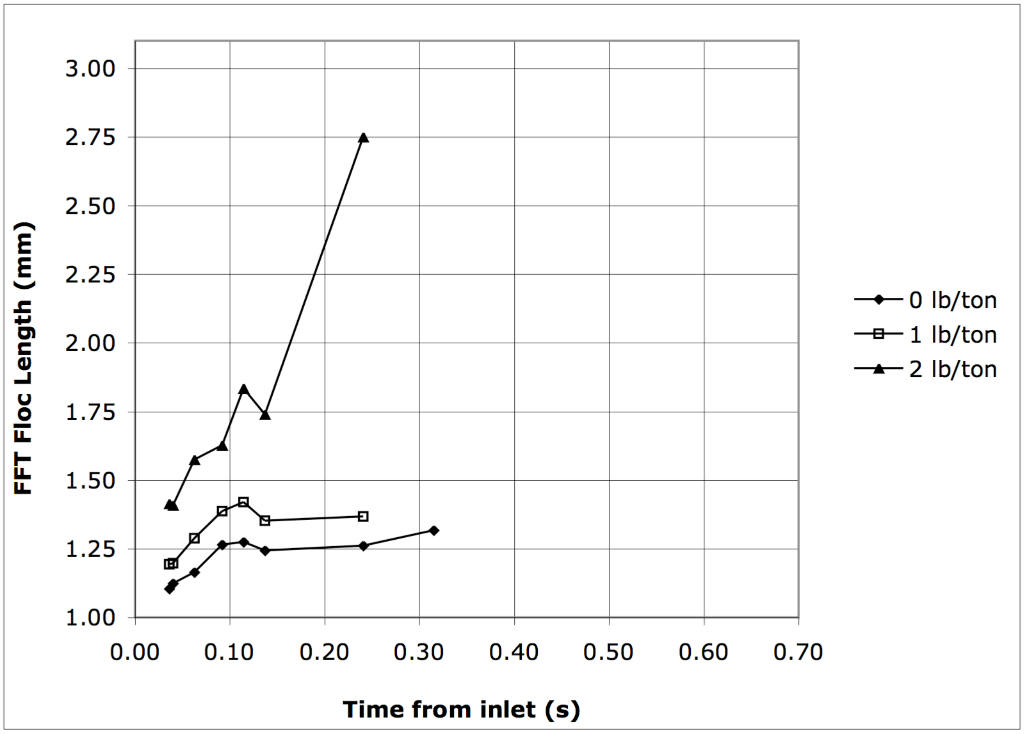

Figure 74. FFT floc length versus time from inlet as a function of retention aid dosage at 2.562 W/m energy dissipation.

Figures 68 through 74 displayed very similar trends to those from the morphological and formation number data. Again we see that increased retention aid dosage results in increased floc size. The addition of retention aid seems to cause problems with measuring floc size as seen in figures 70 and 71. This data shows only a weak indication that increased mechanical energy dissipation decreases the floc size.

DISCUSSION

Figures 52 through 54 summarized floc area and floc number data in an effort to find a relation between the two. It may be instructive to see what happens when area per floc data is plotted along the same data and curves in figures 52 through 54. Using the best fit equation in figure 75, it is possible to calculate a predicted area/floc curve which is displayed in the chart. What becomes apparent is that a maximum area/floc size of approximately 9.1 mm^2 is predicted. Using the actual data to confirm this prediction yields interesting results which are displayed in figures 76 through

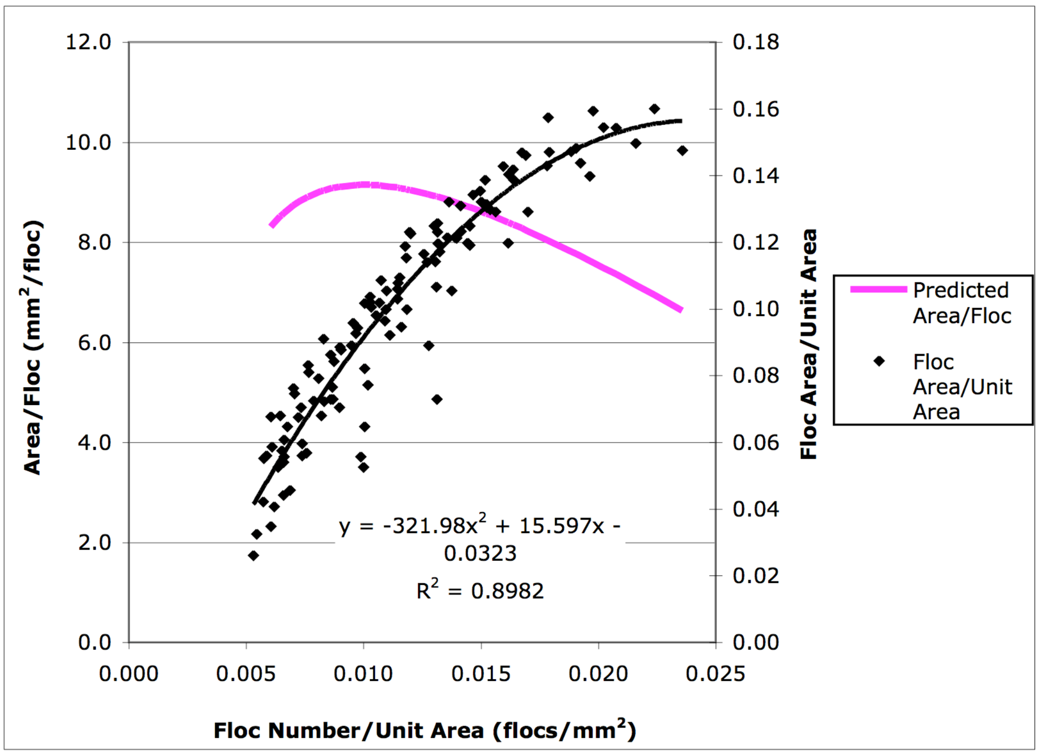

Figure 75. Floc area versus floc number and predicted area/floc versus floc number.

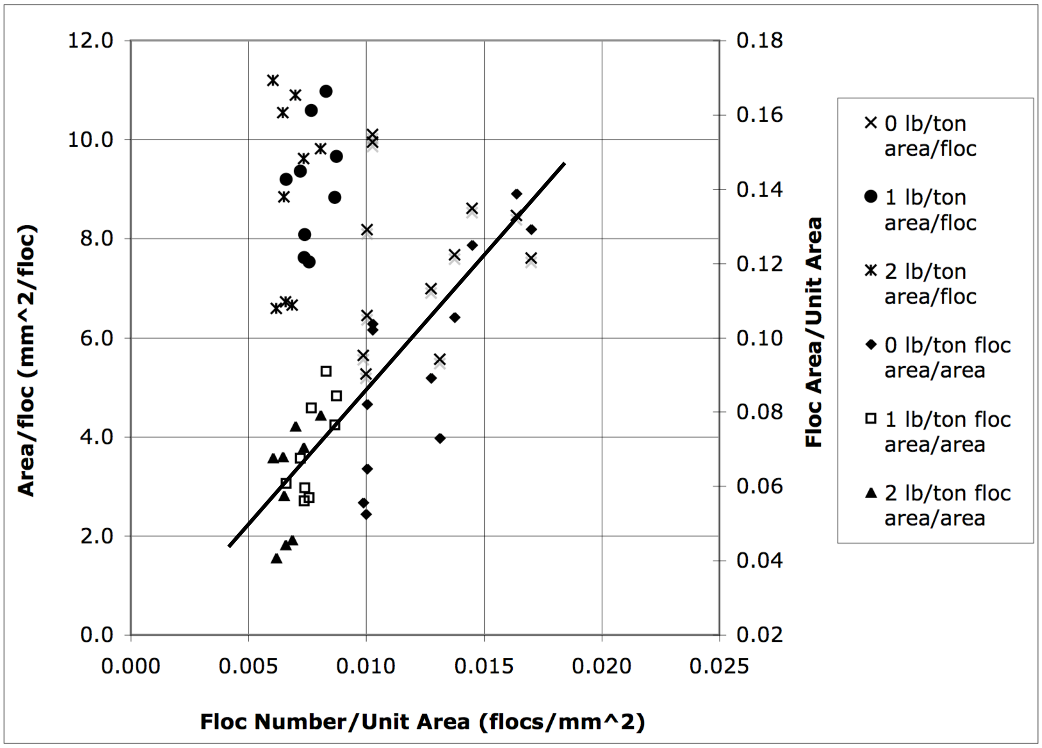

Figure 76. Floc size data and retention aid effect at 0.432 W/m energy dissipation.

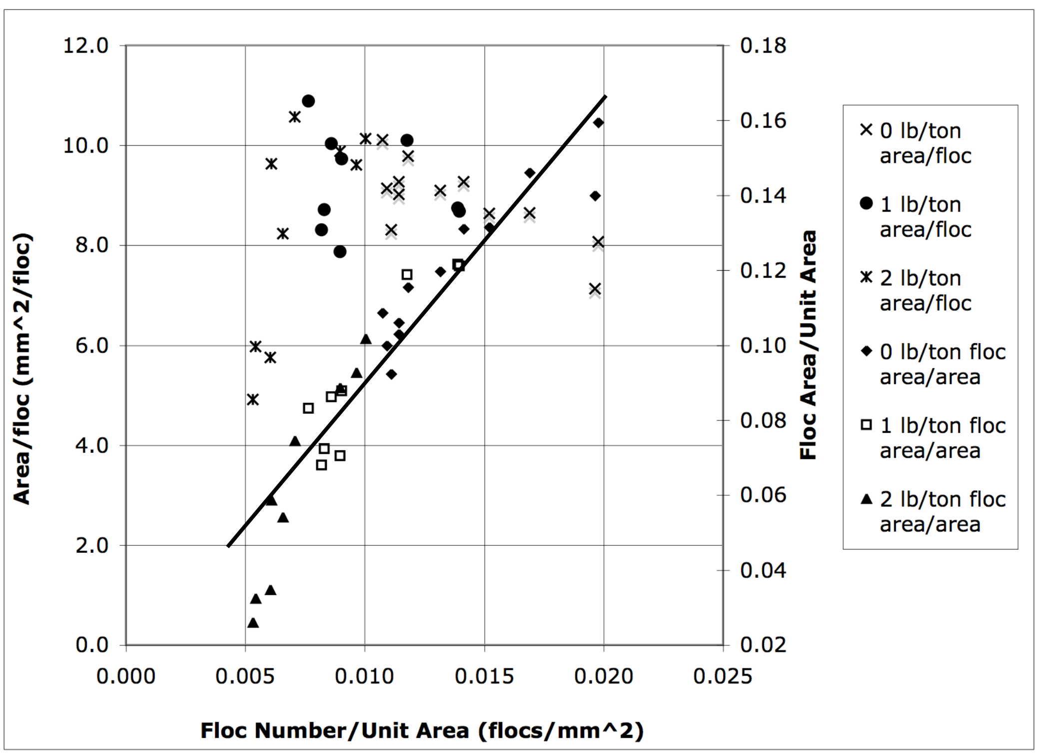

Figure 77. Floc size data and retention aid effect at 0.898 W/m energy dissipation.

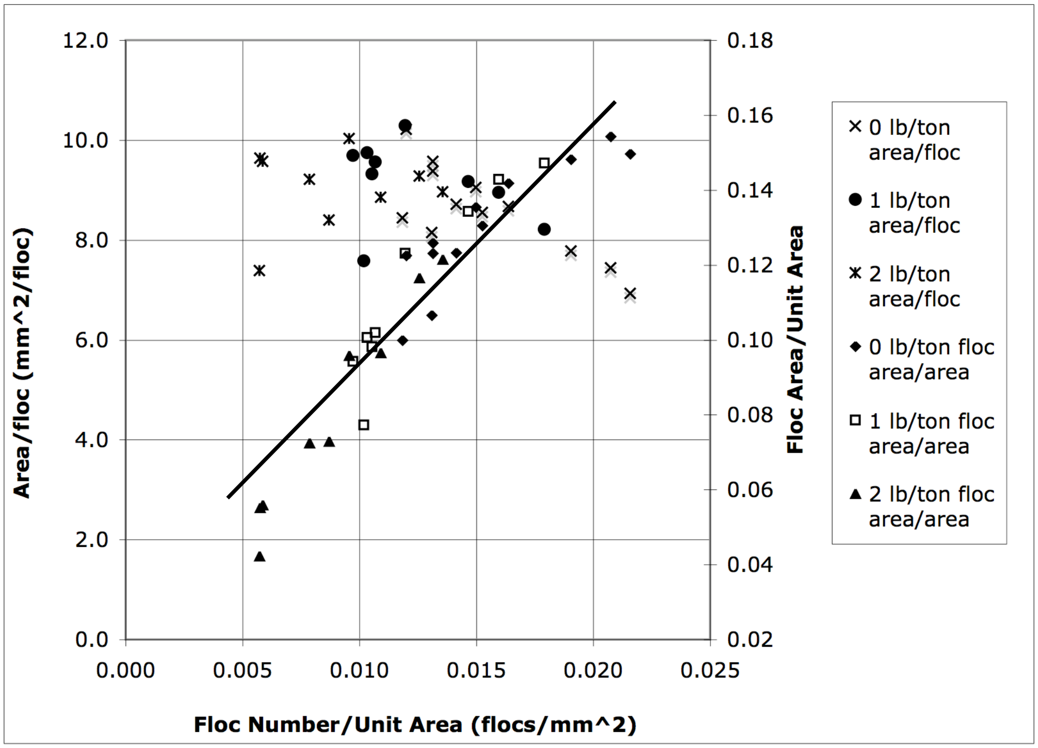

Figure 78. Floc size data and retention aid effect at 1.587 W/m energy dissipation.

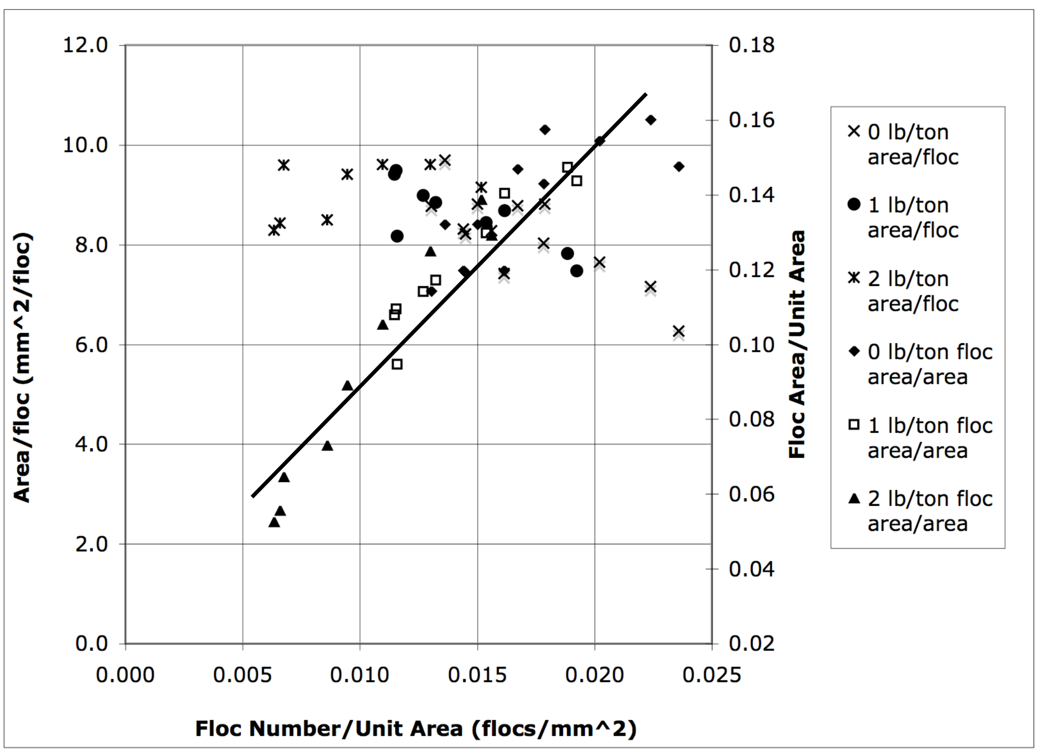

Figure 79. Floc size data and retention aid effect at 2.562 W/m energy dissipation.

Figures 76 through 79 were plotted by taking each retention aid dosage level as a separate data set. This allowed seeing if the retention aid relationship was different between energy level settings. What was seen is that regardless of energy dissipation level, increasing the retention aid dosage had the same effect of decreasing floc area while at the same time decreasing the floc number. The real story, however, is in the area per floc data which does indeed show a maximum floc size. Maximum floc size varies little with energy dissipation, but the point at which the maximum occurs varies. Notice that the maximum shifts right along the floc number axis as the energy dissipation is increased. The maximum floc area is 9.1 mm^2 and this corresponds to an apparent floc diameter of 3.4 mm.

What is the significance of this floc diameter? The FQA length-weighted fiber length for the pulp used in this study was 2.28 mm as was shown in Table I. As covered earlier, the importance of fiber length has not gone unnoticed (Mason, 1954; Kerekes and Schell, 1991). In fact, Wrist states that floc sizes are characteristic of the lengths of the fibers that make up the floc (1961).

Physical Interpretation

Up until this point, there has been no comparison between the data and what is actually shown visually in the collected images. To begin, trends from the images need to be established. This will be accomplished by inspecting key images from specific experimental settings. Once these trends are established, a comparison will be made to the data to evaluate the ability of the image analysis routines.

The next three sets of images compare different experimental settings at three different points in the channel. Figure 80 compares the experimental extremes of the study. Figure 81 compares the effect of energy dissipation, and figure 82 compares the effect of retention aid dosage. Recorded for each image is the floc area per unit image area (A_f), the number of flocs per unit area (N_f), and the formation number (F^2).

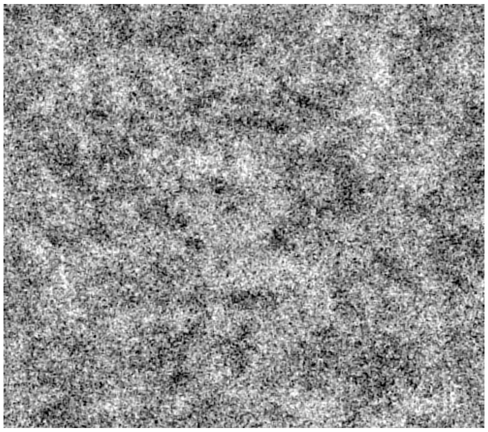

(a) Inlet, 2.562 W/m, 0 lb/ton;
A_f=0.148, N_f=0.024, F^2=0.145

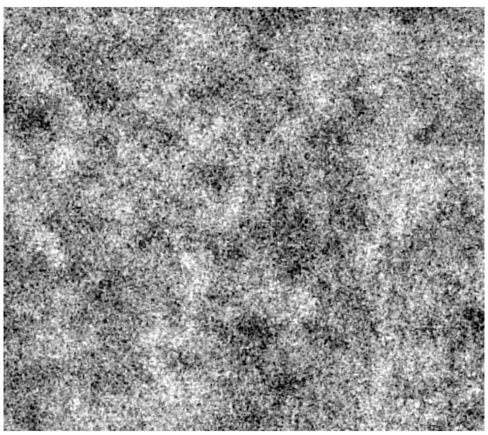

(b) 200 mm downstream, 2.562 W/m, 0 lb/ton;
A_f=0.147, N_f=0.017, F^2=0.150

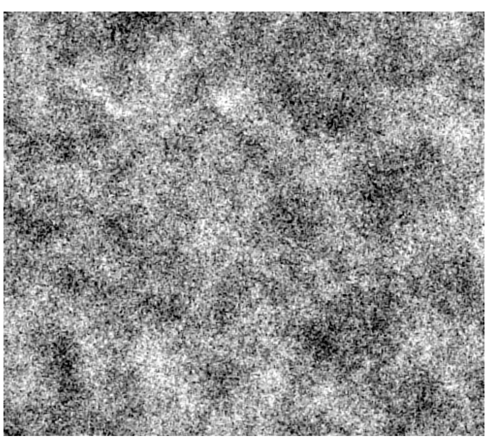

(c) 421 mm downstream, 2.562 W/m, 0 lb/ton;
A_f=0.119, N_f=0.015, F^2=0.156

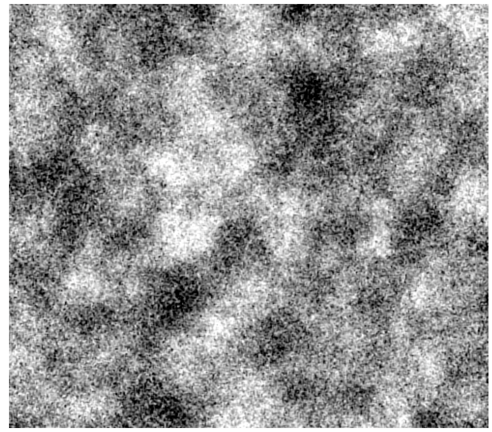

(d) Inlet, 0.432 W/m, 2 lb/ton
A_f=0.071, N_f=0.007, F^2=0.191

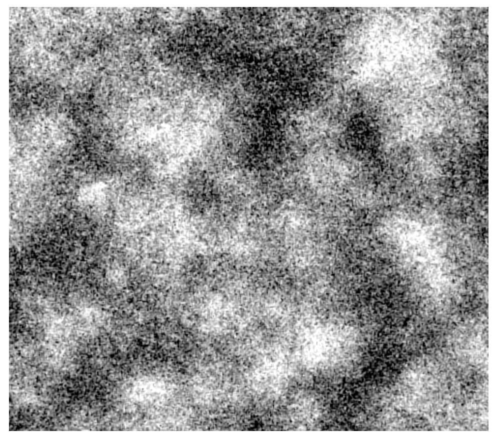

(e) 200 mm downstream, 0.432 W/m, 2 lb/ton
A_f=0.068, N_f=0.006, F^2=0.200

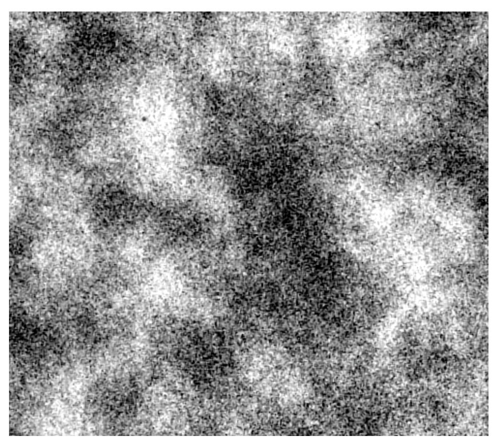

(f) 421 mm downstream, 0.432 W/m, 2 lb/ton
A_f=0.060, N_f=0.007, F^2=0.194

Figure 80. Visual flocculation state comparison between experimental extremes.

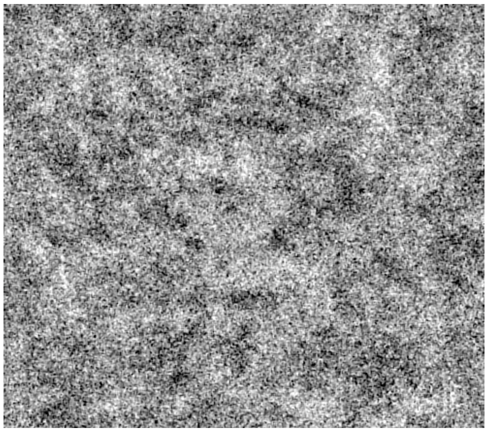

(a) Inlet, 2.562 W/m, 0 lb/ton
A_f=0.148, N_f=0.024, F^2=0.145

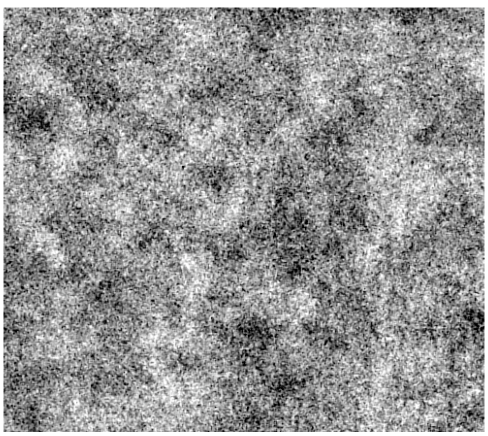

(b) 200 mm downstream, 2.562 W/m, 0 lb/ton
A_f=0.147, N_f=0.017, F^2=0.150

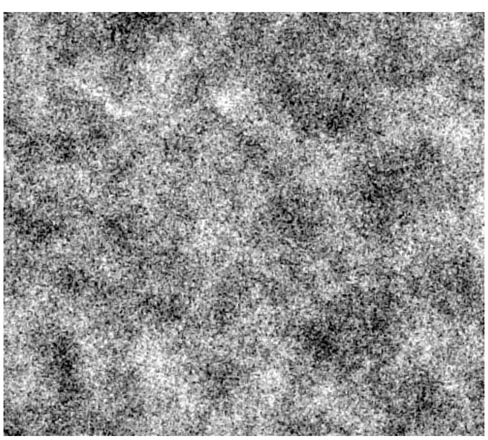

(c) 421 mm downstream, 2.562 W/m, 0 lb/ton
A_f=0.119, N_f=0.015, F^2=0.156

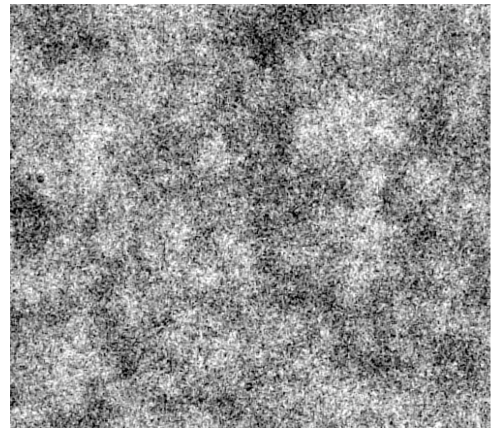

(d) Inlet, 0.432 W/m, 0 lb/ton
A_f=0.129, N_f=0.017, F^2=0.153

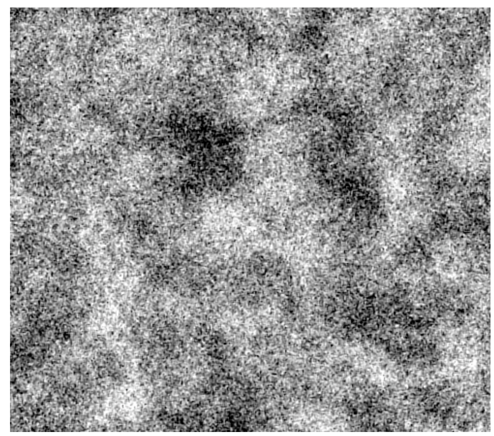

(e) 200 mm downstream, 0.432 W/m, 0 lb/ton
A_f=0.089, N_f=0.013, F^2=0.157

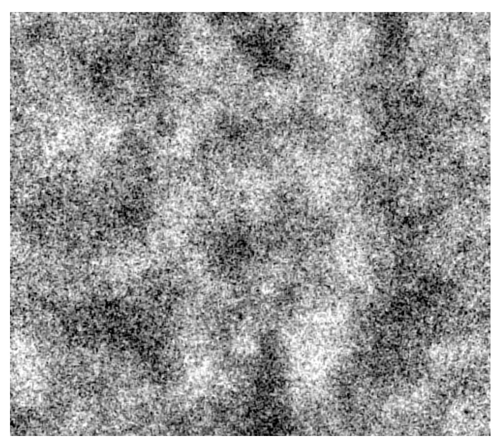

(f) 421 mm downstream, 0.432 W/m, 0 lb/ton
A_f=0.056, N_f=0.010, F^2=0.166

Figure 81. Visual flocculation.state comparing effect of power dissipation.

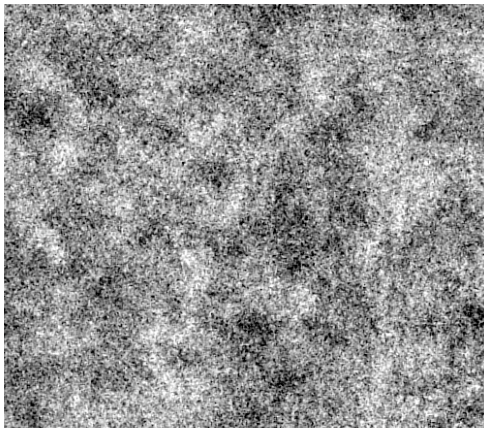

(a) 200 mm downstream, 2.562 W/m, 0 lb/ton
A_f=0.147, N_f=0.017, F^2=0.150

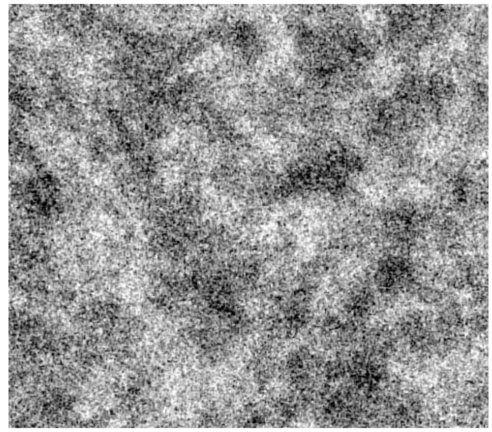

(b) 200 mm downstream, 2.562 W/m, 1 lb/ton
A_f=0.114, N_f=0.013, F^2=0.157

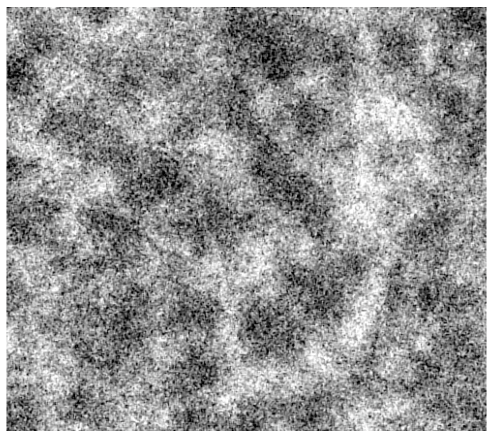

(c) 200 mm downstream, 2.562 W/m, 2 lb/ton
A_f=0.089, N_f=0.009, F^2=0.170

Figure 82. Visual flocculation.state comparing effect of retention aid dosage.

In looking at figures 80 through 82 it becomes apparent that floc size is definitely affected by retention aid dosage, energy dissipation, and position in the imaging channel. Floc growth is what is physically happening in the channel and this occurs while both A_f and N_f decrease. How can the area per floc grow while both the total floc area and total floc number decrease? A first step in answering this question is to confirm that the data does indeed display floc growth in the same fashion. Figures 83 through 85 display floc equivalent diameter distributions at the experimental extremes. These distributions are a measure of what is seen in figure 80.

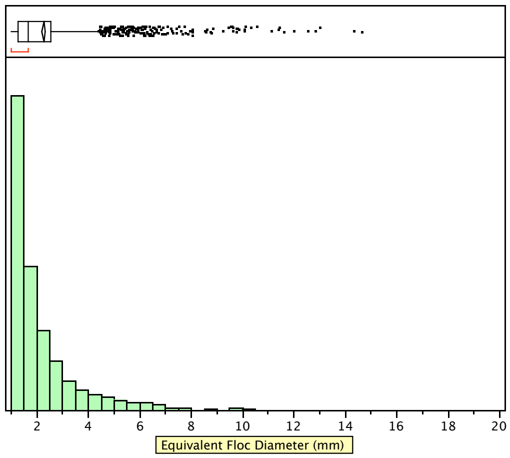

(a) Inlet, 2.562 W/m, 0 lb/ton

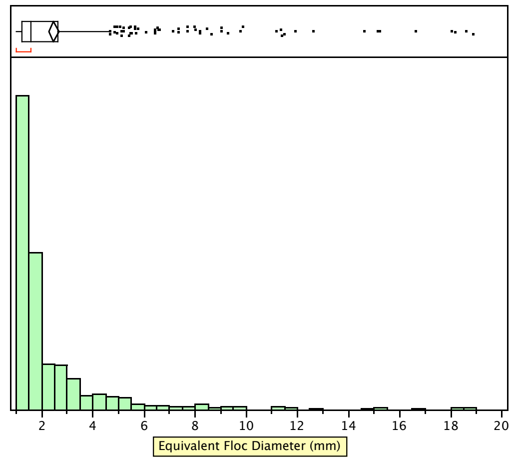

(d) Inlet, 0.432 W/m, 2 lb/ton

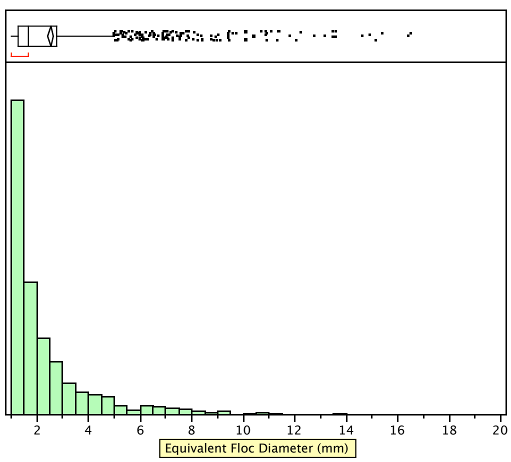

(b) 200 mm downstream, 2.562 W/m, 0 lb/ton

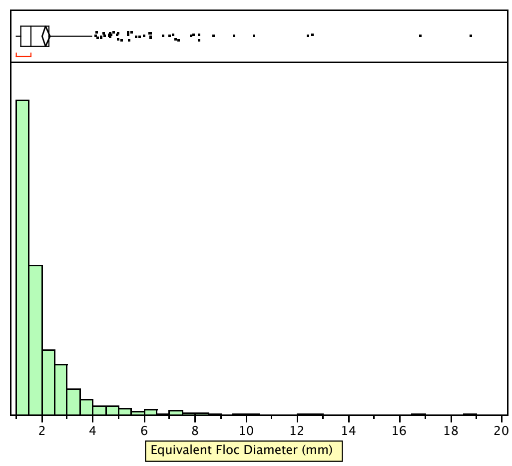

(e) 200 mm downstream, 0.432 W/m, 2 lb/ton

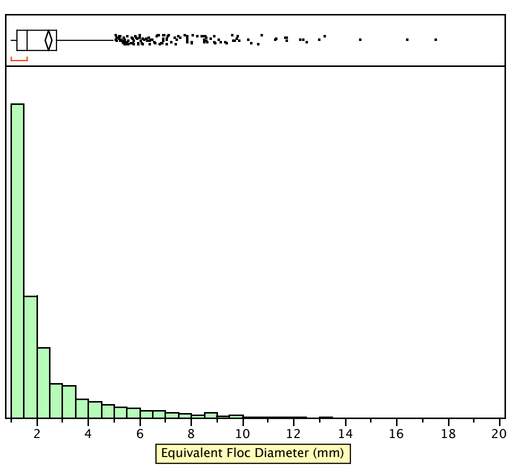

(c) 421 mm downstream, 2.562 W/m, 0 lb/ton

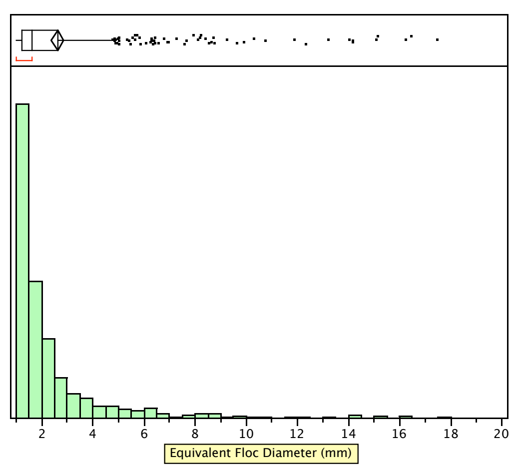

(f) 421 mm downstream, 0.432 W/m, 2 lb/ton

Figure 83. Overall floc area equivalent diameter distributions for experimental extremes.

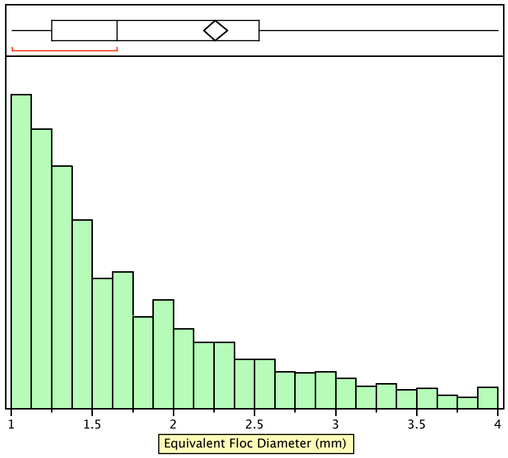

(a) Inlet, 2.562 W/m, 0 lb/ton

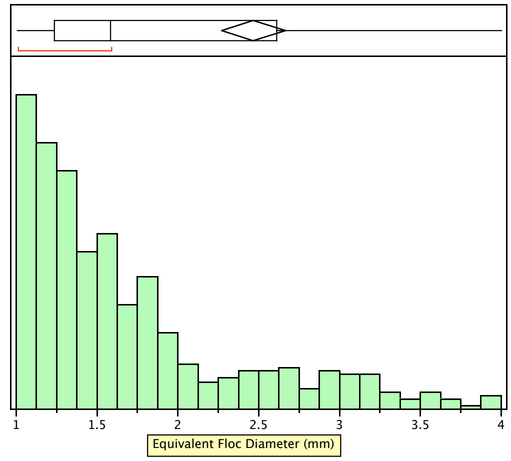

(d) Inlet, 0.432 W/m, 2 lb/ton

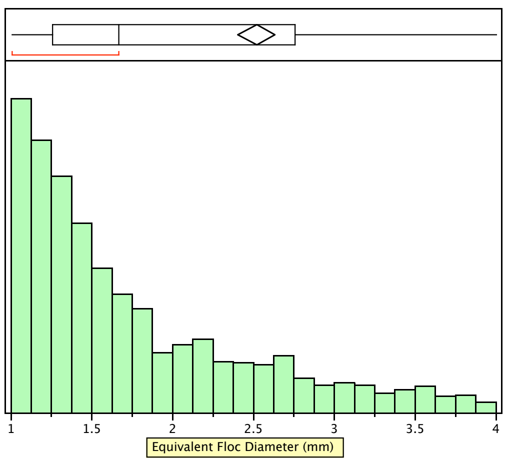

(b) 200 mm downstream, 2.562 W/m, 0 lb/ton

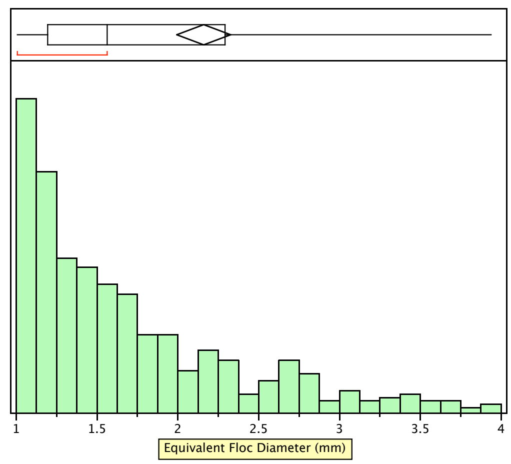

(e) 200 mm downstream, 0.432 W/m, 2 lb/ton

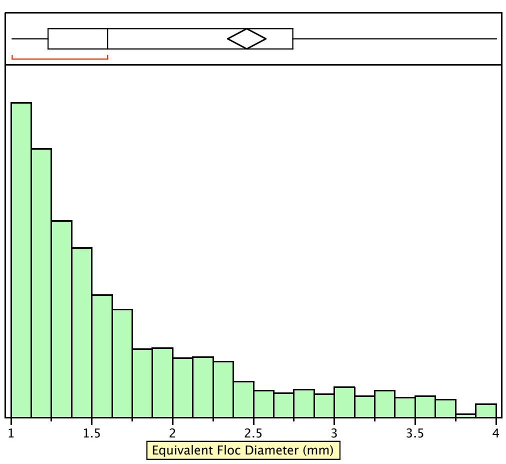

(c) 421 mm downstream, 2.562 W/m, 0 lb/ton

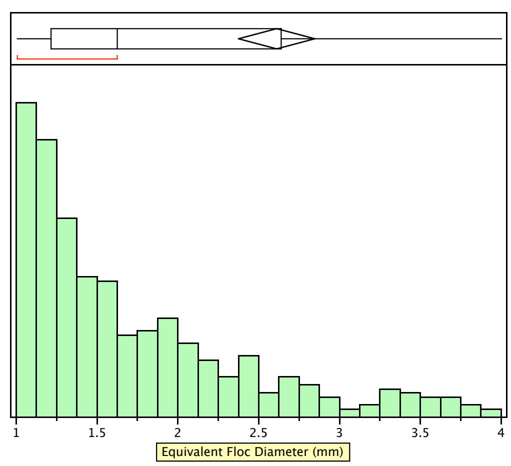

(f) 421 mm downstream, 0.432 W/m, 2 lb/ton

Figure 84. Floc area equivalent diameter distributions for experimental extremes from 1 to 4 mm.

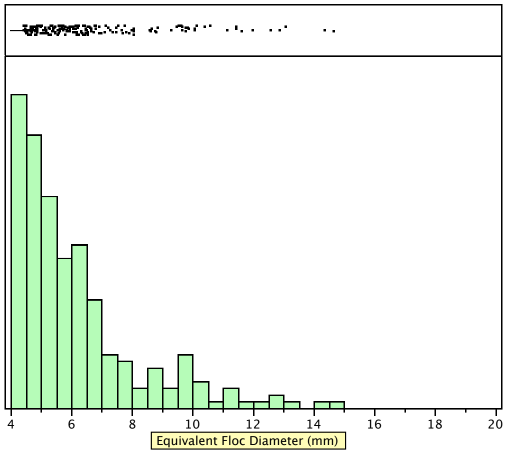

(a) Inlet, 2.562 W/m, 0 lb/ton

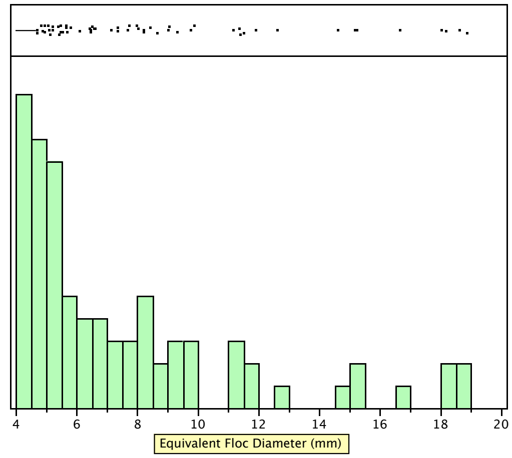

(d) Inlet, 0.432 W/m, 2 lb/ton

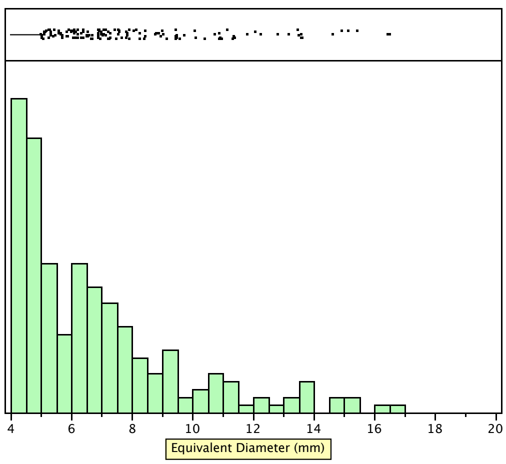

(b) 200 mm downstream, 2.562 W/m, 0 lb/ton

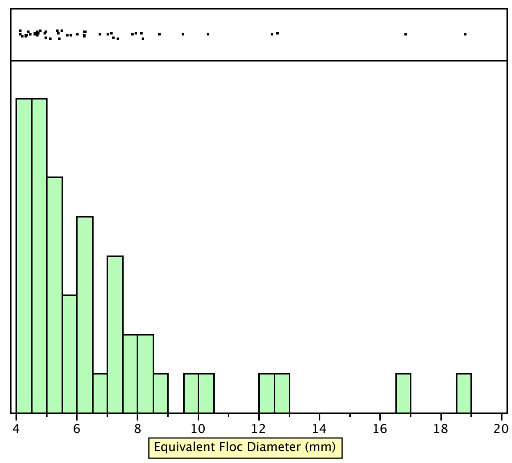

(e) 200 mm downstream, 0.432 W/m, 2 lb/ton

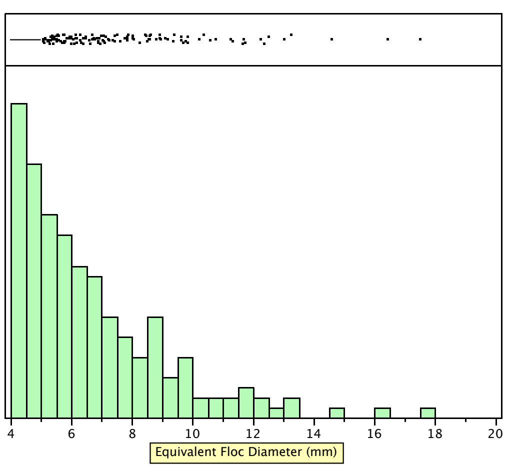

(c) 421 mm downstream, 2.562 W/m, 0 lb/ton

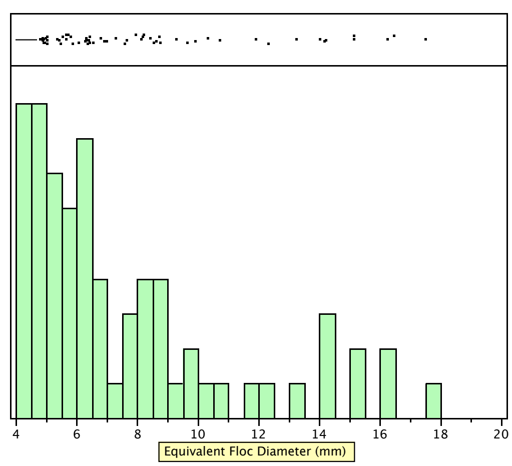

(f) 421 mm downstream, 0.432 W/m, 2 lb/ton

Figure 85. Floc area equivalent diameter distributions for experimental extremes from 4 to 20 mm.

Figure 83 displayed the overall equivalent diameter distribution for the experimental extremes. At this level it is difficult to discern differences between the different distributions. It is necessary to zoom in on the data and inspect different regions of the distributions to highlight differences.

Figure 84 displays the distributions for equivalent diameters of 1 mm to 4 mm. Remember the low pass filter kept everything 1 mm or larger. 4 mm was chosen because approximately 90% of the flocs for all experimental settings and positions in the imaging channel fell below 4 mm. By zooming in on this range of diameters subtle differences start to appear in the distributions. The distributions in figure 84d-84f show a slight skew towards larger diameters.

Figure 85 goes much further in showing the floc size differences. In figure 85d-85f it is clearly shown that floc sizes are larger with the increase in retention aid dosage and the decrease in energy dissipation. *Floc size distributions derived from morphological image operations confirm what is seen visually in the floc images.*

As illustrated in figure 85, the equivalent diameter distributions show an increase in floc size between the two extremes: low retention aid dosage paired with high energy, and high retention aid dosage paired with low energy. This is expected by looking at the floc images. Figures 75-79 attempted to show what happens to the area per floc as retention aid dosage is changed and energy dissipation is changed. It may be more beneficial to actually look at how the equivalent diameter of the flocs changes down the channel. Figures 86-88 do just this at all three retention aid dosages.

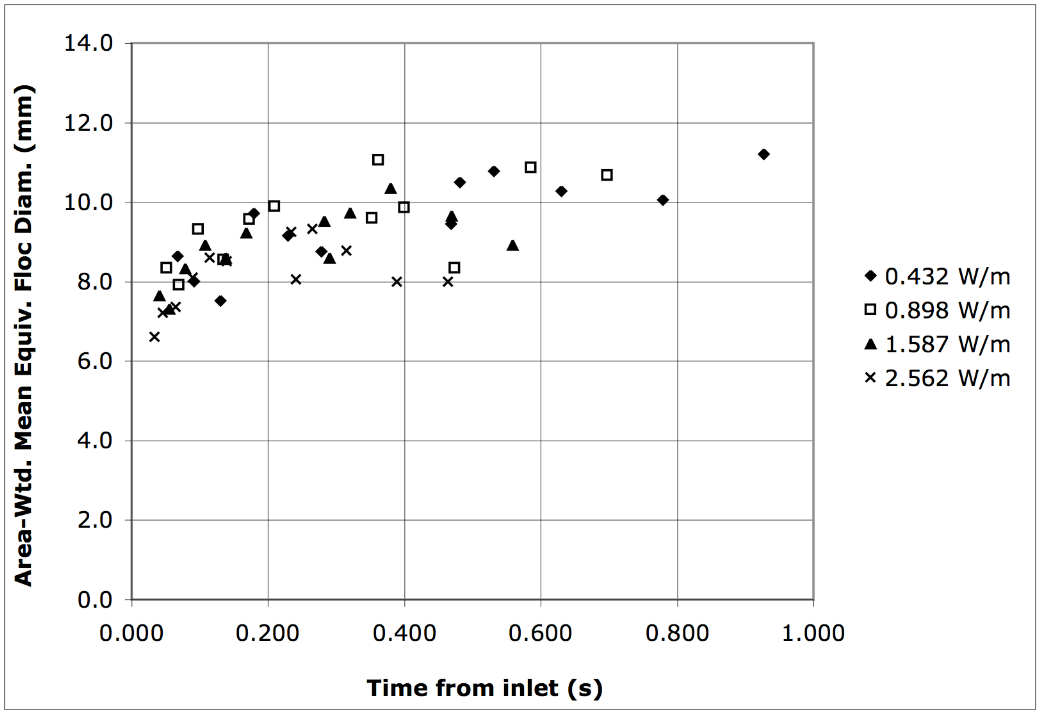

Figure 86. Equivalent floc diameter at 0 lb/ton.

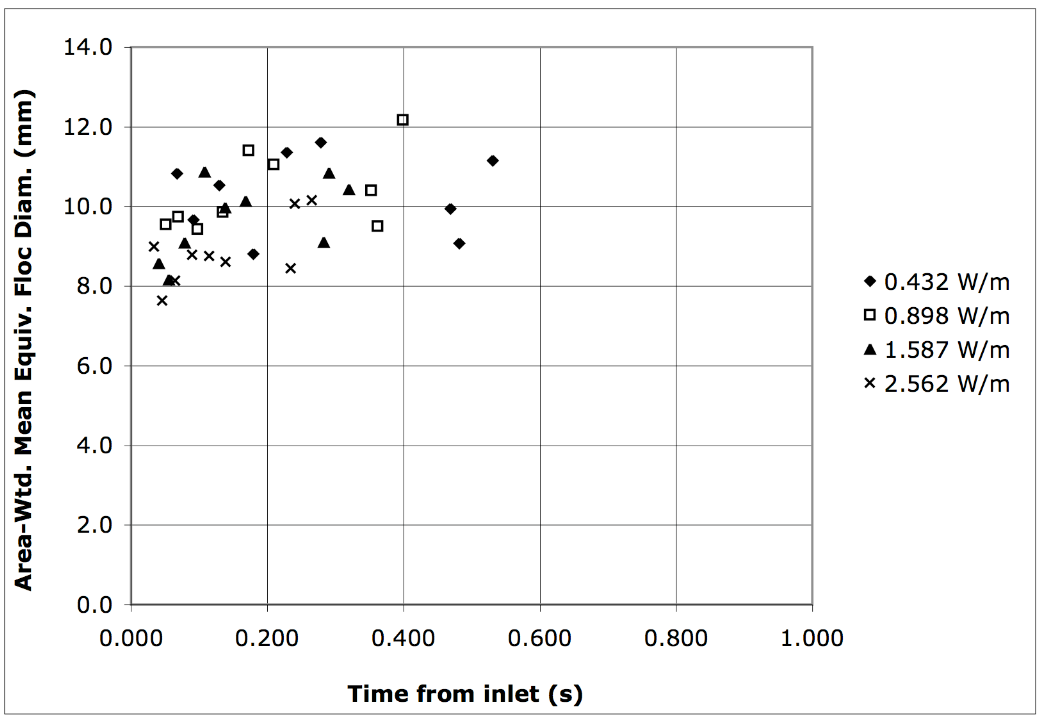

Figure 87. Equivalent floc diameter at 1 lb/ton.

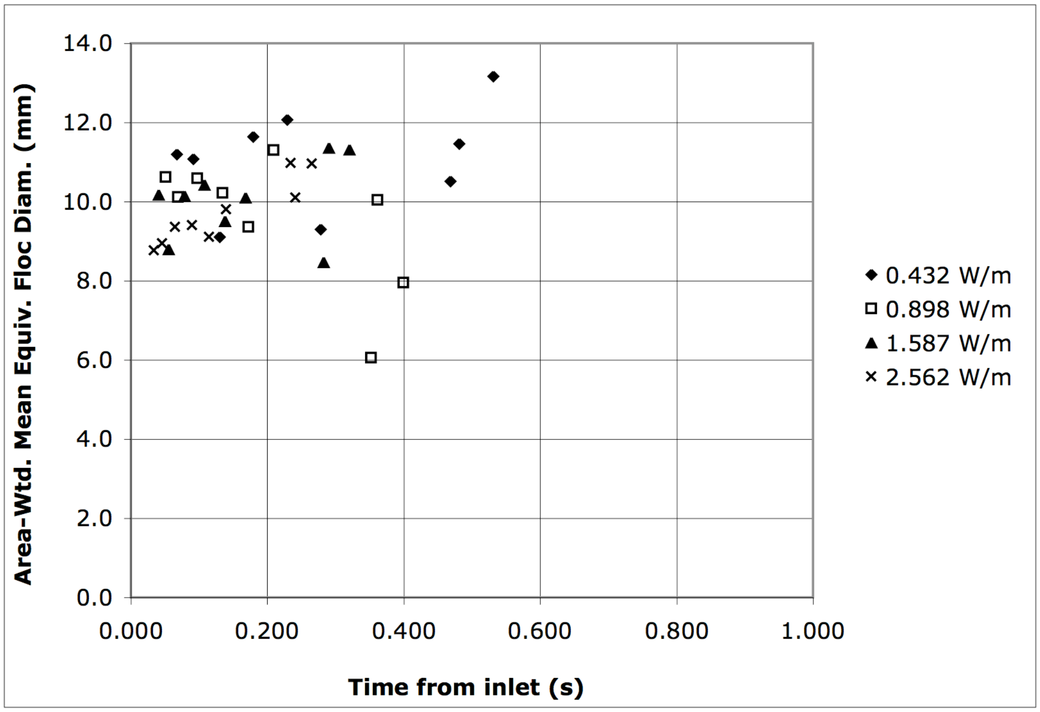

Figure 88. Equivalent floc diameter at 2 lb/ton.

As the distributions confirmed, so does the actual mean equivalent diameters: floc size increases down the channel, with increasing retention aid dosage, and with decreasing energy dissipation. The results are counterintuitive however. Floc size is increasing, but at the same time both the total area of flocs and the total number of flocs decrease. Generally,

$$\frac{\text{area}}{\text{floc}} = \frac{\text{total floc area}}{\text{number of flocs}} \quad \textbf{(14)}$$

The question to be answered is how can area per floc increase if both total floc area and total floc number decrease? To help answer this, let us assume that over any specific area in the channel, total floc volume (V_f) is constant. This means that for the total number of flocs:

$$N_f = \frac{6V_f}{\pi D^3} \quad \text{or} \quad \frac{\text{total floc volume}}{\text{volume of each floc}} \qquad \textbf{(15)}$$

The total area of flocs can be defined in a similar fashion:

$$A_f = \left(\frac{6V_f}{\pi D^3}\right)\left(\frac{\pi D^2}{4}\right) = \frac{1.5V_f}{D} \qquad \textbf{(16)}$$

(total floc number) * (area of one floc)

Solving for D (floc size) in both cases, we get:

$$D_N = \sqrt[3]{\frac{6V_f}{\pi N_f}} \qquad D_A = \frac{1.5V_f}{A_f} \qquad \textbf{(17)}$$

Assuming a constant floc volume, the mean diameter of flocs increases with decreasing total floc number and decreasing total floc area.

Effects of Retention Aid and Energy Dissipation

We have seen the separate effects of retention aid and energy dissipation on floc area and floc number. Increasing the retention aid dosage decreases both the number of flocs (N_f) and the area of flocs (A_f) in the image. This results in an increase of floc diameter as shown by equation 17. Increasing the energy dissipation rate increases both N_f and A_f. This results in a decrease of floc diameter as shown by equation 17.

What has not been presented here yet and not extensively in the literature, is the relative effect of these variables and any interaction between the two on floc size. There are several studies in the literature that have looked at the effect of either retention aid dosage or shear rate (i.e. energy dissipation level) on flocculation state or floc size, but none have attempted to combine the two variables and ascertain any combination effects that may exist. Lindström et al. (1977) completed a Britt jar study using bleached sulfite pulp. Cationic polyacrylamide was added at the rates of 0.02%, 0.1% and 1.0%. Flocculation state or intensity was measured by a correlation with turbidity of the suspension. Low turbidity corresponded to high flocculation. Lindström concluded that there was an optimum polymer dosage because the most flocculation occurred at 0.1% dosage (i.e. not the highest dosage studied). In addition, the effect of shear rate on flocculation while keeping polymer dosage and type constant was investigated. Shear rate was varied by changing the mixer speed. Reynolds numbers were not given, but linear mixing rates of 10.7 m/min to 21.4 m/min were used. Results showed that the most flocculation occurred at a mixing rate of 10.7 m/min.

Wågberg and Lindström (1987) used a previously published FFT technique (Wågberg, 1985) to study the flocculation of cellulosic fibers by cationic polyacrylamides with different charge densities. The technique was based on FFT analysis of back-scattered laser light and yielded both a floc index value and an average floc diameter. Cationic polyacrylamide dosage was varied from 0.03% to 0.1%. As expected the flocculation index increased as the retention aid dosage was increased, but average floc diameter was unchanged. An explanation for the floc diameter was that it was being controlled by the turbulence scale. The effect of shear rate was also investigated. A higher flocculation index was noted at the lowest shear rate. The lowest floc diameter occurred with the intermediate shear rate. The Reynolds number used in the study was approximately 29,000.

Wågberg and Nordqvist (1999) used a new FFT image analysis technique to analyze flocculation while varying cationic polyacrylamide dosage. One uncertainty about this work was the flow channel had a height of 3 mm. Reynolds numbers for this study were only 6000 which is just inside the turbulent regime. This low Reynolds number surely affects the polymers by increasing the time it takes for them to adsorb onto the fibers. This study only looked at the effect of polymer dosage on flocculation. Cationic polyacrylamide dosage was varied from 0.02% to 0.2%. Over this range flocs grew to 3 mm (from 2 mm) at a dosage of 0.06%, then decreased to an equilibrium size of 2.5 mm at the 0.2% dosage.

In this broad snapshot we have seen that over the past 30 years there has been a significant amount of work around measuring flocculation and how it varies with different parameters (e.g. polymer dosage and turbulence level). What has been absent from the vast majority (if not all) of these analyses is the investigation into the relative importance of polymer dosage and turbulence level and possibly the importance of combination effects of the two variables. The current study has shown significant, repeatable changes in flocculation state whether it is measured by floc number, total floc area or average floc equivalent diameter occur as a result of varying polymer dosage and energy dissipation rate. What would be more valuable is combining the two variables into a model to determine the additive effects of the two variables.

One type of regression model could be constructed by looking at the equilibrium values of both the floc area per unit image area and the floc number per unit image area. The equilibrium values for either floc area or floc number are the values at the furthest distance down the channel from the inlet. The general model would look something like this:

$$N_f = \alpha_1 R + \beta_1 E + \gamma_1 RE \qquad A_f = \alpha_2 R + \beta_2 E + \gamma_2 RE$$

$$N_f = \frac{\text{number of flocs}}{\text{unit image area}} \qquad A_f = \frac{\text{area of flocs}}{\text{unit image area}} \tag{18}$$

$R =$ retention aid dosage
$E =$ energy dissipation rate
$\alpha, \beta, \gamma =$ model coefficients

Using an appropriate statistical software package, in this case JMP, and the raw data from Appendix I, models similar to equation 18 can be constructed. The output from the statistical analysis follows.

Floc Number

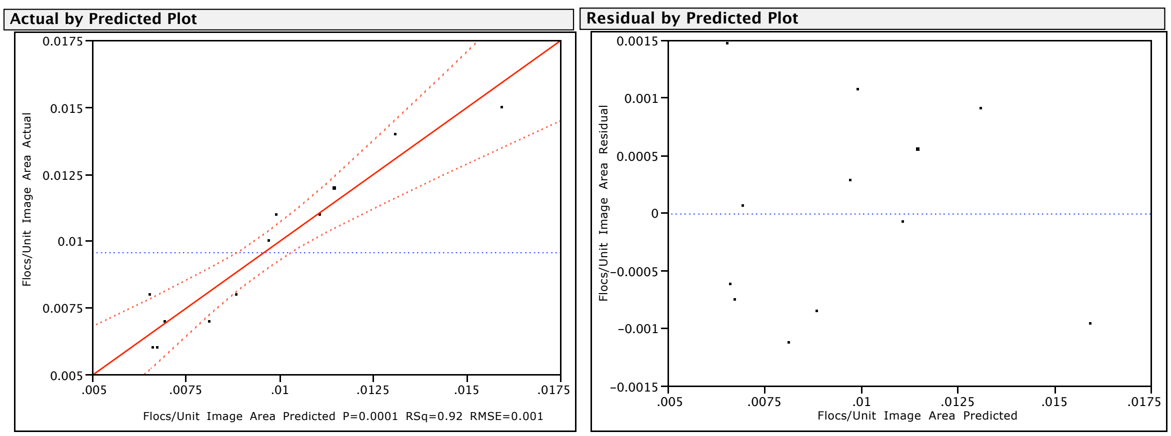

(a) (b)

Figure 89. (a) Actual versus model-predicted floc number per unit image area; **(b)** residual plot of the regression model.

Summary of Fit

RSquare	0.918685
RSquare Adj	0.888191
Root Mean Square Error	0.001023
Mean of Response	0.009583
Observations (or Sum Wgts)	12

Analysis of Variance

Source	DF	Sum of Squares	Mean Square	F Ratio
Model	3	0.00009455	0.000032	30.1274
Error	8	0.00000837	0.000001	**Prob > F**
C. Total	11	0.00010292		0.0001

Parameter Estimates

Term	Estimate	Std Error	t Ratio	Prob>|t|
Intercept	0.0103209	0.000687	15.02	<.0001
Retention Aid Dosage (lb/T)	-0.002875	0.000362	-7.95	<.0001
Energy Dissipation (W/m)	0.0015604	0.000368	4.24	0.0028
(Retention Aid Dosage (lb/T)-1)*(Energy Dissipation (W/m)-1.36975)	-0.00137	0.000451	-3.04	0.0162

Effect Tests

Source	Nparm	DF	Sum of Squares	F Ratio	Prob > F
Retention Aid Dosage (lb/T)	1	1	0.00006612	63.2116	<.0001
Energy Dissipation (W/m)	1	1	0.00001878	17.9507	0.0028
Retention Aid Dosage (lb/T)*Energy Dissipation (W/m)	1	1	0.00000964	9.2200	0.0162

Floc Area

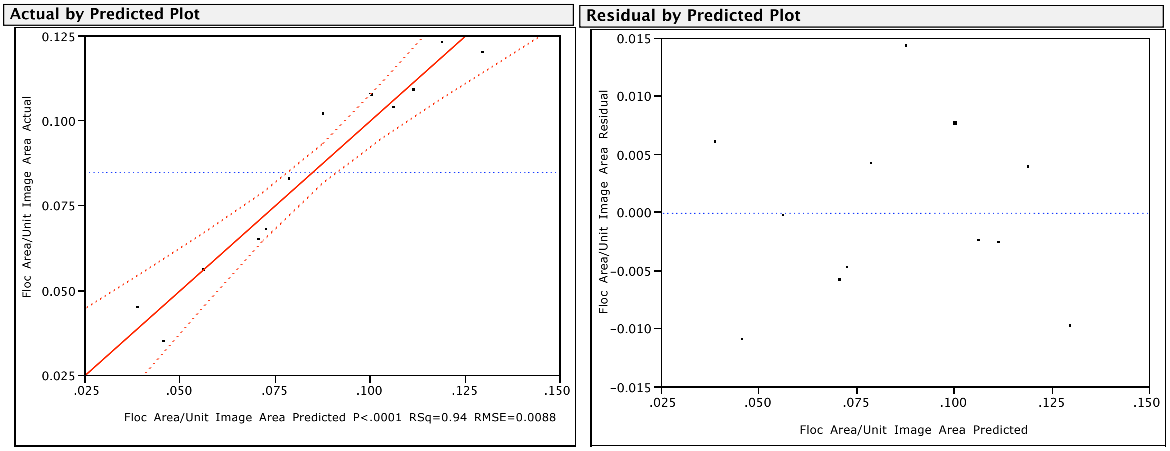

(a) **(b)**

Figure 90. (a) Actual versus model-predicted floc area per unit image area; **(b)** residual plot of the regression model.

Summary of Fit

RSquare	0.938535
RSquare Adj	0.915486
Root Mean Square Error	0.008791
Mean of Response	0.084833
Observations (or Sum Wgts)	12

Analysis of Variance

Source	DF	Sum of Squares	Mean Square	F Ratio
Model	3	0.00943947	0.003146	40.7185
Error	8	0.00061819	0.00007[illegible]	**Prob > F**
C. Total	11	0.01005767		<.0001

Parameter Estimates

Term	Estimate	Std Error	t Ratio	Prob>|t|
Intercept	0.0989824	0.005908	16.76	<.0001
Retention Aid Dosage (lb/T)	-0.031875	0.003108	-10.26	<.0001
Energy Dissipation (W/m)	0.012941	0.003165	4.09	0.0035
(Retention Aid Dosage (lb/T)-1)*(Energy Dissipation (W/m)-1.36975)	0.0019659	0.003877	0.51	0.6258

Effect Tests

Source	Nparm	DF	Sum of Squares	F Ratio	Prob > F
Retention Aid Dosage (lb/T)	1	1	0.00812813	105.1854	<.0001
Energy Dissipation (W/m)	1	1	0.00129148	16.7129	0.0035
Retention Aid Dosage (lb/T)*Energy Dissipation (W/m)	1	1	0.00001987	0.2571	0.6258

Each of the models for floc area and floc number account for more than 90% of the variation around the mean as witnessed by the r-square value of each model. Residuals for both responses appear to be random. The predictive models for each response are:

$$N_f = 0.0103 - 0.0029R + 0.0016E - 0.0014(R-1)(E-1.3698) \tag{19}$$

$$A_f = 0.0990 - 0.0319R + 0.0129E + 0.0020(R-1)(E-1.3698) \tag{20}$$

Things that were not apparent before constructing these models have now been illuminated. As before, we see that increased retention aid dosage results in decreased floc number and floc area, and that increased energy dissipation results in increased floc number and floc area. What was not apparent before was the interaction effect of retention aid dosage and energy dissipation. We see that floc number has a negative correlation with *RE* and floc area has a positive correlation with *RE*.

The p-values for the parameter estimates (labeled "Prob>|t|" in the output for each response variable) serve as the gauge for the significance of each of the parameters and the interaction effect. Typically, a p-value < 0.05 is considered significant (Sall, et al. 2005). For N_f, we see that all parameters in the model are significant as all p-values are less than 0.05. The results are slightly different for A_f where all parameters are significant except for the interaction effect *RE*.

In addition to whether or not a parameter is significant, comparing the p-values allows us to see the relative significance of the parameters. For both N_f and A_f, the retention aid dosage is the most significant parameter as witnessed by the lowest p-value in either case. Energy dissipation is significant in both models, but is slightly more significant with respect to N_f. The one stark difference between the two models is with the interaction effect *RE*. With a p-value of 0.63, *RE* has absolutely no significance with respect to A_f.

How does the model compare with the data and trends already discussed? First, we can look at the general behavior of the model with respect to each parameter. As we saw earlier in the results section, increased retention aid dosage resulted in both decreased N_f and A_f. Both models account for this as we see a negative correlation for R. We also saw that increased energy dissipation resulted in both increased N_f and A_f. This too is accounted for in both models where a positive correlation exists for E. Physically, the models perform according to what was seen in the data.

A way to determine the predictive capability of the models would be to test them against the data collected from the image analysis routines. A good comparison would be the data contained in figure 75. Figure 75 plotted A_f versus N_f for all the data. We see in figure 91 that the predicted values follow closely the actual data gathered from the image analysis routines. A more clear representation of this is seen in figure 92.

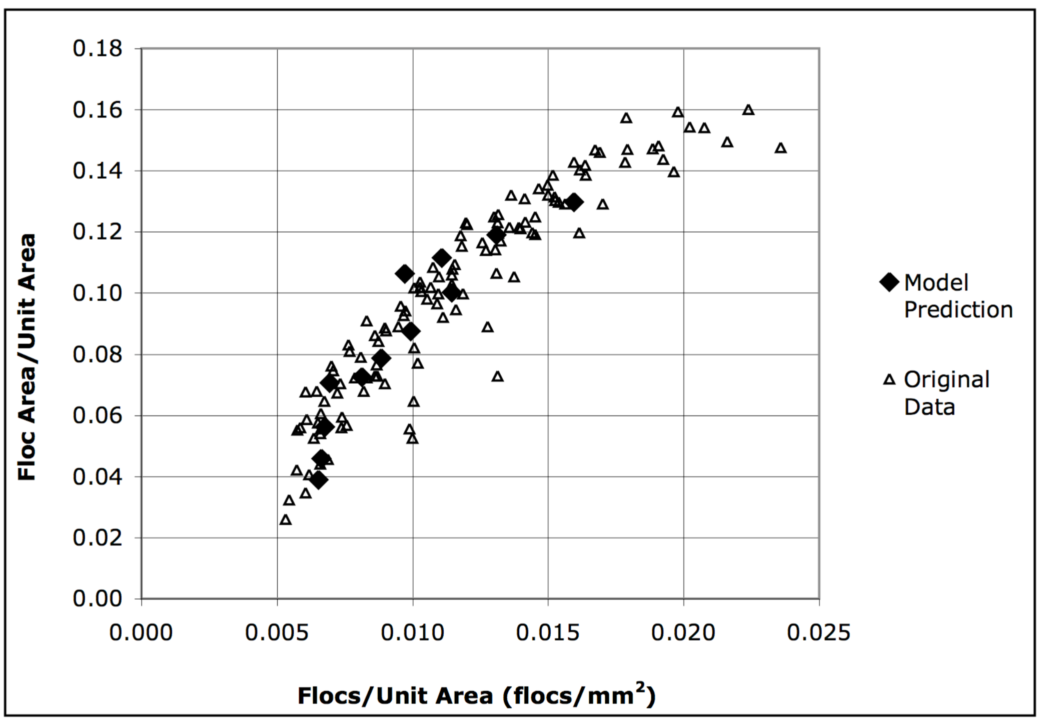

Figure 91. Comparison of regression model data and original floc data.

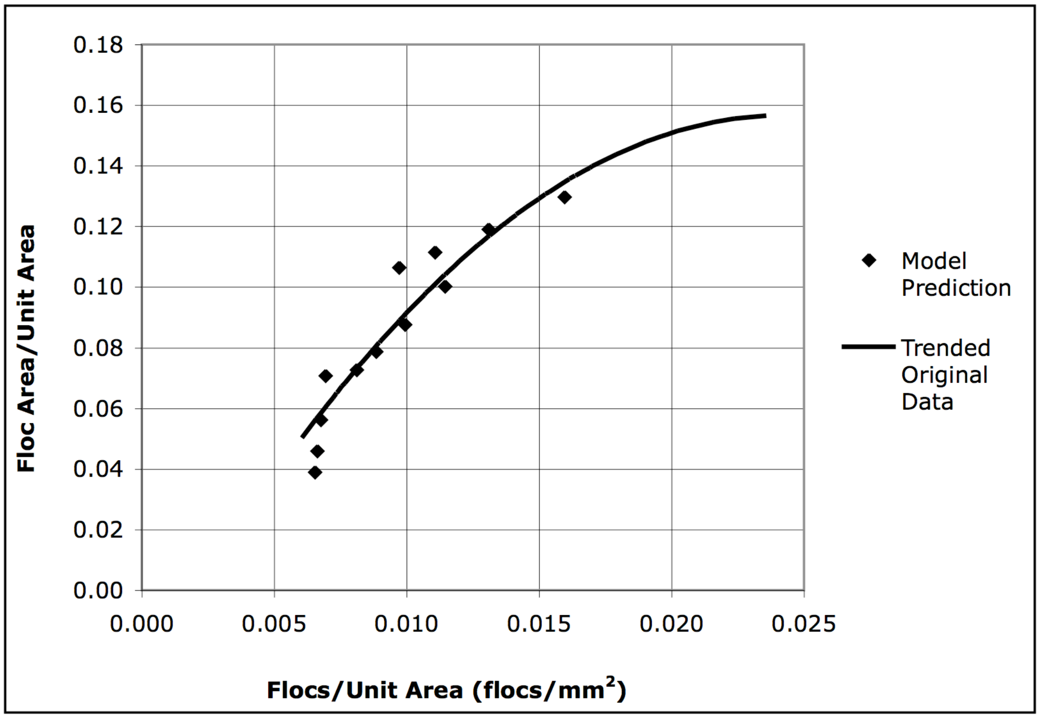

Figure 92. Comparison of regression model data and the original floc data trendline.

Physically, the regression models behave as they should. Changes in retention aid dosage and energy dissipation produce expected results. When compared against the actual data, the models are in agreement. One more aspect of the models agrees with the data. Please refer to figure 53. Notice how figure 53 is almost identical to figure 75, but in this case, the data is separated out into the three retention aid dosage levels. Figure 53 shows how the data actually has a different trend for each retention aid dosage level. This trend (an increasing slope with increasing dosage) is reflected in the model prediction as three distinct sets of points can be seen. Although the slopes are not exactly the same as in figure 53, the model is predicting their existence. A more elaborate model may predict this better.

Taking the analysis one step further, it would interesting to use equation 19 to predict F^2 (formation number squared) with the help of the trendline equation in figure 64. Solving the equation in figure 64 for F^2, we get:

$$F^2 = \frac{1}{2204.555 N_f} + 0.123839 \qquad \textbf{(21)}$$

Substituting the regression model for N_f from equation 19, we get:

$$F^2 = \frac{1}{2204.555(0.0103 - 0.0029R + .0016E - 0.0014(R-1)(E-1.3698))} + 0.123839 \qquad \textbf{(22)}$$

Figure 93 displays F^2 versus E for the three retention aid dosages.

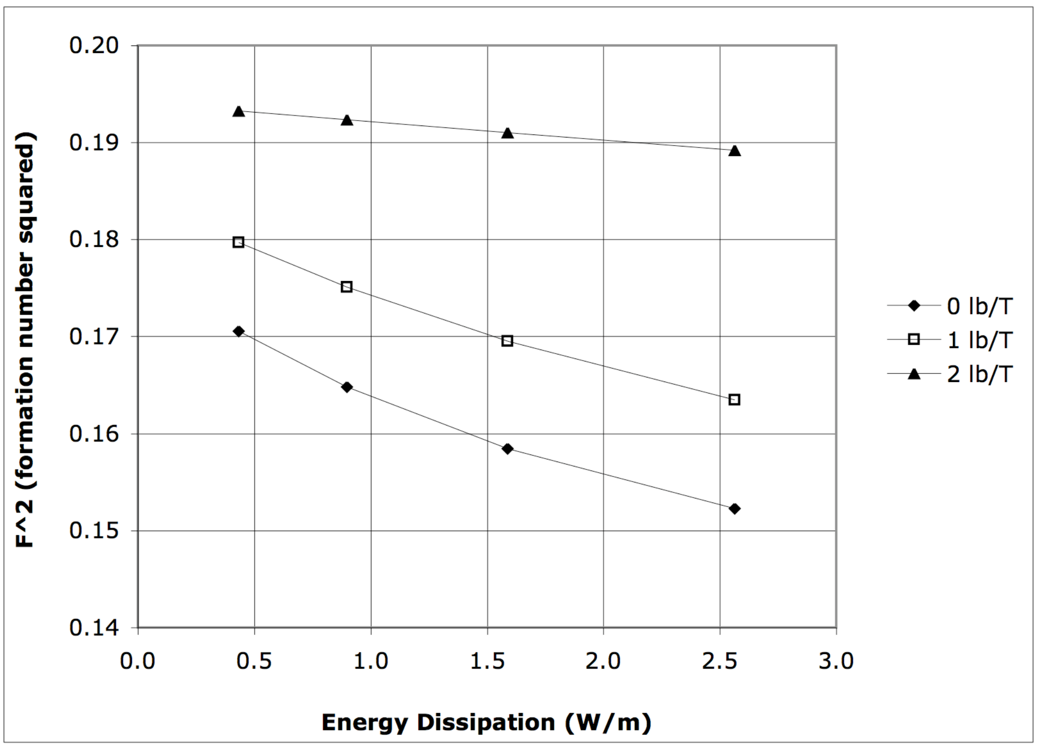

Figure 93. Energy dissipation as a predictor of F^2.

Figure 93 is very exciting because paper formation is now being predicted by production parameters (i.e. energy dissipation and retention aid dosage). Notice how the curves makes physical sense because as energy dissipation is increased formation gets better (F^2 decreases). Increased retention aid dosage results in poorer formation (F^2 increases).

To visualize the changes in F^2 and to better understand what is physically happening, it is helpful to refer to figure 80 where the floc images of the experimental extremes are displayed. Notice how figure 93 highlights the importance of the interaction effect *RE*. This is shown by the different slopes of the three curves. At the 2 lb/T dosage level where the curve is very flat, energy dissipation has little effect on F^2. The lower dosages display a different relationship where F^2 falls off (formation improves) with increasing energy dissipation. The differences in slopes of the three curves may indicate an opportunity for optimizing dosage levels of the retention aid. If that is the case, this model and technique may prove to be a useful tool in optimizing retention aids.

CONCLUSIONS

This study utilized three different image analysis procedures to analyze fiber flocs in a flowing suspension. Morphological image analysis is not typically used in situations such as these, but this study has shown that it can be used to accurately measure the flocculation state of a flowing fiber suspension. Image analysis data provided by the other two methods (FFT and formation number) served to confirm the ability of the morphological image analysis to measure floc size in this situation.

Floc size grew with increasing retention aid dosage, decreasing energy dissipation, and with time down the channel. This was expected and could be confirmed by inspecting the floc images. The success of the morphological image analysis hinged on its ability to measure and report what was seen in the floc images. Initially, results were confusing in that total floc area and total floc number were decreasing with time and retention aid dosage. How could floc size be getting larger in that situation? Floc size distributions using data from the morphological image analysis showed an increase in floc size. Equivalent floc diameter data did indeed show that floc size was increasing. By assuming a constant total floc volume, it became apparent that floc diameter could increase while total floc area and total floc number decreased. Floc diameter was shown to have an inverse relationship with total floc area and an inverse cube root relationship with total floc number.

Knowing that flocs change as retention aid dosage and energy dissipation is varied is important, but what was more instructive in this study was the creation of a regression model to *predict* the response of the floc by knowing the changes in retention aid dosage and energy dissipation. This predictive capability was confirmed by the actual data collected in the study. Retention aid dosage was found to be the most significant parameter. The interaction effect when predicting A_f was the only parameter found to not be significant. What needs to be remembered is that the model was constructed using data gathered from a laboratory flow channel and not a paper machine headbox. Results may not be easily extrapolated, but using what is known about retention aids and turbulence, estimates about what would happen to flocculation on a paper machine should be possible.

First, we know that the biggest difference between the current experimental setup and a typical paper machine is the level of turbulence. We discussed briefly that a typical paper machine slice would experience Reynolds numbers in the area of 770,000. This is well over an order of magnitude higher than what was experienced in the laboratory. Second, we know that even at the lower (turbulent) Reynolds numbers in the laboratory, retention aid adsorption onto fibers occurs in a fraction of a second. This would most likely not change on a paper machine. Third, past work by other researchers, has theorized or shown that floc growth/decay is significantly affected by or, in the absence of chemicals, governed by turbulent intensity and scale.

Using these three points, we may be able to make some predictions about what might happen on a paper machine with respect to turbulence and retention aid dosage. Because retention aid adsorption is so fast and complete at the turbulence levels seen in the laboratory (i.e. it is a collision process), it stands to reason that at the much elevated turbulence levels on a paper machine, the significance that retention aid dosage has with respect to the flocculation model should not change appreciably. On the other hand, it also stands to reason that the much elevated levels of turbulence on the paper machine may allow energy dissipation to become more significant with respect to flocculation because of the wider range of scales and intensities in the system. A model, such as the one constructed in this study, which is properly applied and adjusted to work on a paper machine may allow optimization of retention aids through feed points, dosages, and retention aid type. With respect to turbulence level, the model may help in the design of machine equipment that control or affect turbulence such as headbox tubes or formation table dewatering elements.

The contribution of this study to the body of knowledge in flocculation goes beyond just seeing what retention aid dosage and energy dissipation do to the flocculation state of a flowing fiber suspension. What we have seen for the first time are the relative contributions of retention aid dosage and energy dissipation on fiber flocculation. By relating the two parameters in a regression model, the significance of each variable and the significance of the combination effect of the two variables have been elucidated. The added benefit of using the model to help predict F^2 has shown that, at the conditions in the study, the interaction effect *RE* plays an important role-especially at the higher retention aid dosage levels. Because *RE* has different effects at the retention aid dosage levels, there may be an opportunity for retention aid optimization. This would make the model and technique used in this study a useful tool.

<u>Recommendations for Future Work</u>

Although mechanical energy dissipation (turbulence level) and retention aid dosage are important and interesting variables, they indeed do not provide a complete description of a flowing pulp suspension. Fiber properties (e.g. fiber length, coarseness, and flexibility), turbulence scale, and fiber suspension consistency would be prime candidates for further study using these analysis techniques. A detailed kinetic study comparing retention aid dosage, energy dissipation, and possibly some of the aforementioned fiber properties would be a valuable addition to the knowledge in this area of concern. Further development of a more elaborate model to relate retention aid dosage and energy dissipation may prove to be interesting. Expansion of the test conditions, especially a widening of the *E* variable, might allow easier application of the model to the paper machine.

ACKNOWLEDGEMENTS

First, I would like to thank IPST and the IPST member companies for the opportunity to complete this research. Without their financial support, this project would not have been possible. Completing my degree at IPST has been an honor and I am thankful for the unique atmosphere that existed while I was here.

I would like to thank Dr. Fred Ahrens for being both a great advisor and friend. Fred stepped in as my advisor after my original advisor left IPST and I thank him for that.

Two very important items were donated to this project. I would like to thank Tony Colasurdo and Eka Chemicals in Marietta, GA for their generosity in donating retention aid chemicals. Without pulp, this project would not have gone far. I thank Harvey Persinger, Bill Herring, Steve Olsen, and Weyerhaeuser Company for their donation of market pulp to use in this project.

Mark Urbin and the IEC machine shop have been instrumental in crafting the pieces of equipment to use in my research. Mark's suggestions and expertise has been greatly appreciated.

The last person I would like to thank is simply the most important person to me over the past 11 years. That person is my wonderful wife Sarah. Without her love, devotion, and patience I would not have made it this far. Her sacrifices have allowed me to finish my degree and for this I am truly thankful.

LITERATURE CITED

Beghello, L., and D. Eklund. "Some Mechanisms That Govern Fiber Flocculation." *Nordic Pulp and Paper Research Journal 12*, no. 2 (1997): 119-123.

Beghello, L., and M. Toivakka, and D. Eklund. "A Device For Measuring Fiber Floc Sizes in Highly Turbulent Fiber Suspensions." *Nordic Pulp and Paper Research Journal 12*, no. 4 (1996): 249-253.

Britt, K. "Sheet Formation—Advances In Retention and Drainage Concepts." *Pulp and Paper Canada 80*, no. 6 (June 1979): 67-72.

Eklund, D., and T. Lindström. *Paper Chemistry: An Introduction*. Grankulla, Finland: DT Paper Science, 1991.

Göttsching, L. "Influence of Paper Formation on Different Strength Properties." *Wocheblatt für Papierfabrikation 107*, no. 7 (April 15, 1979): 232-235.

Gruber, E., and P. Müller. "Investigations of the Flocculation Behavior of Microparticle Retention Systems." *TAPPI Journal 3*, no. 12 (December 2004): 17-22.

Jacobsen, B., and E. Arvin. "Biodegradation of Kinetics and Fate Modelling of Pentachlorophenol in Bioaugmented Activated Sludge Reactors." *Water Research Journal 30*, no. 5 (May 1996): 1184-1194.

Kajanto, I. "Effect of Formation on Print Unevenness." In *The Proceedings of the Technical Association of the Pulp and Paper Industry International Paper Physics Conference Held in Kona, HI, 22-26 September 1991*, 281-290.

Kerekes, R. "Perspectives on Fiber Flocculation in Papermaking." In *The Proceedings of the International Paper Physics Conference, 1995*, 23-31.

Kerekes, R, and C. Schell. "Characterization of Fibre Flocculation Regimes by a Crowding Factor." In *The Proceedings of the CPPA Annual Meeting Held in Montreal, 31 January-1 February 1991*, B223-230.

Kerekes, R. and C. Schell. "Effects of Fiber Length and Coarseness on Pulp Flocculation." *TAPPI Journal 78*, no. 2 (February 1995): 133-139.

Kerekes, R., R. Soszynski, and P. Tam Doo. "The Flocculation of Pulp Fibers." In *The Proceedings of the Papermaking Raw Materials Conference* edited by Punton, 1985, 265-310.

Kulikova, Y., M. Schaepe, and W. Robbins. "Assessment of the Influence of Paper Formation on the Fluorescence Contribution to Brightness." *Color Research and Application 20*, no. 2 (April 1995): 87-92.

Libertucci, M., M. Kortschot, and T. Yuhara. "The Effect of Formation on the Fracture Toughness of Paper." In *The KCL Paper Physics Seminar Held in Otaniemi, Finland, 8-11 June 1992*, 40-43.

Lindström, T., C. Söremark, and L. Eklund. "Kinetic Aspects of the Flocculation of Cellulosic Fiber Dispersions with Polyacrylamides." *CPPA Transactions of the Technical Section 3*, no. 4 (December 1977): 114-118.

Madsen, V., and A. Aneliunas. "The Effect of Formation on Print Quality." *TAPPI Journal 51*, no. 7 (July 1968): 309-314.

Mason, S. "Fiber Motions and Flocculation." *TAPPI Journal* 37, no. 11 (November 1954): 494-501.

McCabe, W., and J. Smith, and P. Harriott. *Unit Operations of Chemical Engineering*. New York: McGraw-Hill, 1993.

Mills, B. Personal communication with a scientist at Eka Chemicals of Marietta, GA: August 1999.

Norman, B., K. Moller, R. Ek, and G. Duffy. "Hydrodynamics of Papermaking Fibers in Water Suspension." In *The Transactions of the BPBIF Symposium on Fiber-Water Interactions in Papermaking Held in Oxford, September 1977*, 195-249.

Norman, B., and D. Wahren. "A Comprehensive Method for the Description of Mass Distribution in Sheets and Flocculation and Turbulence in Suspensions." *Svensk Papperstidning 75*, no. 20 (15 November 1972): 807-818.

Norman, B., and D. Wahren. "Mass Distribution and Sheet Properties of Paper." In *The Transactions of the BPBIF Symposium on the Fundamental Properties of Paper Related to Its Uses Held in Cambridge, September 1973*, 7-70.

Norman, B., and D. Wahren. "The Measurement of Mass Distribution in Paper Sheets Using a Beta Radiographic Method." *Svensk Papperstidning 77*, no. 11 (August 1974): 397-406.

Ödberg, L., and A. Swerin, and H. Tanaka. "Some Kinetic Aspects of Wet-End Chemistry." In *The Proceedings of the Technical Association of the Pulp and Paper Industry Papermakers Conference Held in ?, 1995*, 65-70.

Park, C., and C. Aidun, and H. Nanko. "The Floc Dispersion Mechanism in Sudden Expansion Tubes-Part I: The Model Floc Formation and Characterization, and the Visualization of the Floc Dispersion." 1999.

Parker, J. *The Sheet Forming Process*. Atlanta: Technical Association of the Pulp and Paper Industry, 1972.

Penniman, J. "Kinetics of Coagulation and Flocculation." *Paper Trade Journal 162*, no. 11 (June 1978): 37-38.

Popil, R. "On the Causality of Physical Properties on the Printability of Wood Containing Papers." In *The Proceedings of the Technical Association of the Pulp and Paper Industry Process and Product Quality Conference held in Cincinnati, October 1996*, 103-108.

Russ, J. *The Image Processing Handbook*. Boca Raton: CRC Press, 2002.

Sall, J., and L. Creighton, and A. Lehman. *JMP Start Statistics*. Belmont, CA: Thomson, 2005.

Scott, William. *Principles of Wet End Chemistry*. Atlanta, GA: TAPPI PRESS, 1996.

Shahalam, A., R. El-Samra, G. Ayoub, and A. Acra. "Parametric Sensitivity of Comprehensive Model of Aerobic Fluidized-Bed Biofilm Process." *Journal of Environmental Engineering 122*, no. 12 (December 1996): 1085-1093.

Shallhorn, P., and H. Heintze. "Offset Printing and the Formation of Uncoated Fine Papers." In *The Proceedings of the Technical Association of the Pulp and Paper Industry Process and Product Quality Conference Held in Cincinnati, October 1996*, 109-112.

Shaw, D. *Introduction to Colloid and Surface Chemistry*. Oxford, England: Butterworth-heinemann, 1992.

Steen, M. *Turbulence and Flocculation in Fibre Suspensions*. Ph.D. Dissertation: University of Trondheim, Norway, 1990.

van de Ven, T. *Fundamentals of Papermaking*, 1:471 (1989). Transactions of the Ninth Fundamental research Symposium, Cambridge. Sept. 1989. Mechanical Engineering Publications Limited, London 1989.

Wågberg, L. "A Device for Measuring the Kinetics of Flocculation Following Polymer Addition in Turbulent Fiber Suspensions." *Svensk Papperstidning 88*, no. 6 (April 4, 1985):R48-R56.

Wågberg, L., and J. Eriksson. "New Equipment for Detection of Polymer Induced Flocculation of Cellulosic Fibres By Using Image Analysis—Application to Microparticle Systems." *Chemical Engineering Journal 80*, (2000): 51-63.

Wågberg, L., and T. Lindström. "Flocculation of Cellulosic Fibers By Cationic Polyacrylamides With Different Charge Densities." *Nordic Pulp and Paper Research Journal 2*, no. 4, (December 1987): 152-160.

Wågberg, L., and T. Lindström. "Kinetics of Polymer-Induced Flocculation of Cellulosic Fibers in Turbulent Flow." *Colloids and Surfaces 27*, no. 1/3 (October 1987): 29-42.

Wågberg, L., and T. Nordqvist. "Detection of Polymer Induced Flocculation of Cellulosic Fibers by Image Analysis." *Nordic Pulp and Paper Research Journal 14*, no. 3 (1999): 247-255.

Weseman, B. *The Effects of Refining On Polyacrylamide Adsorption Onto Cellulose Fibers*. Masters Thesis: Institute of Paper Science and Technology, Atlanta, 1999.

Wrist, P. "Formation and Structure of Paper." Ed. F. Bolam, Tech. Sect., BP&BMA, London, 839 (1961).

Wrist, P. "The Science of Paper Manufacture." *TAPPI Journal 44*, no. 1 (January 1961): 181A-199A.

Xu, H. *Measurement of Fiber Suspension Flow and Forming Jet Velocity Profile By Pulsed Ultrasonic Doppler Velocimetry*. Ph.D. Dissertation: Institute of Paper Science and Technology, Atlanta, 2003.

APPENDIX I: PROCESSED MORPHOLOGICAL AREA AND NUMBER DATA

Flow Rate (LPM)	Sector Midpoint (mm)	Time from inlet (s)	Reten Dosage (#/ton)	Total Number of Flocs	Flocs per Unit Image Area	Floc Area Sum (mm^2)	Total Floc Area per Unit Image Area	Mean Area/Floc (mm^2)	AWA Equiv. Diam. (mm)
100	58.9	0.067	0	1447	0.017	11715	0.129	7.603	8.646
100	80.2	0.092	0	1394	0.016	10182	0.139	8.472	8.007
100	113.4	0.130	0	1235	0.015	8485	0.125	8.615	7.517
100	156.7	0.179	0	1170	0.014	10333	0.105	7.673	9.722
100	200.0	0.229	0	1086	0.013	9285	0.089	6.986	9.154
100	243.4	0.278	0	1117	0.013	9691	0.073	5.566	8.765
100	409.9	0.468	0	850	0.010	8378	0.053	5.267	9.457
100	421.0	0.481	0	840	0.010	7630	0.056	5.642	10.503
100	464.4	0.531	0	854	0.010	8969	0.065	6.448	10.777
100	551.1	0.630	0	874	0.010	8689	0.102	9.941	10.285
100	681.1	0.778	0	855	0.010	6994	0.082	8.180	10.062
100	811.1	0.927	0	874	0.010	8828	0.104	10.101	11.215
133	58.9	0.051	0	1671	0.020	11910	0.140	7.128	8.356
133	80.2	0.069	0	1683	0.020	13576	0.159	8.067	7.919
133	113.4	0.097	0	1439	0.017	12440	0.146	8.645	9.321
133	156.7	0.135	0	1296	0.015	11197	0.132	8.639	8.557
133	200.0	0.172	0	1120	0.013	10191	0.120	9.100	9.572
133	243.4	0.209	0	1203	0.014	11154	0.131	9.272	9.894
133	409.9	0.352	0	973	0.011	8771	0.103	9.014	9.597
133	421.0	0.362	0	1005	0.012	9829	0.115	9.780	11.060
133	464.4	0.399	0	931	0.011	8505	0.100	9.136	9.865
133	551.1	0.474	0	946	0.011	7856	0.092	8.304	8.350
133	681.1	0.585	0	973	0.011	9020	0.106	9.271	10.866
133	811.1	0.697	0	914	0.011	9243	0.109	10.113	10.677
166	58.9	0.041	0	1838	0.022	12744	0.150	6.933	7.657
166	80.2	0.055	0	1766	0.021	13137	0.154	7.439	7.313
166	113.4	0.078	0	1622	0.019	12619	0.148	7.780	8.330
166	156.7	0.108	0	1393	0.016	12079	0.142	8.671	8.921
166	200.0	0.138	0	1298	0.015	11106	0.130	8.556	8.594
166	243.4	0.168	0	1274	0.015	11533	0.135	9.053	9.231
166	409.9	0.282	0	1008	0.012	8505	0.100	8.437	9.529
166	421.0	0.290	0	1114	0.013	9077	0.107	8.148	8.599
166	464.4	0.320	0	1118	0.013	10482	0.123	9.376	9.736
166	551.1	0.379	0	1022	0.012	10435	0.123	10.211	10.360
166	681.1	0.469	0	1119	0.013	10710	0.126	9.571	9.656
166	811.1	0.558	0	1204	0.014	10498	0.123	8.719	8.932
200	58.9	0.034	0	2007	0.024	12571	0.148	6.263	6.612
200	80.2	0.046	0	1905	0.022	13630	0.160	7.155	7.219
200	113.4	0.065	0	1721	0.020	13154	0.155	7.643	7.359
200	156.7	0.090	0	1517	0.018	12173	0.143	8.024	8.098
200	200.0	0.114	0	1424	0.017	12506	0.147	8.782	8.597
200	243.4	0.139	0	1521	0.018	13411	0.158	8.817	8.514
200	409.9	0.234	0	1160	0.014	11248	0.132	9.696	9.253
200	421.0	0.241	0	1235	0.015	10147	0.119	8.216	8.059
200	464.4	0.265	0	1277	0.015	11250	0.132	8.810	9.326
200	551.1	0.315	0	1110	0.013	9727	0.114	8.763	8.783
200	681.1	0.389	0	1374	0.016	10201	0.120	7.424	8.003
200	811.1	0.464	0	1227	0.014	10203	0.120	8.316	7.997

APPENDIX I CONTINUED

Flow Rate (LPM)	Sector Midpoint (mm)	Time from inlet (s)	Reten Dosage (#/ton)	Total Number of Flocs	Flocs per Unit Image Area	Floc Area Sum (mm^2)	Total Floc Area per Unit Image Area	Mean Area/Floc (mm^2)	AWA Equiv. Diam. (mm)
100	58.9	0.067	1	743	0.009	7179	0.084	9.662	10.833
100	80.2	0.092	1	738	0.009	6518	0.077	8.831	9.668
100	113.4	0.130	1	706	0.008	7745	0.091	10.970	10.543
100	156.7	0.179	1	627	0.007	4777	0.056	7.618	8.805
100	200.0	0.229	1	562	0.007	5171	0.061	9.201	11.364
100	243.4	0.278	1	652	0.008	6904	0.081	10.590	11.606
100	409.9	0.468	1	644	0.008	4848	0.057	7.528	9.944
100	421.0	0.481	1	628	0.007	5074	0.060	8.080	9.072
100	464.4	0.531	1	614	0.007	5747	0.068	9.359	11.161
133	58.9	0.051	1	1189	0.014	10320	0.121	8.680	9.551
133	80.2	0.069	1	1183	0.014	10347	0.122	8.746	9.737
133	113.4	0.097	1	1002	0.012	10121	0.119	10.101	9.436
133	156.7	0.135	1	768	0.009	7475	0.088	9.732	9.862
133	200.0	0.172	1	732	0.009	7344	0.086	10.033	11.399
133	243.4	0.209	1	707	0.008	6163	0.072	8.718	11.045
133	409.9	0.352	1	697	0.008	5793	0.068	8.311	10.399
133	421.0	0.362	1	763	0.009	6006	0.071	7.871	9.510
133	464.4	0.399	1	650	0.008	7075	0.083	10.885	12.176
166	58.9	0.041	1	1525	0.018	12529	0.147	8.216	8.578
166	80.2	0.055	1	1358	0.016	12159	0.143	8.953	8.170
166	113.4	0.078	1	1247	0.015	11438	0.134	9.172	9.096
166	156.7	0.108	1	1018	0.012	10476	0.123	10.291	10.871
166	200.0	0.138	1	878	0.010	8562	0.101	9.752	9.980
166	243.4	0.168	1	828	0.010	8028	0.094	9.695	10.143
166	409.9	0.282	1	867	0.010	6576	0.077	7.585	9.101
166	421.0	0.290	1	896	0.011	8355	0.098	9.325	10.845
166	464.4	0.320	1	908	0.011	8682	0.102	9.562	10.430
200	58.9	0.034	1	1604	0.019	12540	0.147	7.818	8.991
200	80.2	0.046	1	1638	0.019	12240	0.144	7.473	7.634
200	113.4	0.065	1	1376	0.016	11950	0.140	8.684	8.139
200	156.7	0.090	1	1309	0.015	11051	0.130	8.443	8.788
200	200.0	0.114	1	1081	0.013	9716	0.114	8.988	8.757
200	243.4	0.139	1	1127	0.013	9971	0.117	8.848	8.604
200	409.9	0.234	1	987	0.012	8064	0.095	8.170	8.447
200	421.0	0.241	1	982	0.012	9317	0.109	9.487	10.064
200	464.4	0.265	1	976	0.011	9183	0.108	9.408	10.156
100	58.9	0.067	2	624	0.007	6003	0.071	9.619	11.201
100	80.2	0.092	2	596	0.007	6495	0.076	10.897	11.085
100	113.4	0.130	2	554	0.007	4900	0.058	8.844	9.107
100	156.7	0.179	2	549	0.006	5787	0.068	10.540	11.650
100	200.0	0.229	2	515	0.006	5766	0.068	11.195	12.071
100	243.4	0.278	2	526	0.006	3465	0.041	6.587	9.308
100	409.9	0.468	2	584	0.007	3887	0.046	6.657	10.518
100	421.0	0.481	2	560	0.007	3766	0.044	6.726	11.472
100	464.4	0.531	2	687	0.008	6744	0.079	9.817	13.174
133	58.9	0.051	2	855	0.010	8662	0.102	10.131	10.615
133	80.2	0.069	2	822	0.010	7895	0.093	9.605	10.122
133	113.4	0.097	2	764	0.009	7549	0.089	9.881	10.589
133	156.7	0.135	2	601	0.007	6355	0.075	10.573	10.224
133	200.0	0.172	2	560	0.007	4609	0.054	8.230	9.360
133	243.4	0.209	2	519	0.006	4996	0.059	9.626	11.306
133	409.9	0.352	2	452	0.005	2221	0.026	4.913	6.054
133	421.0	0.362	2	463	0.005	2765	0.032	5.972	10.049
133	464.4	0.399	2	515	0.006	2962	0.035	5.751	7.962
166	58.9	0.041	2	1154	0.014	10345	0.122	8.965	10.171
166	80.2	0.055	2	1069	0.013	9921	0.117	9.280	8.806
166	113.4	0.078	2	928	0.011	8219	0.097	8.857	10.148
166	156.7	0.108	2	813	0.010	8159	0.096	10.035	10.431
166	200.0	0.138	2	740	0.009	6214	0.073	8.397	9.514
166	243.4	0.168	2	670	0.008	6173	0.073	9.213	10.108
166	409.9	0.282	2	487	0.006	3599	0.042	7.390	8.480
166	421.0	0.290	2	488	0.006	4705	0.055	9.642	11.363
166	464.4	0.320	2	498	0.006	4769	0.056	9.576	11.320
200	58.9	0.034	2	1329	0.016	11002	0.129	8.278	8.769
200	80.2	0.046	2	1291	0.015	11810	0.139	9.148	8.942
200	113.4	0.065	2	1107	0.013	10639	0.125	9.611	9.368
200	156.7	0.090	2	934	0.011	8977	0.105	9.611	9.407
200	200.0	0.114	2	806	0.009	7587	0.089	9.413	9.118
200	243.4	0.139	2	732	0.009	6218	0.073	8.494	9.814
200	409.9	0.234	2	540	0.006	4477	0.053	8.291	10.970

APPENDIX II: RUN ORDER OF EXPERIMENTS

Run	Flow Rate (LPM)	Retention Aid (#/ton)	Image
1	100	2	1
2	100	0	1
3	200	0	1
4	133	1	1
5	133	0	1
6	200	2	1
7	166	2	1
8	100	1	1
9	133	0	1
10	100	2	1
11	200	0	1
12	166	1	1
13	166	0	1
14	133	1	1
15	166	0	1
16	200	1	1
17	200	1	1
18	100	0	1
19	133	2	1
20	166	1	1
21	200	2	1
22	200	2	1
23	100	1	1
24	100	0	1
25	166	0	1
26	133	0	1
27	100	2	1
28	166	2	1
29	166	2	1
30	100	1	1
31	200	1	1
32	133	2	1
33	133	1	1
34	166	1	1
35	200	0	1
36	133	2	1
37	133	2	2
38	200	2	2
39	100	0	2
40	166	1	2
41	100	2	2
42	100	2	2
43	133	0	2
44	133	0	2
45	200	1	2
46	166	0	2
47	200	1	2
48	100	1	2
49	133	1	2
50	166	0	2
51	133	2	2
52	100	2	2
53	100	1	2
54	166	0	2
55	166	1	2
56	200	2	2
57	200	0	2
58	200	1	2
59	133	0	2
60	166	2	2
61	100	0	2
62	133	1	2
63	200	0	2
64	100	1	2
65	200	2	2
66	166	2	2
67	133	2	2
68	166	1	2
69	166	2	2
70	200	0	2
71	133	1	2
72	100	0	2
73	166	2	3
74	133	1	3
75	200	0	3
76	166	0	3
77	133	2	3
78	200	2	3
79	133	0	3
80	100	2	3
81	200	1	3
82	166	1	3
83	100	0	3
84	100	1	3
85	200	0	4
86	166	0	4
87	133	2	4
88	100	2	4
89	133	0	4
90	133	0	4
91	133	0	4
92	100	1	4
93	166	1	4
94	166	1	4
95	166	2	4
96	200	0	4
97	200	2	4
98	200	2	4
99	100	1	4
100	166	2	4
101	200	0	4
102	100	0	4
103	133	2	4
104	166	1	4
105	166	0	4
106	166	2	4
107	200	1	4
108	166	0	4
109	100	2	4
110	100	2	4
111	133	1	4
112	200	1	4
113	100	0	4
114	133	1	4
115	100	1	4
116	133	1	4
117	133	2	4
118	200	1	4
119	200	2	4
120	100	0	4
121	133	0	5
122	100	0	5
123	166	0	5
124	200	0	5
125	200	0	6
126	133	0	6
127	166	0	6
128	100	0	6
129	200	0	7
130	133	0	7
131	100	0	7
132	166	0	7

APPENDIX III: AVERAGED FORMATION NUMBER DATA

Flow Rate (LPM)	Retention Aid (#/ton)	Time from inlet (s)	Sector Midpoint (mm)	Mean Brightness	Brightness Std Deviation	Formation Number (s/y-bar)	Formation Number-sq (s^2/y-bar^2)
100	0	0.067	58.9	130.76	51.12	0.391	0.153
100	0	0.092	80.2	131.48	51.28	0.390	0.152
100	0	0.130	113.4	131.53	51.77	0.394	0.155
100	0	0.179	156.7	131.92	51.82	0.393	0.154
100	0	0.229	200.0	131.89	52.28	0.396	0.157
100	0	0.278	243.4	130.52	52.41	0.402	0.161
100	0	0.468	409.9	130.98	53.45	0.408	0.167
100	0	0.481	421.0	131.35	53.57	0.408	0.166
100	0	0.531	464.4	131.41	53.65	0.408	0.167
100	0	0.580	507.7	130.83	53.07	0.406	0.165
100	0	0.630	551.1	131.30	53.41	0.407	0.165
100	0	0.679	594.4	130.41	53.22	0.408	0.167
100	0	0.729	637.7	130.94	53.13	0.406	0.165
100	0	0.778	681.1	131.38	53.27	0.405	0.164
100	0	0.828	724.4	130.98	52.93	0.404	0.163
100	0	0.877	767.7	131.06	53.21	0.406	0.165
100	0	0.927	811.1	131.52	53.54	0.407	0.166
100	0	0.977	854.4	130.50	53.52	0.410	0.168
133	0	0.051	58.9	131.08	50.60	0.386	0.149
133	0	0.069	80.2	131.75	50.58	0.384	0.147
133	0	0.097	113.4	131.77	51.03	0.387	0.150
133	0	0.135	156.7	131.93	51.54	0.391	0.153
133	0	0.172	200.0	131.79	51.93	0.394	0.155
133	0	0.209	243.4	130.85	52.08	0.398	0.158
133	0	0.352	409.9	131.11	52.79	0.403	0.162
133	0	0.362	421.0	131.22	52.73	0.402	0.161
133	0	0.399	464.4	131.60	53.07	0.403	0.163
133	0	0.436	507.7	130.90	52.70	0.403	0.162
133	0	0.474	551.1	131.49	52.68	0.401	0.160
133	0	0.511	594.4	130.32	52.68	0.404	0.163
133	0	0.548	637.7	130.90	52.89	0.404	0.163
133	0	0.585	681.1	131.73	52.95	0.402	0.162
133	0	0.623	724.4	131.00	52.51	0.401	0.161
133	0	0.660	767.7	131.16	52.69	0.402	0.161
133	0	0.697	811.1	131.77	53.06	0.403	0.162
133	0	0.734	854.4	130.98	52.46	0.401	0.160
166	0	0.041	58.9	130.95	50.20	0.383	0.147
166	0	0.055	80.2	131.73	50.27	0.382	0.146
166	0	0.078	113.4	131.67	50.75	0.385	0.149
166	0	0.108	156.7	132.10	50.96	0.386	0.149
166	0	0.138	200.0	131.83	51.55	0.391	0.153
166	0	0.168	243.4	130.88	51.61	0.394	0.155
166	0	0.282	409.9	131.27	52.30	0.398	0.159
166	0	0.290	421.0	131.54	52.31	0.398	0.158
166	0	0.320	464.4	131.57	52.34	0.398	0.158
166	0	0.350	507.7	131.14	52.27	0.399	0.159
166	0	0.379	551.1	131.64	52.34	0.398	0.158
166	0	0.409	594.4	130.89	52.01	0.397	0.158
166	0	0.439	637.7	131.02	52.07	0.397	0.158
166	0	0.469	681.1	131.62	52.09	0.396	0.157
166	0	0.499	724.4	131.00	52.13	0.398	0.158
166	0	0.529	767.7	131.19	51.88	0.395	0.156
166	0	0.558	811.1	131.87	51.94	0.394	0.155
166	0	0.588	854.4	131.15	52.01	0.397	0.157

APPENDIX III CONTINUED

Flow Rate (LPM)	Retention Aid (#/ton)	Time from inlet (s)	Sector Midpoint (mm)	Mean Brightness	Brightness Std Deviation	Formation Number (s/y-bar)	Formation Number-sq (s^2/y-bar^2)
200	0	0.034	58.9	131.06	49.97	0.381	0.145
200	0	0.046	80.2	131.60	49.91	0.379	0.144
200	0	0.065	113.4	131.69	50.30	0.382	0.146
200	0	0.090	156.7	132.20	50.72	0.384	0.147
200	0	0.114	200.0	131.97	51.13	0.387	0.150
200	0	0.139	243.4	130.90	51.28	0.392	0.153
200	0	0.234	409.9	130.21	51.67	0.397	0.157
200	0	0.241	421.0	130.59	51.53	0.395	0.156
200	0	0.265	464.4	130.64	51.74	0.396	0.157
200	0	0.290	507.7	131.22	51.80	0.395	0.156
200	0	0.315	551.1	131.70	51.95	0.394	0.156
200	0	0.340	594.4	130.59	51.77	0.396	0.157
200	0	0.364	637.7	129.43	51.57	0.398	0.159
200	0	0.389	681.1	130.13	51.46	0.395	0.156
200	0	0.414	724.4	129.17	51.45	0.398	0.159
200	0	0.439	767.7	131.03	51.63	0.394	0.155
200	0	0.464	811.1	131.98	51.57	0.391	0.153
200	0	0.488	854.4	131.02	51.39	0.392	0.154
100	1	0.067	58.9	130.59	54.67	0.419	0.175
100	1	0.092	80.2	131.25	54.76	0.417	0.174
100	1	0.130	113.4	131.32	55.14	0.420	0.176
100	1	0.179	156.7	131.66	55.94	0.425	0.181
100	1	0.229	200.0	130.95	56.36	0.430	0.185
100	1	0.278	243.4	130.36	56.17	0.431	0.186
100	1	0.468	409.9	130.06	56.60	0.435	0.189
100	1	0.481	421.0	130.39	56.69	0.435	0.189
100	1	0.531	464.4	130.53	56.90	0.436	0.190
133	1	0.051	58.9	131.25	52.05	0.397	0.157
133	1	0.069	80.2	131.67	52.12	0.396	0.157
133	1	0.097	113.4	131.58	52.91	0.402	0.162
133	1	0.135	156.7	129.99	54.56	0.420	0.176
133	1	0.172	200.0	130.88	55.14	0.421	0.177
133	1	0.209	243.4	129.78	55.42	0.427	0.182
133	1	0.352	409.9	129.05	54.70	0.424	0.180
133	1	0.362	421.0	129.51	54.83	0.423	0.179
133	1	0.399	464.4	129.65	54.75	0.422	0.178
166	1	0.041	58.9	131.04	51.06	0.390	0.152
166	1	0.055	80.2	131.66	51.16	0.389	0.151
166	1	0.078	113.4	131.69	51.83	0.394	0.155
166	1	0.108	156.7	131.17	52.64	0.401	0.161
166	1	0.138	200.0	131.35	53.29	0.406	0.165
166	1	0.168	243.4	130.44	53.43	0.410	0.168
166	1	0.282	409.9	129.82	53.89	0.415	0.172
166	1	0.290	421.0	130.28	54.07	0.415	0.172
166	1	0.320	464.4	130.23	53.75	0.413	0.170
200	1	0.034	58.9	130.87	50.69	0.387	0.150
200	1	0.046	80.2	131.51	50.74	0.386	0.149
200	1	0.065	113.4	131.42	51.26	0.390	0.152
200	1	0.090	156.7	131.18	51.53	0.393	0.154
200	1	0.114	200.0	131.20	52.03	0.397	0.157
200	1	0.139	243.4	130.19	52.23	0.401	0.161
200	1	0.234	409.9	130.04	52.86	0.407	0.165
200	1	0.241	421.0	130.64	52.81	0.404	0.163
200	1	0.265	464.4	130.58	53.28	0.408	0.166

APPENDIX III CONTINUED

Flow Rate (LPM)	Retention Aid (#/ton)	Time from inlet (s)	Sector Midpoint (mm)	Mean Brightness	Brightness Std Deviation	Formation Number (s/y-bar)	Formation Number-sq (s^2/y-bar^2)
100	2	0.067	58.9	128.66	56.25	0.437	0.191
100	2	0.092	80.2	129.85	56.76	0.437	0.191
100	2	0.130	113.4	130.05	57.91	0.445	0.198
100	2	0.179	156.7	130.83	57.54	0.440	0.193
100	2	0.229	200.0	129.75	58.08	0.448	0.200
100	2	0.278	243.4	130.67	57.04	0.437	0.191
100	2	0.468	409.9	128.10	56.89	0.444	0.197
100	2	0.481	421.0	128.87	56.81	0.441	0.194
100	2	0.531	464.4	128.30	55.88	0.436	0.190
133	2	0.051	58.9	129.35	54.00	0.417	0.174
133	2	0.069	80.2	130.56	54.15	0.415	0.172
133	2	0.097	113.4	131.59	54.77	0.416	0.173
133	2	0.135	156.7	130.86	55.84	0.427	0.182
133	2	0.172	200.0	130.91	56.82	0.434	0.188
133	2	0.209	243.4	130.30	56.93	0.437	0.191
133	2	0.352	409.9	128.57	58.25	0.453	0.205
133	2	0.362	421.0	128.84	58.78	0.456	0.208
133	2	0.399	464.4	128.93	58.08	0.450	0.203
166	2	0.041	58.9	128.08	52.12	0.407	0.166
166	2	0.055	80.2	129.71	52.28	0.403	0.162
166	2	0.078	113.4	129.47	53.42	0.413	0.170
166	2	0.108	156.7	130.00	54.08	0.416	0.173
166	2	0.138	200.0	130.77	54.88	0.420	0.176
166	2	0.168	243.4	129.08	55.25	0.428	0.183
166	2	0.282	409.9	130.25	57.63	0.442	0.196
166	2	0.290	421.0	130.22	57.69	0.443	0.196
166	2	0.320	464.4	129.91	57.94	0.446	0.199
200	2	0.034	58.9	130.90	51.60	0.394	0.155
200	2	0.046	80.2	131.19	51.77	0.395	0.156
200	2	0.065	113.4	131.10	52.55	0.401	0.161
200	2	0.090	156.7	132.00	53.12	0.402	0.162
200	2	0.114	200.0	130.92	54.04	0.413	0.170
200	2	0.139	243.4	129.61	54.39	0.420	0.176
200	2	0.234	409.9	130.30	57.06	0.438	0.192
200	2	0.241	421.0	130.63	56.97	0.436	0.190
200	2	0.265	464.4	130.58	56.89	0.436	0.190

APPENDIX IV: FFT LENGTH DATA

Flowrate (GPM)	Retention Aid (#/T)	Time from inlet (s)	Sector Midpoint (mm)	Mean Floc Length (mm)
100	0	0.072	62.7	1.183
100	0	0.080	70.0	1.201
100	0	0.125	109.6	1.253
100	0	0.183	160.4	1.294
100	0	0.229	200.0	1.349
100	0	0.274	239.6	1.328
100	0	0.481	421.0	1.383
100	0	0.630	551.0	1.457
100	1	0.072	62.7	1.831
100	1	0.080	70.0	1.757
100	1	0.125	109.6	1.965
100	1	0.183	160.4	1.978
100	1	0.229	200.0	1.966
100	1	0.274	239.6	1.954
100	1	0.481	421.0	2.163
100	2	0.072	62.7	2.288
100	2	0.080	70.0	2.454
100	2	0.125	109.6	3.015
100	2	0.183	160.4	1.977
100	2	0.229	200.0	2.802
100	2	0.274	239.6	1.963
100	2	0.481	421.0	2.305
133	0	0.054	62.7	1.140
133	0	0.060	70.0	1.166
133	0	0.094	109.6	1.239
133	0	0.138	160.4	1.335
133	0	0.172	200.0	1.330
133	0	0.206	239.6	1.312
133	0	0.362	421.0	1.408
133	0	0.474	551.0	1.333
133	1	0.054	62.7	1.376
133	1	0.060	70.0	1.353
133	1	0.094	109.6	1.505
133	1	0.138	160.4	1.591
133	1	0.172	200.0	1.666
133	1	0.206	239.6	1.715
133	1	0.362	421.0	1.488
133	2	0.054	62.7	1.607
133	2	0.060	70.0	1.675
133	2	0.094	109.6	1.970
133	2	0.138	160.4	2.132
133	2	0.172	200.0	2.457
133	2	0.206	239.6	2.089
133	2	0.362	421.0	2.768

APPENDIX IV CONTINUED

Flowrate (GPM)	Retention Aid (#/T)	Time from inlet (s)	Sector Midpoint (mm)	Mean Floc Length (mm)
166	0	0.043	62.7	1.126
166	0	0.048	70.0	1.122
166	0	0.075	109.6	1.196
166	0	0.110	160.4	1.270
166	0	0.138	200.0	1.314
166	0	0.165	239.6	1.287
166	0	0.290	421.0	1.322
166	0	0.379	551.0	1.350
166	1	0.043	62.7	1.283
166	1	0.048	70.0	1.283
166	1	0.075	109.6	1.410
166	1	0.110	160.4	1.434
166	1	0.138	200.0	1.549
166	1	0.165	239.6	1.459
166	1	0.290	421.0	1.486
166	2	0.043	62.7	1.316
166	2	0.048	70.0	1.338
166	2	0.075	109.6	1.533
166	2	0.110	160.4	1.635
166	2	0.138	200.0	1.745
166	2	0.165	239.6	1.724
166	2	0.290	421.0	2.717
200	0	0.036	62.7	1.104
200	0	0.040	70.0	1.124
200	0	0.063	109.6	1.164
200	0	0.092	160.4	1.266
200	0	0.114	200.0	1.274
200	0	0.137	239.6	1.245
200	0	0.241	421.0	1.262
200	0	0.315	551.0	1.317
200	1	0.036	62.7	1.193
200	1	0.040	70.0	1.197
200	1	0.063	109.6	1.288
200	1	0.092	160.4	1.387
200	1	0.114	200.0	1.421
200	1	0.137	239.6	1.352
200	1	0.241	421.0	1.369
200	2	0.036	62.7	1.415
200	2	0.040	70.0	1.408
200	2	0.063	109.6	1.574
200	2	0.092	160.4	1.627
200	2	0.114	200.0	1.834
200	2	0.137	239.6	1.739
200	2	0.241	421.0	2.749

APPENDIX V: PRESSURE DROP DATA

Fibers	Flow Rate (LPM)	Pump Speed (RPM)	Flow Velocity in channel (m/s)	V^2 in channel (m^2/s^2)	N_{Re} in Channel	Upstream Port (mm)	Downstream Port (mm)	Diff. Press. (Pa)	dP/dL (Pa/mm)	h_{fs} (J/kg)	f actual
No fibers	38	340	0.33	0.11	7785	20	1617	160	0.10	0.16	0.0106
No fibers	60	460	0.52	0.28	12292	20	1617	290	0.18	0.29	0.0077
No fibers	83	610	0.73	0.53	17004	20	1617	460	0.29	0.46	0.0064
No fibers	100	730	0.87	0.77	20487	20	1617	620	0.39	0.62	0.0059
No fibers	115	820	1.01	1.01	23560	20	1617	760	0.48	0.76	0.0055
No fibers	135	967	1.18	1.40	27658	20	1617	1010	0.63	1.01	0.0053
No fibers	155	1085	1.36	1.84	31755	20	1617	1230	0.77	1.23	0.0049
No fibers	174	1231	1.52	2.32	35648	20	1617	1500	0.94	1.50	0.0047
No fibers	188	1320	1.64	2.71	38516	20	1617	1690	1.06	1.69	0.0046
No fibers	200	1440	1.75	3.06	40975	20	1617	1940	1.21	1.94	0.0046
No fibers	231	1615	2.02	4.08	47326	20	1617	2310	1.45	2.31	0.0041
No fibers	250	1760	2.19	4.78	51218	20	1617	2660	1.67	2.66	0.0041
Fibers present	38	340	0.33	0.11	7785	20	1617	100	0.06	0.10	0.0066
Fibers present	60	460	0.52	0.28	12292	20	1617	180	0.11	0.18	0.0048
Fibers present	83	610	0.73	0.53	17004	20	1617	290	0.18	0.29	0.0040
Fibers present	100	730	0.87	0.77	20487	20	1617	360	0.23	0.36	0.0034
Fibers present	115	820	1.01	1.01	23560	20	1617	450	0.28	0.45	0.0033
Fibers present	135	967	1.18	1.40	27658	20	1617	570	0.36	0.57	0.0030
Fibers present	155	1085	1.36	1.84	31755	20	1617	770	0.48	0.77	0.0031
Fibers present	174	1231	1.52	2.32	35648	20	1617	900	0.56	0.90	0.0028
Fibers present	188	1320	1.64	2.71	38516	20	1617	1070	0.67	1.07	0.0029
Fibers present	200	1440	1.75	3.06	40975	20	1617	1250	0.78	1.25	0.0030
Fibers present	231	1615	2.02	4.08	47326	20	1617	1600	1.00	1.60	0.0029
Fibers present	250	1760	2.19	4.78	51218	20	1617	1900	1.19	1.90	0.0029